# Dynamics of Oily and Solid Soil Removal from Fibres

NHAN T. PHAM

A thesis submitted in partial fulfilment of the requirements of The Nottingham Trent University for the Degree of Doctor of Philosophy

May 2002

# Abstract

This thesis reports the development of a novel single fibre optical method based upon attenuated total internal reflection (ATIR) for the study of the kinetics of the detergency process. This method is assessed for its ability to monitor the extent to which the fibre is soiled by liquids or solids. In this thesis, the focus is upon textile type fibres of polyester and Tencel, with the main focus on polyester fibres of 800 and 80 $\mu$m in diameter. Initial assessment of the method is performed using coiled PMMA optical fibres.

An experimental apparatus based on a lock-in amplifier has been designed, tested and characterised over a range of conditions. The immersion of fibres in a series of alkanes demonstrates the increasing light attenuation as the refractive index of the outer medium approaches that of the fibre. The ability of the system to monitor the wetted length of the fibre via light attenuation was established. The system was then used to monitor the deposition of decane drops from a decane-water emulsion. Subsequently, the wetting of small portions of fibres by drops of water and the deposition of polystyrene particles of sizes 1.9, 3.15, 5 and 10 $\mu$m from suspension drops of a range of concentrations was considered. The particle deposition was forced by the natural evaporation of the drops. These studies showed a linear relationship between the covered area and the light attenuation with significantly higher attenuation due to the final deposition of particles compared to the initial wetted area. This study was then extended to the deposition of clay particles via evaporation. The interpretation of the trends in the ATIR light transmission signal in the particle deposition experiments has been developed using videomicroscopy and the quartz crystal microbalance (QCM) method. It was found that the penetration depth of the evanescent wave in the ATIR method is larger than that of the QCM. Furthermore, the contact line pinning during evaporation which was observed by videomicroscopy has also been recorded by the ATIR transmission signals. Clay deposition from aqueous solutions in which the fibres are immersed has also been studied. The rate of the deposition of the particles can be manipulated by adding electrolytes to the solution.

To support the experimental work a simple quantitative model of the light transmission based on meridional rays in multimode fibres has been developed. Good agreement between model and experiments are found for the immersion study of polyester and the deposition of polystyrene particles onto polyester.

# Acknowledgements

# Table of Contents

# Chapter 5: Liquid Soiling of Fibres

# Chapter 1: Introduction

Detergency is broadly defined as the process of removal of soil or dirt from a substrate material. There are two types of soil: solid (particulate soil), or liquid (oily soil). Soils normally differ from the textile fibres in shape and composition, but are however of comparable size. Oily soil has to be persistent, therefore, it must be non-volatile [1]. In the following a concise introduction to the historical background of the detergency industry is given and its drastic changes during the last century described.

## 1.1. The history of detergency

One might rightly claim that the synthetic detergency industry started as the soap industry. Carboxylate soaps had been used for centuries before fat shortages during the first World War led to the development of synthetic detergents. The new products comprised one or more surface active agents (surfactants) and subsidiary constituents. Surfactants are organic chemicals which enable the cleaning solution to wet the surface of the products to be cleaned by lowering the surface tension of water, so that soil can be readily loosened and removed. Surfactants also emulsify oily soils and keep them in dispersion. Despite the fact that the first synthetics proved to be only fair to moderately good detergents, (but good wetting agents) they are still being produced in large quantities for use as textile auxiliaries. The production of synthetic detergents rose sharply after the second World War and it is still rising whereas the production of soaps seems to have settled down [2].

The most important reason for this increase in the production of synthetic detergents is that by blending with the correct inorganic or organic additives, synthetics can perform many detergent operations much better than the soaps. In addition the problem of precipitation does not arise with some of the new compounds. The calcium and magnesium ions, which give hardness to the water, form insoluble salts with the fatty acid in soap and a curd-like precipitate occurs and settles on what ever is being washed. By using a large excess of

soap, it is possible to redisperse the precipitate, but it is extremely sticky and difficult to move. This problem with soap can be overcome by using synthetic detergents because their salts remain water soluble throughout the washing procedure. Another advantage of synthetic detergents is that by blending them with the right additives new compositions can be obtained to be used for each individual purposes [3]. The additives include builders which were introduced to improve the performance of synthetic detergents. The primary function of these chemicals is to reduce water hardness. Also, it was noticed that, although, the detergent was able to lift the dirt from the textile, it could not keep it in suspension and the soil become uniformly redeposited giving a grey appearance on white textiles. The first example of builders was carboxymethylcellulose (or zeolites, phosphates) and it was found that by their addition the problem of redeposition was eliminated.

Another type of additive, which caused a revolutionary trend in the detergent industry in the 70s, was enzymes. Enzyme - an organic catalyst - aims at proteinaceous stains since it breaks down protein into amino acids and, therefore, eases their removal. It is sometimes an ingredient of detergents which are used in connecting with a pre-soak cycle prior to a proper washing cycle. Other additives which have to be mentioned are optical brighteners (whitener) and bleaches. Nowadays, it is not unusual for a detergent formulation to contain around twelve components in all [1].

## 1.2 Types of synthetic detergents

There are several types of detergents each comprising of a mixture of several surfactants but they all have one property in common. The surfactant molecule possesses a unique property called amphiphilicity. This means that the molecule comprises of a hydrophilic (water loving) and a hydrophobic (oil loving) group. It is because of this dual character that detergents have remarkable wetting and emulsifying properties and that they foam and are capable of cleaning soiled surfaces.

There are four main classes of surfactants: anionic, cationic, non-ionic and amphoteric. These four groups of organic chemicals will be discussed separately below as well as their differences and their areas of application.

### 1.2.1 Anionic surfactants

Anionics as the name suggested are compounds in which the detergency is vested in the anion, which has to be neutralised with an alkaline or basic material before the full detergency is developed [2]. This type of detergent has a low temperature sensitivity, low water hardness tolerance, high foaming and is the most widely used as Table 1.1 shows. The reason is the ease and low cost of their manufacture [4]. Therefore, they can be found in most of the common household products, such in laundry and hand dishwashing detergents and personal cleansing products. Anionic compounds are good in removing particulate soil and especially effective at cleaning fabrics that absorb water readily, such as those made of natural fibres, (e.g. cotton).

### 1.2.2 Non-ionic surfactants

Non-ionics are low sudsing and are typically used in laundry and automatic dishwasher detergents and rinse aids. They do not ionise in solution and thus have no electrical charge, they are resistant to water hardness and clean well on most soils. However, they are more efficient in removing oily and organic dirt than inorganic or polar dirt. They are widely used in blends with anionics, with the latter in larger proportions [4]. Because of their complementary nature, non-ionic and anionic surfactants are utilised together to take advantage of the beneficial properties of each [5]. The most widely used non-ionics are alcohol ethoxylates.

### 1.2.3 Cationic surfactants

Cationic detergents are of relatively little interest to the cleaning materials manufacturer. Compared with the anionic and non-ionic compounds their detergency is relatively poor and their cost is high. However, they are still used as cleaners but their special properties make them very effective germicides and,

therefore, they are widely used in antiseptic soaps and mouthwashes. Due to their positive charges they adhere to many fabrics that normally carry negative electrical charges, and hence, they can be found in fabric softeners.

### 1.2.4 Amphoteric surfactants

The amphoterics are the least widely used type of surfactants in detergents as Table 1.1 suggests, however, they are of some interest. Due to their chemical structure they possess the characteristics of both anionic detergents and cationic fabric softeners. Amphoteric surfactants in general are stable in highly acid solutions, and have thus found use in acid cleaners based on hydrofluoric acid. It has been found that amphoteric compounds are non-irritating to the skin and do not produce either eye sting or irritation and they give very excellent foam, which makes them suitable for foam cleaners which are to work at neutral pH, such as hair and rug shampoos [2].

| Type of deterrents | Usage in % |
|--------------------|------------|
| Anionics | 66 |
| Non-ionics | 29 |
| Cationics | 5 |
| Amphoterics | < 1 |

Table 1.1: The estimated usage of detergents in 1975 [2]

### 1.3 Efficiency of detergents

Combinatorial chemistry has enabled researchers to develop vast numbers of formulae of detergent solutions and one would like to have a reliable method to investigate the efficiency of removing of soil from a material of each individual solution. There are many methods currently used to evaluate the performance of the detergents, but the undoubtedly most common one dealing with particulate soils is by reflectance measurements. In this evaluation, a standard size of fabric is soiled with standard soil, such as coffee powder or vacuum cleaner dust. The reflectance of the soiled cloth is then measured before it is washed in a Ter-O-

Tometer (or Tergotometer) with the detergent under investigation. After the washing cycle the reflectance of the washed cloth is recorded and the efficiency of the detergent in removing the soil is determined using the equation below:

$$Detergent\ efficiency = \frac{R_W - R_S}{R_C - R_S} \times 100 \ ; \qquad\qquad (1.1)$$

where $R$ is the reflectance and the subscripts $w, s$ and $c$ refer to washed, soiled and clean condition [3]. Although, the idea of this method is simple and the test is easily realised the reflectance is normally influenced by the optical geometry of the reflectometer and this method is only sensitive at a low level of soiling. Alternative approaches have been put forward to overcome that problem but with only minor improvements. If one wants a representative result of the efficiency of the detergent with this method many tests have to be done and it is therefore, very time consuming. Hence, a reliable and quick method to determine the efficiency of detergents is sought. Although, this method might represent the conditions in the washing machine very well and should be used as the final test, one might wish to have a model approach which only focuses on the detergent ability of surfactants solutions in idealised conditions. Naturally, the fact that a cloth is used complicates the test in the sense that the travelling of soil between neighbouring fibres in the cloth due to capillary action needs to be considered. Furthermore, the water-surfactant mixture flow in the drum of the washing machine is difficult or impossible to quantify. In the following an idealised single fibre technique is proposed which can be used to overcome some of the difficulties mentioned. It allows one to directly investigate and visualise the detergency process, it gives quantitative signals and enables the liquid flow to be controlled.

## 1.4 Project overview

This report develops a technique to characterise aspects of wetting of fibres and the detergency process. This novel approach uses the natural light guiding properties of fibres to determine the interaction of liquid or particles with a single fibre. There are numerous optical fibre sensors using the same principle of light

guiding to investigate the fibre surface interaction with its environment. However, the investigation in this thesis is unusual in being aimed at using textile fibres since they are used in the detergency process. .

The aim of the project was to design an experimental system capable of performing measurements with textile type fibres to study the feasibility of the proposed technique. The system then had to be tested and characterised using both optical and textile type fibres. Its limitations have been explored and its performance was improved. Model experiments using both types of fibres were conducted and the results were compared with each other to gain a greater understanding of the sensing technique as well as the experimental system.

In subsequent chapters, a detailed literature review of work related to the project is given. Since this work is interdisciplinary the review Chapter covers several areas of research starting with the basics of the theory of detergency. This is followed by some material on the wetting of solids emphasising the differences due to the geometrical nature of cylindrically shaped fibres to planar solids. Then the report moves on to describe the structure of optical fibres which enable them to guide light so efficiently and to the more relevant textile type fibres of this project. The chapter concludes with some examples of fibre optic sensors which provides a general idea of the principles used in this report.

Chapter 3 discusses the relevant theoretical background of the project. It starts with a description of the theory of detergency. This is followed by a concise treatment of the basics of light guiding in optical fibres as well as a simplified approach developed to explain light transmission in textile fibres. Furthermore, some relevant ideas of colloid science related to the experiments on particle interactions will be described. Finally, the fundamentals of the quartz crystal microbalance, which is used in this project with particle deposition experiments, will be outlined.

The experimental development and the apparatus used are described in Chapter

4. A chronological project plan of the experimental procedures is outlined and the equipment used for the different experiments is explained in detail. Furthermore, some preliminary experiments to illustrate the feasibility of the sensing principle as well as the functioning of the equipment are given. These experiments will play an important role in discussing more complex investigation in subsequent chapters.

Chapter 5 is the first part of the results and discussion dealing with the liquid interaction of different media with the fibre. This chapter describes experiments where the fibre probe is fully immersed in liquids with different refractive indices and the deposition of oily drops from an aqueous environment onto the fibre. Since the aim of these experiments was to test and characterise the model system, they have been performed with both textile type and optical fibres. It was found that the results for both types of fibres were quite similar, and the results are in good agreement with those existing in the literature.

The second part of the results and discussion is given in Chapter 6. The interactions of textile fibres with particles deposited from aqueous suspension has been investigated. Evaporation experiments of drops from suspension on the fibre surface have been carried out to force deposition of particles onto the surface. Deposition is the inverse process to removal of particulates and knowledge of the mechanisms involved in the attachment of particles to a surface will certainly help to characterise their detachment process as a part of the detergency. Monodisperse latex particles were used and these offer a more controllable deposition process than the multi-sized drops of oil in the previous chapter. After familiarising with the effects of monodisperse particles, attention was focused towards a problem of industrial relevance: the deposition of clay particles onto textile fibres. The process has been investigated and explanations suggested for characterising the different stages of deposition. The same type of measurements was carried out using a quartz crystal microbalance (QCM) equipment and comparisons were drawn from the two sets of results. The experimental results are also discussed using the light guiding model suggested

in Chapter 3.

Finally, Chapter 7 summarises the results obtained and gives ideas for further improvement of the method. So far, only a relatively large fibre has been used, but with improvement of the light source the method is capable of dealing with reduced fibres of much smaller diameter. In this section possible applications of the method will be suggested and their feasibility will be discussed.

## References

[1] B.J.Carroll, *Physical aspects of detergency*, Colloids and Surfaces A: Physicochemical and Engineering Aspects, **74**, (1993), 131

[2] A.Davidsohn, B.M.Milwidsky, *Synthetic detergents*, George Godwin Limited, London, (1978),

[3] K.Durham, *Surface activity and detergency*, Macmillan & Co. Ltd, London, (1961), VII

[4] M.R.Porter, *Handbook of surfactants*, Blackie & Son Ltd., London, (1991), 128

[5] K.H.Raney, *Optimization of nonionic/anionic surfactant blends for enhanced oily soil removal*, Journal of the American Oily Chemists Society, **68**, (1991), 525

# Chapter 2: Literature Review

This chapter provides a general literature review of previously published work in the areas of detergency, wetting of fibres and optical fibre sensors, that are relevant to this project. The first area covered in this section will be the theory of detergency. The processes of how dirt attaches to the fabrics and how it is removed from fabrics will be introduced. Both solid and liquid soil will be covered. The second area will be the wetting of fibres. This part of the chapter emphasises the difference of fibres to planar substrates and sets it within the context of the detergency process. After the macroscopic view of fibres, attention will be turned to the microscopic structure of fibres. The properties of optical fibres and of the textile fibres used in this project will be described. Finally, the chapter concludes with some examples of fibre sensors recently developed by academic researchers or already in industrial use.

## 2.1 Detergency

Due to the important role of detergents and their applications in every day life, there is a significant interest in developing more advanced surfactant solutions. Therefore, research activity in the detergency industry is very high. However, the detergency process is highly complicated and it is dependent on many factors which are not all easily controllable. Not only has one to deal with the surfactant solution under investigation but also with the woven fabric material, the nature of the soil and the hydrodynamic flow during the cleaning process. The woven fabric complicates matters due to interactions of neighbouring fibres allowing dirt between fibres to change location. This makes both the reproducibility of the location of the soil and knowing the location of the soil difficult. Naturally, the type of the soil plays an important role in the detergency process. Whether it is of liquid or solid origin, whether it is a mixture of both or whether it is electrically neutral or charged can all be important. In fact the variety of soils found on textiles is vast. Table 2.1 shows only a few examples.

| Soil | Origin | Major component |
|---|---|---|
| Skin cells | Body | Protein, lipids |
| Oil (sebum) | Body | Lipids |
| Sweat residues | Body | Inorganic -NaCl Organic - Urea |
| Medicaments | Body | Various organics |
| Sand/clays | Environmental | Siliceous matter |
| Stains | Food, drink | Fats, dyes |

Table 2.1. Examples of soils commonly found on fabrics before laundering [1].

Clearly, these soils are unsuitable for use in controlled studies of detergency due to their complexity and lack of reproducibility. Researchers have therefore introduced standard soils which are reproducible and are used in the detergency testing experiments. Table 2.2 shows a few examples of these standard soils.

| Soil | Classification |
|---|---|
| Iron oxide | Particulate |
| Vacuum cleaner dust | Particulate |
| Mineral oil | Mineral oil |
| Olive oil | Natural oil |
| Artificial sebum | Natural oil |
| Used car oil | Mineral oil/particulate |
| Blood | Natural stain |
| Red wine | Food, drink |

Table 2.2. Standard artificial soils used in detergent studies [1].

Finally, the characteristics of the hydrodynamic flow in the washing machine needs to be controlled. It is this flow which actually removes the soil from garments.

The complexity of the detergency process makes it necessary for researchers to design idealised investigation methods which enable them to control some of the factors described above. In the next section some of the methods developed to investigate the detergency process will be reviewed with the emphasis on the performance of the detergents.

## 2.1.1 Studies of the removal of liquid soil

Soils which can be found on textiles are very wide ranging and are often a mixture of solid and liquid components. However, it has been found helpful to separate the discussion of soils using their basic natures into those which are of solid type and those which are of liquid type. First, consider the methods used to investigate the removal of oily soil from solid.

### 2.1.1.1 Ellipsometric techniques

Ellipsometry is an optical technique, which relies on the fact that light changes its state of polarisation when reflected at a surface [2]. If the surface is clean, the technique will give its refractive index. On the other hand, if a film is deposited on the surface, ellipsometry will give the average thickness and refractive index of the film [3]. In detergency this method enables the amount of, for example, fat deposited on the surface to be determined, assuming the refractive index of the soil is known. Therefore, ellipsometry can be used to study the efficiency of surfactants by determination of the amount of soil at the surface as a function of time during the detergency process.

Malmsten and Lindman using the same technique found that the removal process starts with the adsorption of surfactant molecules at the soil/water and soil/substrate interfaces [3]. Due to the adsorption of surfactants the adhesion energy of the soil towards the substrate will be lowered and, hence, less force is needed to remove the soil from the surface. Naturally, the packing of the surfactant molecules at the interfaces is crucial for the removal efficiency and it was suggested that the optimal surfactant packing for maximal removal of soil is in planar layers, i.e. zero curvature toward water and soil [3].

In a similar work it was found that the efficiency of ionic surfactants can be enhanced by addition of inorganic salts [4]. The salt enables the surfactant molecules to pack themselves more densely on the interfaces and so the lowering of the adhesion forces between soil and substrate is more effective. Addition of salt also lowers the critical micelle concentration which also favours

the cleaning process; this will be described in detail later in Chapter 3. Backstrom, *et al* further found that the efficiency of non-ionic surfactants can be enhanced by adding hydrocarbons [4]. This fact can also be explained with the packing pattern of the surfactant molecules at the interfaces. However, the effect on the removal of soil of adding hydrocarbons is dependent on the nature of the surfactant itself.

### 2.1.1.2 Shear flow analysis

In this type of investigation the detachment of oil drops from surfaces via a flow of water, or more generally, of an aqueous phase, is characterised. A small drop of pristane, which is an alkane ($C_{19}H_{40}$), is formed at the tip of a capillary tube of a syringe and detached by mechanical shock [5]. Due to gravitational forces the pristane drop rises through the water vessel towards the substrate, which forms one wall of a channel. The diameter of the oil drop, typically 0.1 to 0.5 mm, is small compared to the channel width. Once the drop has been attached to the substrate a Poiseuille flow of water is formed in the channel, as illustrated in Figure 2.1. The shear rate, $\gamma_{shear}$, of the hydrodynamic flow at the wall of the channel is measured. The rate of the hydrodynamic flow is increased to the point where the oil drop starts to detach and the critical value of shear $\gamma_c$ is reached. As long as $\gamma_{shear}$ remains lower than $\gamma_c$ the contact line of the drop and the surface of the substrate does not move, despite visible deformation of the droplet due to the flow. When the shear rate reaches its critical value $\gamma_c$ the upstream part of the contact line starts to move slowly and the contact area starts to decrease gradually. Finally, the drop is detached when the near part of the drop catches up with the front part [5]. It was often observed that a sliding motion of the droplet along the surface preceded the actual removal process.

The experimental results show that the critical shear rate, $\gamma_c$ , is a decreasing function of the drop diameter, which seems logical since the larger the drop, the larger the hydrodynamic forces exerted on it [5]. The condition for detachment of the drop from the substrate surface is that the adhesion forces are overcome by

the hydrodynamic forces.

This method was also used to investigate the effect of roughness of the substrate on the detachment process. It was found that the contact angle hysteresis $(\cos\theta_r - \cos\theta_a)$, where $\theta_r$ and $\theta_a$ are the receding and advancing contact angles, respectively, was nearly double for a rough substrate compared to a polished substrate indicating an increase in the critical shear value for detachment [6].

The same researchers studied the effects of adding surfactants into the system. Dodecyl trimethyl ammonium bromide (DTAB), a cationic surfactant, was added to the alkane phase. It was found that the contamination of the system with DTAB resulted in an increase in contact angle hysteresis compared with the pure pristane-water system [7]. This means that higher force is needed to remove the pristane drop in the contaminated system, suggesting that DTAB does not favour detachment of alkane drops.

Yamamoto and colleagues used the same principle to design a flow cell capable of the investigation of the detachment of single particles from a surface [8]. The system enabled them to study the detachment and reattachment of latex polystyrene particles on hard surfaces. They found that higher hydrodynamic force is needed to detach agglomerated particles compared to single particles. A significant effect is also the decease of the removal efficiency of the particles from the surface with their drying time. This could be explained with the adhesion-induced deformation of the contact area, which will be discussed later in Chapter 3.
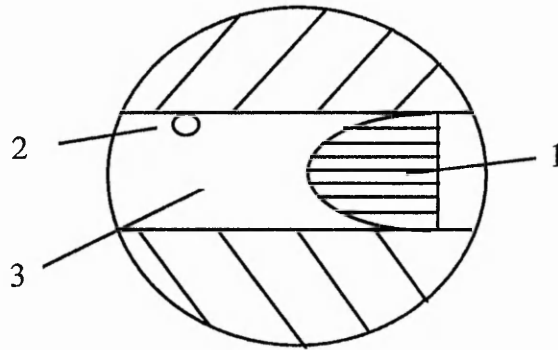
Figure 2.1. Poiseuille flow. (1) Poiseuille flow profile, (2) droplet attached to a wall of a capillary (3) [5].
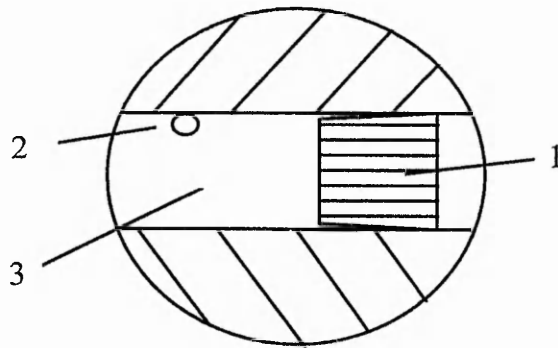


Figure 2.2. Electro-osmotic flow. (1) Piston flow profile, (2) particle attached to a wall of a capillary (3).

### 2.1.1.3 Videomicroscopy

Visual methods can also be found in detergency studies. Raney *et al* investigated the optimum detergency conditions for non-ionic surfactants with the aid of enhanced videomicroscopy [9]. With this method they could visualise the process of surfactant adsorption at the soil-water and soil-substrate interfaces. When pure straight chain hydrocarbons and non-ionics were used as soil and surfactant, respectively, they found that the optimum detergency effect was observed near the phase inversion temperature (PIT). The PIT may be defined as the temperature where the separation of the three phases occurs, or alternatively, at which the surfactant-oil-water system forms a middle-phase (or a surfactant phase) microemulsion containing equal volumes of oil and water in equilibrium with the excess oil and water phase [9]. It was shown that under these conditions ultralow interfacial tensions can be observed [10,11] which favours the emulsification of oil into the surrounding water, leading finally to a lift off of the oily soil. Another favourable effect is the high solubilisation of oil which occurs near the PIT since it was found that the main process of oil removal in this case was a combined solubilisation-emulsification mechanism [9,11,12].

Raney and co-workers also investigated the effects of hydrophobic additives in the system described above [12,13]. In this work it was established that the optimum detergency correlates with the PIT of the soil-surfactant-water system. Investigations were then undertaken which aimed to see whether the point of optimum detergency could be manipulated by lowering the PIT of the surfactant system. Therefore, hydrophobic or lipophilic compounds such as long-chain alcohol (e.g. dodecanol) were added to the oil-surfactant-water system [12,13]. The studies showed that it is possible to lower the PIT considerably and the new point for optimum detergency correlates with the new PIT. In this manner the researchers found a way to develop surfactant systems for soil removal at low temperatures.

Raney went further and applied the PIT theorem to blends of anionic and ionic surfactants for removal studies of soil (hexadecane) from polyester/cotton fabric

[11]. It was shown that not only the correlation of PIT and optimum detergency holds, but that one should also be able to determine the PIT of the anionic-nonionic blend given their weight ratio and vice versa. The author also speculated on how to develop temperature-insensitive surfactant formulations [11].

## 2.1.2 Studies of the removal of particulate soil

The cleaning of particulates from surfaces is enjoying renewed attention due to its relevance in several industries. For example, it is critical in the semiconductor industry that silicon wafers are exceptionally clean of dust particles of sizes around 1 μm and smaller. There are many studies investigating the adhesion and removal of particles on surfaces and a selection is mentioned below.

### 2.1.2.1 Electro-osmotic washing

If one considers the parabolic velocity profile of Poiseuille flow in Figure 2.1, it becomes apparent that the hydrodynamic force acting on the soil at the wall of the fibre is negligible and it is therefore claimed that particles smaller than 0.1 μm are hardly removable by ordinary mechanical washing [14]. One way to increase the force acting on the soil is to modify the velocity profile towards a piston flow, as shown in Figure 2.2. Watanabe and Tagawa reported that electro-osmosis flow shows a piston-like velocity profile. They applied the method to the investigation of the removal of particulate soil from the capillary walls of cotton [15,16]. A soiled cotton cloth is placed between two electrodes in a water bath. An electric field is generated perpendicular to the cloth and this field contributes to the velocity flow profile illustrated in Figure 2.2.

Additionally, the particles adhering to the substrate are themselves usually charged and are thus subject to the force tending to cause electrophoretic flow and so can be collected by the electrodes [17]. Electro-osmotic flow in this case can be seen as a movement of the liquid without any distortion effects on the substrate. Therefore, not only does electro-osmosis give a higher hydrodynamic drag on particles but it is also substrate friendly. The increase in pure

hydrodynamic drag force acting on the particles at the wall can be explained by the Bernoulli effect. According to the Bernoulli Theorem the hydrostatic pressure $p_S$ is defined as,

$$p_s = p + \frac{1}{2}\rho u^2 \tag{2.1}$$

where $\rho$ is the density of the liquid and $u$ is the bulk velocity flow. Hence, the soil particles experience a lift force $f$ which is given by

$$f = p_s - p = \frac{1}{2}\rho u^2 \tag{2.2}$$

To determine the effectiveness of detergency the reflectance of the cloths was measured and the Kubelka-Munk equation was applied to determine the detergency D [14]:

$$D = \frac{\left(\frac{K}{S}\right)_s - \left(\frac{K}{S}\right)_w}{\left(\frac{K}{S}\right)_s - \left(\frac{K}{S}\right)_o} \tag{2.3}$$

where $\left(\frac{K}{S}\right) = \left(\frac{(1-R)^2}{2R}\right)$ $\tag{2.4}$

$K$ is the coefficient of reflectivity, $S$ is the light-scattering coefficient, $R$ is the reflectance, and the subscripts $w$, $s$ and $o$ stand for washed, soiled and white cloths, respectively.

Watanabe and Tagawa showed that the detergency D increases with increasing voltage between the electrodes up to 50 V, and that it is linearly dependent of the flow field velocity [15]. They also claimed that electro-osmotic washing gives higher detergency without damage to the fabric than the standard mechanical washing. Moreover, the method has the advantage of removing soil particles on surfaces under cover and on irregular surfaces, where ordinary mechanical methods are ineffective [15]. In the presence of an anionic surfactant, it was reported that the detergency was highly improved with increasing potential between the electrodes [18,19].

## 2.1.2.2 Quartz crystal microbalance

An acoustic method recently employed to investigate some of the processes in detergency is the quartz crystal microbalance (QCM). In principle, the QCM is a gravimetric technique that can be used to detect very small mass changes in the amount of material deposited on or removed from a surface, both in air and in liquid environment [20]. In the case of rigid mass, the mass deposited onto, or depleted from, the quartz crystal surface, can be calculated from the change in its resonance frequency. According to the Sauerbrey equation [21],

$$\Delta f = -\frac{2f_o^2}{A\sqrt{(\rho_q \mu_q)}}\Delta m \qquad (2.5)$$

where $\Delta f$ is the measured shift in resonance frequency, $f_o$ the fundamental resonance frequency, $\Delta m$ is the mass change, $A$ is the electrode area, $\rho_q$ is the density of the quartz (2648 kg m$^{-3}$), $\mu_q$ is the shear modulus ($2.947\times10^{10}$ kg m$^{-1}$s$^{-2}$) for AT-cut quartz, and the minus sign indicates that a loss in mass causes an increase in frequency and vice versa.

The deposition of mass from an aqueous solution normally causes a downward shift in the resonance frequency of the crystal. However, since the mass is surrounded by a liquid which has a viscosity and density, this would lead also to a dissipation of the crystal energy. Only changes within a penetration depth are sensed.

Caruso *et al* used the QCM method to monitor the adsorption of non-ionic surfactants on hard surfaces from an aqueous solution [22]. They immersed the quartz crystal in a temperature controlled bath of an aqueous solution in which the surfactant was injected. It was found that for the two non-ionics under investigation, the frequency immediately decreases upon the addition of the surfactants, indicating a rapid adsorption of the surfactants onto the crystal [22].

Weerawardena and co-workers showed that the technique is capable of monitoring the removal process of solid organics soil by surfactants [23]. Organic

soil, tripalmitin and dotriacontane, was deposited onto the crystal surface. Subsequently, the crystal was immersed in water and then in a surfactant solution. The immersion of the soiled crystal in the water bath showed that the organic soil tended to absorb water which is reflected by a decrease in resonance frequency of the crystal. When the surfactant was injected into the water bath, a decrease in frequency was observed before the removal process, indicated by a rise of the frequency signal. The initial decrease in frequency of the signal can be understood by a picture of the soil removal process as normally starting with the adsorption of surfactant molecules at the soil-water interface, thus adding more mass onto the crystal. Although, the Sauerbrey equation is not valid when the crystal is immersed in liquids, the QCM method is able to monitor the efficiency of the surfactant in removing solid organic soil from hard surfaces in real time [23].

Weerawardena and co-workers also looked at the removal of solid organic soil from hard surfaces by glucose-derived surfactants [24]. They reported that the performances of the surfactants were poor below the critical micelle concentration (CMC) and optimal at concentrations higher than the CMC. However, in this concentration region the removal is also dependent on the degree of polymerisation, and alkyl chain length, of the surfactant molecule [24].

### 2.1.2.3 Rotational rinsing

The removal of particulates has been well studied since it has a variety of industrial applications. For example in the semiconductor industry, it is vital that the surface of the silicon wafer is clean for the functioning of the semiconductor chips. Busnaina and co-workers studied the critical force necessary to remove submicrometer particles from a surface [25,26]. In their studies polystyrene particles were deposited onto the surface of a silicon wafer and the removal was realised by rotating the wafer around its centre and simultaneously introducing water at its centre - rotational rinsing. In this system, the particles experience three individual forces. A drag force $F_d$ arises due to the pressure difference

across the surface as the water flows across the particles. The shear stresses in the flow give rise to a hydrodynamic lift force or Saffman lift force $F_l$ [25-27]. Finally, the particles on the rotated wafer also experience the centrifugal force $F_{cent}$. The total removal force acting on one particle is the sum of the three individual forces which are given below for the laminar case,

$$F_d = 3\pi\mu dV \tag{2.6}$$

$$F_l = 1.62\mu d^2\left(\frac{1}{\upsilon}\frac{\partial U}{\partial x}\right)^{1/2}V \tag{2.7}$$

$$F_{cent} = mr\omega^2 \tag{2.8}$$

where $\mu$ is the viscosity of the fluid, $d$ is the particle diameter, $V$ is the relative velocity between particle and fluid, $\upsilon$ is Poisson's ratio for the substrate, $U$ is the shear flow velocity, $x$ is the co-ordinate of the particle on the substrate, $m$ is the mass of one particle, $r$ is the distance from the centre and $\omega$ is the rotational speed of the wafer.

It was reported that the previously neglected Saffman lift force plays an important role in the removal process and nearly complete removal of the particles from the wafer surface could be achieved using the rotational rinsing method. In addition, it was found that the removal of the particles depended in a sensitive manner on their radius. Calculations showed that the hydrodynamic forces are proportional to the square of the particle radius, while the adhesion force is linearly proportional to the radius [25]. Thus, the smaller the particle, the harder it is to remove, since in this region the adhesion forces exceed the removal forces [25].

Interestingly, it was also reported that the longer the particles were on the substrate the harder it is to remove them [25,26]. This phenomenon has been investigated and it has been found that it can be explained by the adhesion-induced deformation of the particle [25,26]. The area of contact between a particle and a surface increases with time due to the surface forces acting at the boundary. Depending on the material properties of the particle and the surface, either elastic or plastic deformation can occur [26]. This naturally, influences the

removal process drastically. Krishnan and colleagues, using the rotational method, reported that the decrease in removal efficiency correlates well with the increase in contact area, and so the adhesion of the particle to the surface of the substrate [26].

### 2.1.2.4 Rotating cylinder

Visser suggested a different approach for the investigation of adhesion forces of particulates on surfaces [28,29]. The particles were deposited on a cylinder surface which then rotates in a liquid bath in the presence of a hydrodynamic flow along the length of the cylinder surface. Due to the rotation of the cylinder in the liquid, the particles sitting on the cylinder surface will experience a hydrodynamic force. It was reported that the adhesion of carbon-black particles on a cellulose film is dependent on the pH value of the aqueous phase and has its maximum around a value of pH=3.3. The investigation also showed that the removal efficiency is a function of the speed of rotation [28]. Therefore, the critical adhesion force to remove the particles can be determined and has been discussed in terms of the classical Lifshitz - van der Waals theory [28].

A similar investigation looked at the adhesion of polystyrene particles on a cellophane surface [29]. The outcome confirmed the results stated above and Visser gave an expression for the adhesion forces involved and discussed them within well-known classical treatments. Furthermore, the relationship between the efficiency of removal and the hydrodynamic force was also given in this work [29].

### 2.2 The wetting of fibres

Interfacial tensions and the contact angle between the oily and the solid phase are important for the adhesion/removal of liquid soil onto/from a surface. Therefore, it is possible to characterise the detergency by investigating the behaviour of the contact angle during the removal process. Since the removal process normally involves the immersion of soiled substrates, mostly fibres, in surfactant solutions the wetting behaviour of fibres is critical in detergency.

Additionally, some understanding of the wetting process on fibres should be beneficial for further investigation of the kinetics of the removal process. Therefore, the wetting behaviour of fibres will be discussed in this section separately with applications of the contact angle method to detergency study mentioned where appropriate.

The wetting of fibres has many applications in important industrial fields [31]. However, the spreading of a liquid on a fibre is far less understood than the wetting on a plane surface. Determination of the contact angle of a liquid on a flat substrate is fairly simple and the theory behind it is well understood [32-35]. On a flat surface a non-volatile droplet spreads out partially until an equilibrium contact angle is established or it spreads completely to form a thin film on the substrate. This spreading behaviour is related to the spreading coefficient $S$, see Figure 2.3.

$$S = \gamma_{SV} - \left( \gamma_{SL} + \gamma_{LV} \right)$$  (2.9)

In terms of the contact angle

$$S + \gamma_{LV} = \gamma_{LV} \cos\theta$$  (2.10)

where $\gamma_{SV}, \gamma_{LV}, \gamma_{SL}$ are, respectively, the solid-gas, liquid-gas and solid-liquid interfacial tensions. Therefore, partial wetting is observed when the spreading coefficient $S < 0$. For a small drop, the liquid will form a spherical cap and the contact angle $\theta$ is given by Young's equation.

$$\cos\theta = \frac{\gamma_{SV} - \gamma_{SL}}{\gamma_{LV}}$$  (2.11)

$S > 0$ corresponds to complete wetting where the liquid forms a thin film on the substrate and the thickness $e(S)$ of the film can be determined with the following equation.

$$e(S) = a\sqrt{\frac{3\gamma_{LV}}{S}} \; ;$$  (2.12)

where $a$ is a molecular size.

On a fibre, the situation is more complicated. The threshold between wetting and

non-wetting cannot be exactly at $S = 0$ [36]. As a consequence of the fibre geometry, a new value the critical spreading parameter $S_c$ is introduced.

$$S_c = \frac{3}{2}\gamma_{LV}\left(\frac{a}{x_1}\right)^{2/3} \tag{2.13}$$

where $x_1$ is the fibre radius. For $S > S_c$, the droplet spreads out on the fibre and forms a film. For $S < S_c$, the droplet is stable and an equilibrium contact angle is established.

There are two conformations of stable drops on a fibre as seen in Figure 2.4. An axi-symmetrical barrel shape is observed when the contact angle is low and the drop volume rather high. The other type is a clam shape which can be observed by reducing the drop volume and/or increasing the contact angle.

The axially symmetrical conformation becomes metastable when the contact angle exceeds a certain value which is related to the drop volume and to the fibre radius. Beyond this point the axially unsymmetrical conformation, the clam shell, is favoured. Carroll estimated the critical value for the contact angle of the barrel shaped droplet [38]. The transition between the two conformations is accompanied by a reduction of drop contact area, and it is known as the classical roll-up process of detergency as first described by Adam [39]. In the detergency process, the removal of a drop in a clam shape is easier than the removal of one in the barrel shape. This fact is due to the contact area between the drop and the fibre which is larger in the barrel type than in the clam type. Therefore, the roll up process is of great importance in the laundry process.
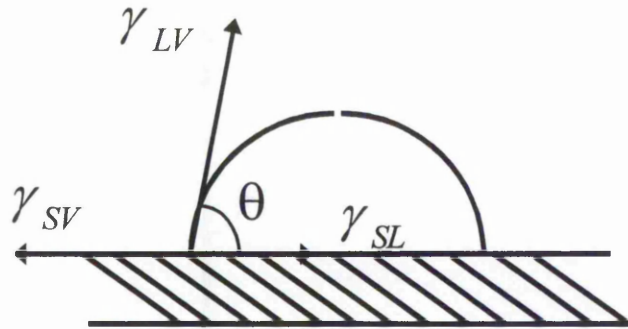
Figure 2.3. Force balance giving a static contact angle. Note: inflection angle at three phase contact line, which always exists, not shown for purposes of simplification.
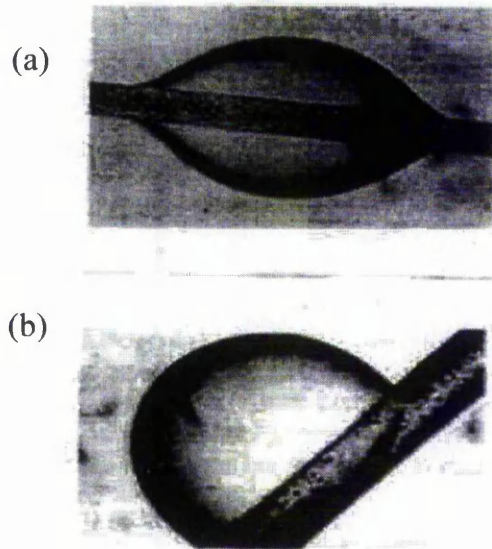


Figure 2.4. Conformations of liquid drop on cylindrical fibres. Barrel shape (a), clam shape (b) [37].

The special geometry of the fibre system, emphasised by the small radii of curvature of the fibres of relevance and the high droplet curvature induced by the fibre, as seen near the contact line in Figure 2.4(a), makes it difficult to apply traditional techniques to investigating the physicochemical factors important in the detergency process. Contact angle measurements are also very difficult due to the high droplet curvature at the three-phase line induced by the fibres. This is the main reason why methods for the determination of contact angle that work well on flat plates do not give very accurate or reproducible results when applied to fibres. Therefore, several new techniques have been introduced to overcome the problems accompanied with fibres, for example [40-43]. One method, the drop length-height method, was introduced by Song and co-workers [43]. This technique improves the reliability and accuracy of the results by using a large part of the drop profile in its calculations. McHale *et al* introduced a method where the contact angle was calculated via the maximum slope, the inflection angle, in the profile [44]. This method only applies for the axis-symmetrical conformation.

As on flat plates, the surface properties of the fibres play a significant role in the wetting process. Carroll investigated the effects of surface roughness on the wetting behaviour [45]. The results showed that the behaviour of the wetting liquid was determined by the geometry of the roughening. Although, on a smooth surface, the liquid could not spread out over the surface when the contact angle was zero, it did when the grooving was parallel to the cylinder axis and the contact angle was less than a certain value, which is closely related to the groove profile.

There is some work investigating the wetting behaviour of some industrially used fibres. Wolf and colleagues found that in glass fibres the surface roughness of the mono-filaments has only a weak contribution to the inhomogeneity of the wetting properties, whereas the chemical heterogeneity of the fibre surface causes a large distribution in the wetting results and in the contact angle hysteresis [46].

Another investigation involving nylon fibre assemblies, showed that the minimum wetting rate and maximum contact angle were observed near pH 4, which coincided with the isoelectric point of the nylon fibres used [47]. In the presence of ionic surfactant, the surfactant concentration, which gave minimum wetting rate, is closely correlated with the concentration for charge neutralisation. These results indicate that the capillary wetting rates in nylon assemblies are affected by electrical phenomena at the nylon/solution interfaces (electrowetting).

A study of the contact angle of polyester at a three phase line was undertaken by Perwuelz and co-workers [48]. The advancing and receding contact angles of the fibre with two liquid phases were measured. The results for the contact angles were quite different and a large hysteresis of 60° to 80° was found.

Ghenaim and colleagues investigated the effect of fluorination of polyester fibre on contact angles with liquids [49]. Fluorination is normally used to make fibres oil resistant and water repellent. Increasing the degree of fluorination made the fibre more hydrophobic and therefore the contact angle with water increased.

Bargeman and colleague investigated the effect of surfactants on the contact angles of water-oil systems on non-polar solids [50]. The conclusion from their investigation was that the contact angles in water-oil systems are not significantly affected by the presence of surfactants, unless the interfacial tension is very low [50]. A theoretical treatment of the influence of surfactants on the contact angle on non-polar solids is also given in the reference.

## 2.3 The structure of fibres

In the course of this project experiments were performed using first optical and then textile-like fibres to look into some aspects of the detergency process. Therefore, it is necessary to consider the structure of the relevant fibres. In the following section, a closer look will be taken at optical fibres and the reasons why they are so efficient in guiding light. Subsequently, attention will be turned towards the more relevant type of fibre for this project, which are textile-like

fibres.

### 2.3.1. Optical fibres

Optical fibres are dielectric waveguiding devices used to confine and guide light. The majority of optical fibres in sensing applications have silica glass cores, but some special materials, such as fluoride glasses and doped polymers, are also utilised for certain applications. A dielectric material called the cladding surrounds the core and its refractive index must be lower than that of the core to satisfy Snell's Law for total internal reflection and thus propagation of the light along the fibre. A barrier layer of plastic (the "buffer") is normally used to jacket the fibre; this provides the fibre with mechanical strength and protects it from damage and moisture absorption.

The propagation of light within an optical fibre can be understood from ray theory. When a ray is incident on an interface between two dielectrics of differing refractive indices (e.g. glass - air), refraction occurs, as shown in Figure 2.5 (a). If the dielectric on the other side of the interface has a refractive index $n_2$ which is less than $n_1$, then the refraction is such that the ray path in the lower index medium is at an angle $\alpha_2$ to the normal at the surface interface, where $\alpha_2$ is greater than $\alpha_1$. The angles of incidence $\alpha_1$ and refraction $\alpha_2$ are related to each other and the two refractive indices of the dielectrics by Snell's law of refraction, equation (2.15).

$$\frac{\sin \alpha_1}{\sin \alpha_2} = \frac{n_2}{n_1} \qquad (2.15)$$

Since $n_1 > n_2$ there is a value for $\alpha_1$ where the angle of refraction is 90°, so that the refracted light travels along the interface of the two media, see Figure 2.5 (b). In this case the angle of incidence is called $\alpha_c$, the critical angle for total internal reflection, and it is given by:

$$\sin \alpha_c = \frac{n_2}{n_1} \qquad (2.16)$$

Further increasing the angle of incidence results in total internal reflection (TIR), where "the exit" ray is completely reflected back into the higher index medium at the interface, as shown in Figure 2.5 (c). This is the mechanism by which light may be considered to propagate down an optical fibre via a series of total internal reflections at the interface between the fibre core and the cladding, which has a slightly lower refractive index.

Total internal reflection offers a sensing method called attenuated total internal reflection (ATIR). Changing the refractive index of a medium surrounding a textile fibre, which does not have a cladding, affects the critical angle for TIR and thus the intensity of the transmitted light. This is the main sensing mechanism used in this project. At its simplest level, an oil drop deposited onto a fibre from the aqueous phase opens up an "optical window" for a range of angles of light being guided down the fibre.

There is also another mechanism that causes loss of light even when the TIR condition is satisfied. Whenever light propagates through a medium an electric field will be generated. A ray of light, which is launched into the fibre, can be treated as a plane wave. When such a ray is reflected at the core-cladding interface, the field associated with the plane wave extends beyond the interface into the cladding region. The amplitude of this field in the cladding decreases exponentially with increasing the distance from the interface. Such a field is often referred to as an evanescent field [51].

If this field interacts with absorbing media, outside the fibre, attenuation of the power of the propagating field will result. If $P_0$ is the power transmitted by the fibre in the absence of an absorbing medium, e.g. fluid, then the power transmitted in the presence of the fluid is given by [52]
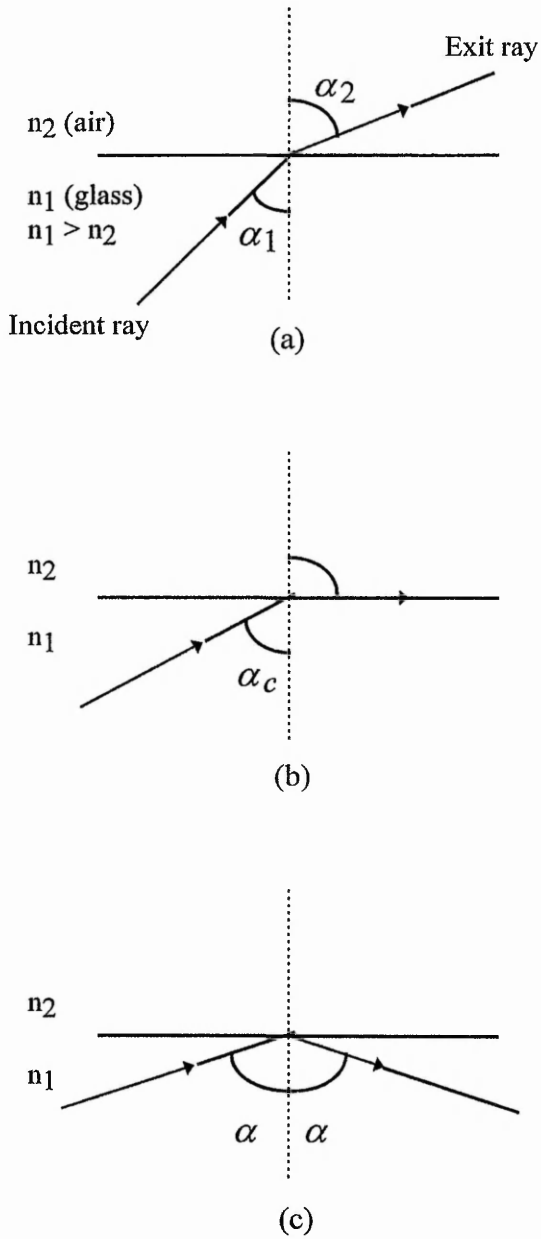
$$P = P_0 \, e^{(-\lambda L)}$$

(2.17)

Figure 2.5. The incidence of light onto an interface with different refractive indices. Illustration of the total internal reflection mechanism.

where $\lambda$ is the evanescent absorption coefficient of the fluid and $L$ is the length of the fibre exposed to the fluid, the sensing region. The amount of absorption depends on both the amplitude of the evanescent field in the absorbing medium and the number of reflections within the sensing region. Some aspects of applications arise from the evanescent field and ATIR are described below in section 2.4.

In the present work, a polymethyl methacrylate (PMMA) polymer optical fibre was used to develop and test a new experimental set-up. Previous work with a PMMA optical fibre has been published by Carroll, and thus provides a controlled test of the experimental set-up developed in this thesis [53]. The PMMA optical fibre has a core refractive index of 1.495 and a cladding of 1.402. The numerical aperture, an angle at which an optical fibre can receive (or emit) the light at the end, is 0.5 and the light acceptance angle is 60°. The polymer fibre chosen has a better light transmittance in the visible region and is more cost-effective compared to glass optical fibre.

## 2.3.2 Textile fibres

For studying the detergency process textile fibres have to be used in the investigation rather than optical fibres to give more relevance to the study. Textile fibres are not made for light-guiding and, therefore, have a much higher light attenuation coefficient which makes the technique more complicated. Another problem is that textile fibres in clothing have very small diameters, typically 10-20 $\mu$m. The fabric fibres use in the investigation were Tencel with a diameter of 57 $\mu$m and polyester with 800 and 80 $\mu$m. Although, some minor damage of the surface of the polyester fibre could be seen it can be considered to have very smooth surface finish, as the pictures in Figure 2.6 suggest.

Polyester (poly-ethylene terephthalate, PET) is probably the most important single synthetic fibre in the textile industry at the present time. PET is generally made by reacting either terephthalic acid or dimethyl terephthalate with ethylene glycol.

Commercial polyester fibres are normally semicrystalline and may be represented as consisting of a spectrum of regions ranging from highly crystalline to virtually non-crystalline. The dimensions and degree of order of these regions depend upon the processing history of the fibre [55]. Polyester is highly oriented, but the orientation is not uniform and differs between the more and less crystalline regions. Due to the semicrystallinity, polyester is optically anisotropic and has two refractive indices, one perpendicular to the fibre axis and one parallel to it. The difference between the two refractive indices is called the birefringence. The higher the spinning speed during the production process of the fibre the larger the birefringence, therefore, its crystallinity is low but it is highly oriented. Hence, birefringence is a useful measure of orientation of the fibre. Table 2.3 gives some typical value of refractive indices for textile fibres.

| Fibre | n‖ | n⊥ | Birefringence |
|---|---|---|---|
| Cellulose | 1.469 | 1.469 | 0 |
| Cotton | 1.577 | 1.529 | 0.048 |
| Polyester | 1.706 | 1.546 | 0.160 |

Table 2.3. Refractive indices of textile fibres [54].

Tencel (or Lyocel) was the third fibre chosen. The fibre was developed by Acordis plc. (Courtaulds) around 1990, it is still quite new on the market and therefore, no physical properties of the fibre could be found in the literature. It is produced from natural cellulose derived from wood pulp using a solvent-spinning process [56]. This fibre combines all the good characteristics of natural and synthetic fibres. Tencel has a high wet modulus that leads to low shrinkage in water, thus it is very stable in washing and dyeing, and it is also thermally stable. In industrial detergency research, it is regarded as a model for examining the detergency process with cotton.
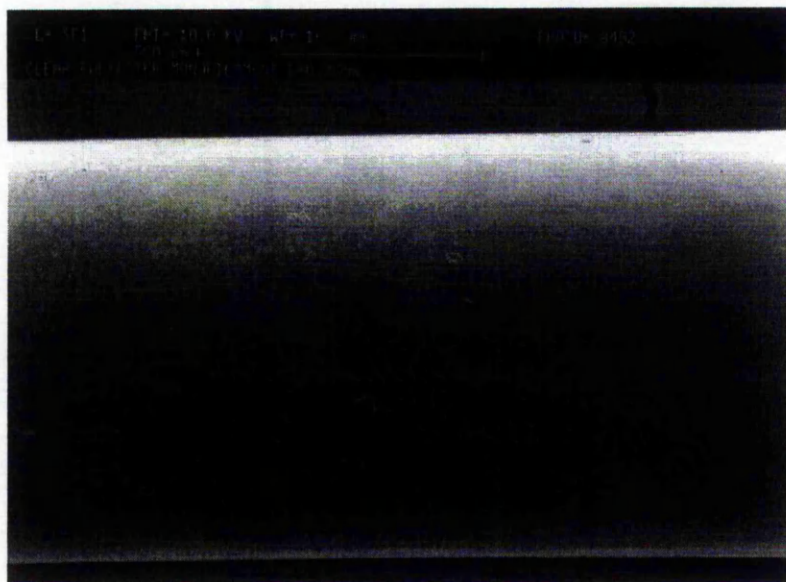
(a)
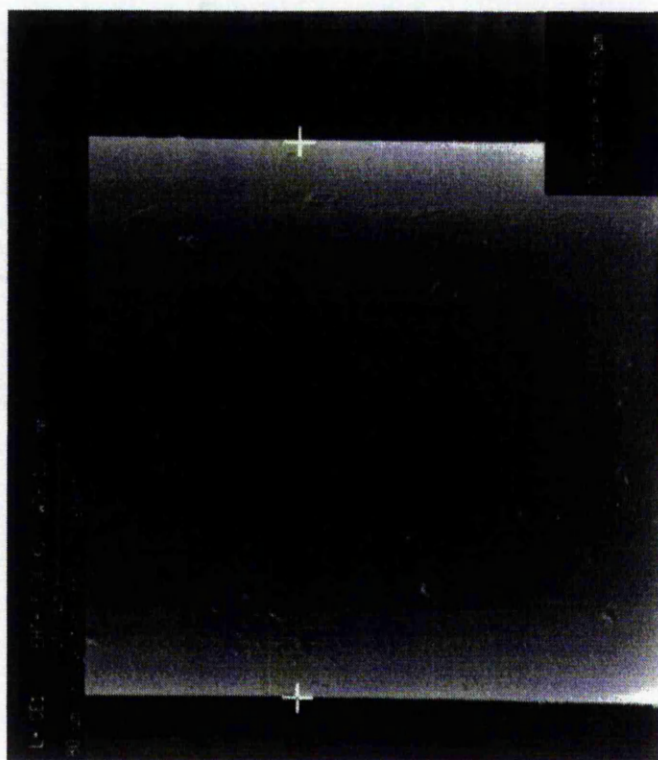


(b)

Figure 2.6. SEM pictures of polyester fibres. (a) 800 μm, (b) 80 μm polyester fibre (with permission of Unilever plc.). Similar pictures can be found in ref. [54] for other textile fibres.

Figure 2.7. SEM pictures of 250 μm PMMA optical fibre (with permission of Unilever plc.).

Figure 2.8. SEM picture of a cross-section of cotton, U-shape (with permission of Unilever plc.).

The reason why Tencel and not cotton, probably the most widely used fabric fibre, has been chosen is that cotton is not suitable for light-guiding at all, as Figure 2.8 shows. Besides its U-shape, which makes liquid drops elongate more than a circular shape, cotton consists of a network of microfibrils which are randomly organised within the inner body of the fibre [55].
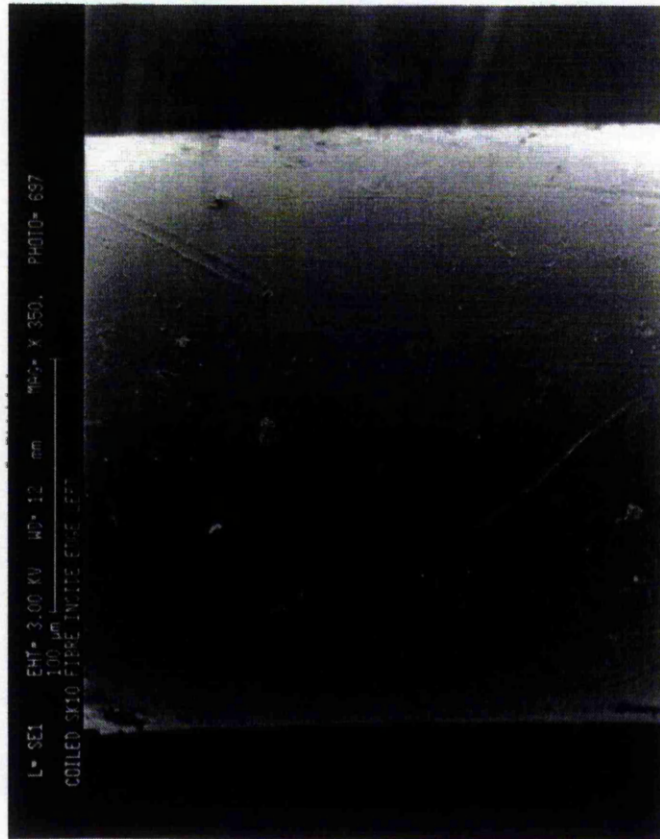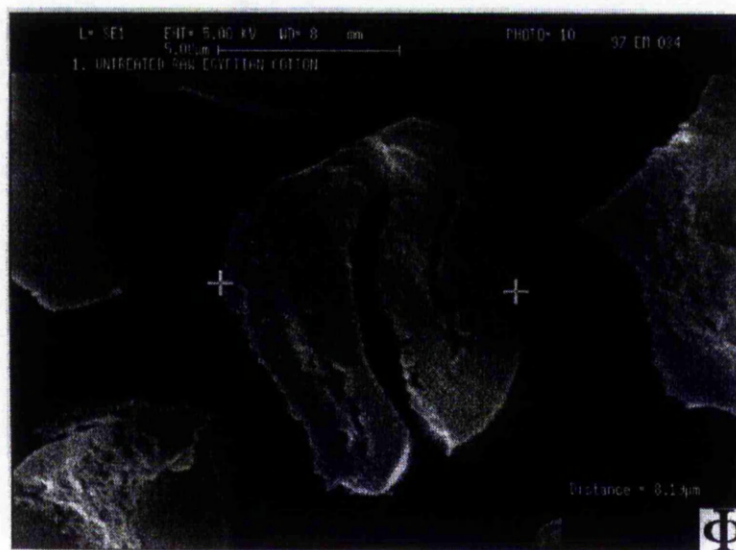
## 2.4 Optical fibre sensing

In recent years there has been remarkable progress in the development of multimode optical fibre evanescent field absorption sensors for industrial applications because of their considerable advantages over traditional sensors [57-59]. Some of their advantages include remote and distributed sensing, on-line measurements, simple design, and low cost [60]. Therefore, there are a number of fibre optic sensors based on the evanescent wave (EW) absorption principle. Below only a few will be mentioned to represent this important optical sensing mechanism.

There are a variety of EW gas sensors which have been successfully developed to measure low concentrations of methane and other flammable gases [61-64]. These sensors show a high sensitivity towards the measurand and hence they are capable of picking up very low quantities of the gas to be measured.

EW sensors can also be used in water quality measurements. It was reported that sensors have been designed to measure hydrocarbon and ammonium ions and ammonia vapour in water, respectively [65-67]. The sensitivity of the sensor was found to be quite high, ppm range, and the response times were quite rapid, of the order of seconds. Optical pH sensors were also found to be very reliable and sensitive [68]. The pH values were obtained by large shifts in the absorption spectrum, hence giving a high sensitivity.

Other applications of EW sensors include the real-time monitoring of physical or biochemical processes. During the deposition of thin films, an optical sensor can be used to monitor the thickness of the film [69]. Not only is this novel method

relatively simple compared to existing methods, it is also very highly sensitive. Optical biosensors are capable of detecting the heart rate, blood pressure variations, breathing frequency and breathing amplitude [70,71]. These type of sensors are found to be user-friendly and they are easily portable and can thus be used at home or in hospital.

EW sensing has so far only been realised in optical fibres. Due to the exponential decay in the EW field high light intensity transmitted by the fibre is needed for the sensing mechanism. Therefore, this method is not likely to be feasible for textile-like fibres as a light guide. Another sensing mechanism in optical fibres is via attenuated total internal reflection (ATIR) which is the main measurement principle of this work. In this technique the surface of the light guiding layer is used as the sensitive interface. Therefore, in most applications the cladding of the optical fibre has to be removed to allow the core to interact with the measurand. Alternatively, one needs to find a way to launch light directly into the cladding layer, in which its intensity goes rapidly toward zero.

Betta *et al* reported an optical fibre for continuous-level sensing based on the ATIR principle [72]. It was found that a fibre with no cladding layer gave a very sensitive response towards the liquid level. However, it reached very quickly a saturation where all the light was lost. This is due to the fact that all light travelling in the core is interacting with the liquid-core interface. A critical thickness of the cladding layer was then proposed for realising a wide-range level sensor with a linear response to the height of the liquid.

Other types of ATIR sensors also exist where the light is launched directly into the cladding layer. An optical fibre sensor has been suggested which can be used to measure liquid droplet parameter, such as refractive index or droplet size [73]. A characterisation of the sensor and theoretical interpretation is also given in the same paper.

# References

[1] E.Kissa, in W.G.Cutler and E.Kissa (Eds.), *Detergency: theory and technology*, Marcel Dekker, New York, 1987

[2] R.M.A.Azzam, N.M.Bashara, *Ellipsometry and polarised light*, North Holland, Amsterdam, 1977

[3] M.Malmsten, B.Lindman, *Ellipsometry studies of cleaning of hard surfaces. relation to the spontaneous curvature of the surfactant monolayer*, Langmuir, **5**, (1989), 1105

[4] K.Backstrom, B.Lindman, S.Engstrom, *Removal of triglycerides from polymer surfaces in relation to surfactant packing. ellipsometry studies*, Langmuir, **4**, (1988), 872

[5] M.Mahe, M.Vignes-Adler, A.Rousseau, C.G.Jacquin, P.M.Adler, *Adhesion of droplets on a solid wall and detachment by a shear flow*, Journal of Colloid and Interface Science, **126**, (1988), 314

[6] M.Mahe, M.Vignes-Adler, P.M.Adler, *Adhesion of droplets on a solid wall and detachment by a shear flow*, Journal of Colloid and Interface Science, **126**, (1988), 329

[7] M.Mahe, M.Vignes-Adler, P.M.Adler, *Adhesion of droplets on a solid wall and detachment by a shear flow*, Journal of Colloid and Interface Science, **126**, (1988), 337

[8] T.Yamamoto, R.Periasamy, R.P.Donovan, D.S.Ensor, J. Adhesion Sci. Technol., **8**, (1994), 543

[9] K.H.Raney. W.J.Benton, C.A.Miller, *Optimum detergency conditions with non-ionic surfactants*, Journal of Colloid and Interface Science, **117**, (1987), 282

[10] H.Saito, K.Shinoda, Journal of Colloid and Interface Science, **32**, (1970), 647

[11] K.H.Raney, *Optimization of nonionic/anionic surfactant blends for enhanced oily soil removal*, Journal of the American Oil Chemists Society, **68**, (1991), 525

[12] K.H.Raney, H.L.Benson, *The effect of polar soil components on the phase inversion temperature and optimum detergency conditions*, Journal of the American Oil Chemists Society, **67**, (1990), 722

[13] K.H.Raney, C.A.Miller, *Optimum detergency conditions with non-ionic surfactants*, Journal of Colloid and Interface Science, **119**, (1987), 539

[14] B.A.Schott, Detergency, *Theory and Test Methods* (W.G.Cutler and R.C.Davis, Eds.), Dekker, New York, 1972

[15] A.Watanabe, M.Tagawa, *On electro-osmotic washing*, Journal of Colloid and Interface Science, **75**, (1980), 218

[16] M.Tagawa, *Removal of particles from substrates by electro-osmotic flow*, Separation and Purification Methods, **15**, (1986), 77

[17] B.J.Carroll, *Physical aspects of detergency, a review*, Colloids and Surfaces A: Physicochemical and Engineering Aspects, **74**, (1993), 131

[18] K.Gotoh, M.Iriya, A.Mitsui, M.Tagawa, *The detachment of nylon particles from quartz plate by electro-osmotic flow*, Colloid & Polymer, **261**, (1983), 805

[19] M.Tagawa, K.Gotoh, *Removal of iron (III) oxide particles from a quartz plate by liquid flow*, Colloid & Polymer Science, **264**, (1986), 1072

[20] D.A.Buttry, M.D.Ward, *Measurement of interfacial processes at electrode surfaces with the electrochemical quartz crystal microbalance*, Chem. Rev., **92**, (1992), 1355

[21] G.Sauerbrey, Z.Phys. **155**, (1959), 206

[22] F.Caruso, T.Serizawa, D.N.Furlong, Y.Okahata, *Quartz crystal microbalance and surface plasmon resonance study of surfactant adsorption onto gold and chromium oxide surfaces*, Langmuir, **11**, (1995), 1546

[23] A.Weerawardena, C.J.Drummond, F.Caruso, M.McCormick, *Real time monitoring of the detergency process by using a quartz crystal microbalance*, Langmuir, **14**, (1998), 575

[24] A.Weerawardena, B.J.Boyd, C.J.Drummond, D.N.Furlong, *Removal of a solid organic soil from a hard surface by glucose-derived surfactants: effect of surfactant chain length, headgroup polymerisation and anomeric configuration*, Colloids and Surfaces A, **169**, (2000), 317

[25] A.Busnaina, J.Taylor, I.Kashkoush, *Measurement of the adhesion and removal forces of submicrometer particles on silicon substrates*, Journal of Adhesion Science and Technology, **7**, (1993), 441

[26] S.K.Krishnan, A.A.Busnaina, D.S.Rimai, L.P.Demejo, *The adhesion-induced deformation and the removal of submicrometer particles*, Journal of Adhesion Science and Techology, **8**, (1994), 1357

[27] P.G.Saffman, J. Fluid Mech., **22**, (1965), 385

[28] J.Visser, *Measurement of the force of adhesion between submicron carbon-black particles and a cellulose film in aqueous solution*, Journal of Colloid and Interface Science, **34**, (1970), 26

[29] J.Visser, *The adhesion of colloidal polystyrene particles to cellophane as a function of pH and ionic strength*, Journal of Colloid and Interface Science, **55**, (1976), 664

[30] D.Bargeman, F.van Voorst Vader, *Effects of surfactants on contact angles at nonpolar solids*, Jornal of Colloids and Interface Science, **42**, (1973), 467

[31] D.Quere, J.M.Di Meglio, F.Brochard, *Wetting of fibre: theory and experiments*, Revue Phys. Appl., **23**, (1988), 1023

[32] P.G.de Gennes, *Wetting: statics and dynamics*, Rev. Mod. Phys., **57**, (1985), 827

[33] L.Leger, J.F.Joanny, *Liquid spreading*, Rep. Prog. Phys., **55**, (1992), 432

[34] A.W.Adamson, *Physical Chemistry of Surfaces*, Wiley, New York, (1982)

[35] D.Li, A.W.Neumann, *Contact angles on hydrophobic solid surfaces and their interpretation*, Journal of Colloid and Interface Science, **148**, (1992), 190

[36] F.Brochard, *Spreading of liquid drops on thin cylinders: the "manchon/droplet" transition*, J. Chem. Phys., **844**, (1986), 4664

[37] B.J.Carroll, *Eqilibrium conformations of liquid drops on thin cylinders under forces of capillarity. A theory for the roll-up process*, Langmuir, **2**, (1986), 248

[38] B.J.Carroll, *The accurate measurement of contact angle, phase contact areas, drop volume, and Laplace excess pressure in drop-on-fiber systems*, Journal of Colloid and Interface Science, **57**, (1976), 488

[39] N.K.Adam, J. Soc. Dyers Colour, **53**, (1937),

[40] B.J.Carroll, *The accurate measurement of contact angle, phase contact areas, drop volume, and Laplace excess pressure in drop-on-fiber systems*, Journal of

Colloid and Interface Science, **57**, (1976), 488

[41] H.D.Wagner, *Spreading of liquid droplets on cylindrical surfaces: accurate determination of contact angle*, J. Appl. Phys., **67**, (1990), 1352

[42] B.J.Carroll, *Direct measurement of the contact angle on plates and on thin fibres: some theoretical aspects*, J. Adhesion Sci. Technol., **6**, (1992), 983

[43] B.Song, A.Bismark, R.Tahhan, J.Springer, *A general drop length-height method for determination of contact angle in drop-on-fiber systems*, Journal of Colloid and Interface Science, **197**, (1998), 68

[44] G.McHale, N.A.Kab, M.I.Newton, S.M.Rowan, *Wetting of a high-energy fiber surface*, Journal of Colloid and Interface Science, **186**, (1997), 186

[45] B.J.Carroll, *The equilibrium of liquid drops on smooth and rough circular cylinders*, Journal of Colloid and Interface Science, **97**, (1984), 195

[46] V.Wolff, A.Perwuelz, A.El Achari, C.Caze, E.Calier, *Determination of surface heterogeneity by contact angle measurements on glass fibres coated with different sizings*, Journal of Material Science, **34**, (1999), 3821

[47] Y.Okamura, K.Gotoh, M.Kosaka, M.Tagawa, *Capillary wetting rates in nylon fibrous assemblies*, J. Adhesion Sci. Technol., **12**, (1998), 639

[48] A.Perwuelz, T.N.De Olivera, C.Caze, *Study of wetting at the silicone oil/water/fibre interface*, Colloids and Surfaces, **A147**, (1999), 317

[49] A.Gheniam, A.Elachari, M.Loutai, C.Caze, *Surface energy analysis of polyester fibers modified by graft fluorination*, Journal of Applied Polymer Science, **75**, (1999), 10

[50] D.Bargeman, F.van Voorst Vader, Journal of Colloids and Interface Science, **42**, (1973), 467

[51] J.M.Senior, *Optical fiber communications, principle and practice*, Prentice Hall, New York, 2nd Ed., 1992

[52] A.W.Snyder, J.D.Love, *Optical waveguide theory*, Chapman and Hall, London, 1983

[53] B.J.Carroll, *Droplet deposition effects on light transmission by an optical fibre*, Colloids and Surfaces, **58**, (1991), 303

[54] P.H.Greaves, B.P.Saville, *Microscopy of textile fibres*, BIOS Scientific Publishers Ltd, 1995

[55] M.Lewin, E.M.Pearce, *Handbook of fiber chemistry*, Marcel Dekker, 1998

[56] The Tencel inforamtion sheet, Courtaulds Fibres Ltd.

[57] P.H.Paul, G.Kychakoff, *Fibre-optic evanescent field absorption sensor*, Appl. Phys. Lett., **51**, (1987), 12

[58] S.Simhony, I.Schnitzer, A.Katzir, E.M.Kosower, *Evanescent wave fibre optic chemical sensor*, Proc. SPIE, (1987), 798

[59] B.D.Gupta, C.D.Singh, *Fibre-optic evanescent field absorption sensor: a theoretical evalutaion*, Fibre Integrated Opt., **13**, (1994), 433

[60] B.D.Gupta, S.K.Khijawania, *Experimental studies on the response of the fibre optic evanescent field absorption sensor*, Fibre Integrated Opt., **17**, (1998), 63

[61] B.Culshaw, G.Stewart, F.Dong, C.Tandy, D.Moodie, *Fibre optic techniques for remote spectroscopic methane detection-from concept to system realisation*, Sensors and Actuators, **B51**, (1998), 25

[62] G.Stewart, C.Tandy, D.Moodie, M.A.Morante, F.Dong, *Design of a fibre optic*

*multi-point sensor for gas detection*, Sensors and Actuators, **B51**, (1998), 227

[63] H.Tai, H.Tanaka, T.Yoshino, *Fibre-optic evanescent-wave methane-gas sensor using optical absorption for the 3.392-$\mu$m line of a He-Ne laser*, Optics Letters, **12**, (1987), 437

[64] F.Farahi, P.Akhavan Leilabady, J.D.C.Jones, D.A.Jackson, *Optical-fibre flammable gas sensor*, J. Phys. E., **20**, (1987), 435

[65] P.Tobiska, M.Chomat, V.Matejec, D.Berkova, I.Huettel, *Investigation of fiber-optic evanescent-wave sensors for detection of liquid hydrocarbons*, Sensors and Actuators, **B51**, (1998), 152

[66] R.A.Potyrailo, G.M.Hieftje, *Distributed fiber-optic chemical sensor with chemically modified plastic cladding*, Applied Spectroscopy, **52**, (1998), 1092

[67] C.Malins, M.Landl, P.Simon, B.D.MacCraith, *Fibre optic ammonia sensing employing novel near infrared dyes*, Sensors and Actuators, **B51**, (1998), 359

[68] C.Egami, K.Takeda, M.Isai, M.Ogita, *Evanescent-wave spectroscopic fibre optic pH sensor*, Optics Communications, **122**, (1996), 122

[69] D.Jose, M.Shelly John, P.Radhakrishnan, V.P.N.Nampoori, C.P.G.Vallaban, *An optical fibre based evanescent wave sensor to monitor the deposition rate of thin films*, Thin Solid Films, **325**, (1998), 264

[70] C.Gagnadre, M.Billon, S.Thuillier, *Fibre optic sensor for physiological parameters*, Electronics Letters, **34**, (1998), 1991

[71] I.B.Bakaltcheva, L.C.Shriver-Lake, F.S.Ligler, *A fiber optic biosensor for multianalyte detection: importance of preventing fluorophore aggregation*, Senosors and Actuators, **B51**, (1998), 46

[72] G.Betta, L.Ippolito, A.Pietrosanto, A.Scaglione, *An optical fiber-based technique for continuous-level sensing*, IEEE Transaction on Instrumentation and Measurement, **44**, (1995), 686

[73] A.K.Das, A.K.Mandal, S.Banerjee, *Measurement of liquid droplet parameters using optical fiber*, Journal of Lightwave Technology, **8**, (1990), 514

# Chapter 3: Theoretical Background

In this chapter an overview of the theoretical background is given. This section starts with a summary of the theory of detergency which forms the background of this study. Due to the complexity of the detergent process this discussion is limited to a simple view of the processes involved, whilst still providing a representative picture of the nature of detergency. The light-guiding in fibres forms a considerable part of the chapter as it represents the sensing principle. A general description of the light guiding effect will be given before a model developed to explain the experimental results is presented. A short introduction into the deposition of particles via evaporation of suspension drops is laid out to help in characterising the outcome of the investigation which will be presented in Chapter 6. Finally, a short treatment of the theory which lies behind the quartz crystal microbalance will be given, which has also been used as a sensing method complementary to the light transmission technique.

## 3.1 Theory of detergency

The removal of soil from surfaces can be achieved in several different ways. Detergency employs the use of surfactants to achieve the removal due to surface chemical effects. One can also obtain the same goal by using physical methods, i.e. mechanical abrasion, and finally by chemical processes [1]. This study is concentrating on the detergency process which is a versatile and cost-effective way for removal of dirt from surfaces. However, the removal of soil is not achieved only by surface chemical processes alone, but also involves mechanical action. Detergency is a complex process involving interactions among aqueous detergent solutions, soils, and fabrics surfaces [2]. The behaviour of particle suspension and emulsion is also governed by the interaction at interfaces. Therefore, it is helpful to consider some principles of surface chemistry in aqueous systems before discussing detergency.

### 3.1.1 Colloid and surface chemistry

There is an intermediate class of materials lying between bulk and molecularly dispersed systems in chemistry. They consist of a dispersed phase or discontinuous phase distributed uniformly in a finely divided state in a dispersion medium or continuous phase. Such systems are termed colloids and they have special properties which are of interest. Examples of colloids may be milk, paints, slurries and many others. In such systems the interfacial interactions between the two phases have a significant contribution to their properties. In the following the interactions at the interfaces will be described using standard terms of surface chemistry.

### 3.1.1.1 Surface tension and surface energy

When a surfactant is added to water the surface tension of the latter will be lowered. Hence the name surfactant or surface active agent. In fact, it is exactly this property which enables them to remove soil from surfaces. The surface energy $W$ is the work necessary to split the column as illustrated in Figure 3.1(a), (b), of a material to form two surfaces of an area $A$; at infinite separation.

$$W = 2\gamma A \tag{3.1}$$

where $\gamma$ is the surface tension.

If one follows this idea further and replaces the bottom half of the column with a different material as seen in Figure 3.1(c), the interfacial tension replaces the surface tension since an interface is created. The work necessary to split the column would then be, where A is set to 1,

$$W = \gamma_a + \gamma_b - \gamma_{ab} \tag{3.2}$$

where $\gamma_{ab}$ is the interfacial tension of material $a$ and $b$ in contact. Material $a$ and $b$ can be of different phases (gas/liquid/solid). The notation of the interfacial tension will be very helpful for the following discussion.

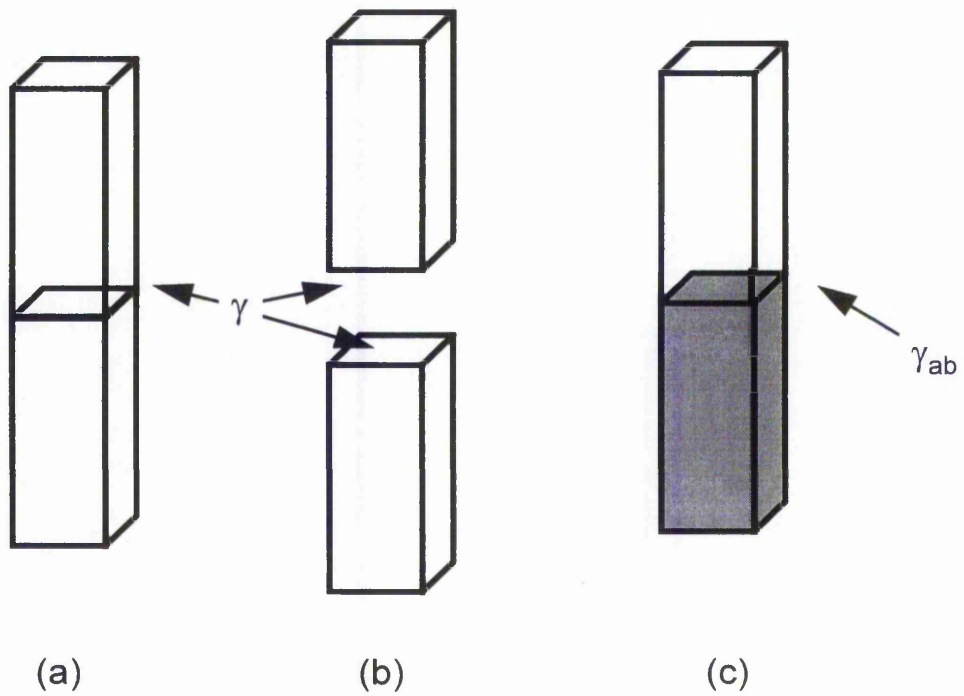(a)                      (b)                      (c)

Figure 3.1. The surface and interfacial tension.

### 3.1.1.2 Surfactants

Surfactants are molecules which have the ability to lower the surface tensions of liquids. They have a unique property which is called amphipathy, which means that the molecules consist of two parts, namely a hydrophilic (water-like) group and a hydrophobic (oil-like) hydrocarbon group. This dual character enables the surfactant molecules to adsorb themselves at the interface of liquids, so that either the hydrophilic or the hydrophobic part of the molecule, dependent on the liquid, orients out of or into the liquid. A uniformly arranged pattern will result which lowers the interaction at the liquid interface giving the liquid a lower interfacial tension.

### 3.1.1.3 Micelles

Surfactant solutions show an interesting behaviour with increasing surfactant concentration. There is a concentration where sharp changes in physical properties, such as surface tension, occur. At this concentration the surfactant molecules aggregate together to form micelles. The concentration at which this occurs is called the critical micelle concentration (CMC). Several structures of micelles can be observed and only two are shown in Figure 3.2.

In aqueous solutions the core of micelles show hydrophobic properties, therefore, they are able to take up substantial quantities of non-polar organic (lipophilic) substances. Micelles are hence very important in detergency because of their ability to solubilise oily soil.

### 3.1.1.4 Emulsion

Emulsions are metastable colloids made out of two immiscible fluids, one being dispersed in the other, in the presence of surfactants [3]. They can be produced by shearing immiscible fluids, which leads to the fragmentation of one phase into the other. According to their droplet volume fraction, which may vary from almost zero to almost one, their properties differ drastically. While diluted emulsions tend to show Newtonian behaviour, more concentrated emulsions act more like viscoelastic solids. The two most common types of emulsion are the direct

emulsion, oil drops dispersed in water (O/W), and the inverse emulsion, water drops dispersed in oil (W/O).

There are two mechanisms which contribute to the destruction of emulsions. Ostwald ripening is due to diffusion of the dispersed phase through the continuous phase. The diffusion leads to a continuous exchange of matter through the continuous phase which increases the average drop diameter whilst reducing their number and eventually to the destruction of the dispersed system and two macroscopic immiscible phases will form. The second mechanism is called coalescence, which is caused by rupture in the thin film forming between two adjacent droplets, leading finally to the fusion of the adjacent droplets. The stability of emulsion varies dependent on the two phases involved, however, it can be increased by adding surfactants which adsorb themselves at the interfaces and therefore, act as stabilisers.

### 3.1.1.5 Particle suspensions

These are stable or metastable dispersions of solids in a liquid, where the stability is obtained by interparticle and intermolecular forces. An understanding of the stability of particle suspensions can be found within the Derjaguin-Landau-Verwey-Overbeek (DLVO) theory. A short description of the relevant ideas will be given in section 3.1.2.3. There are two types of particle suspension. One that contains particles with a variety of sizes and it is called a polydisperse suspension. A monodisperse particle suspension is one, where the particles are roughly the same size.
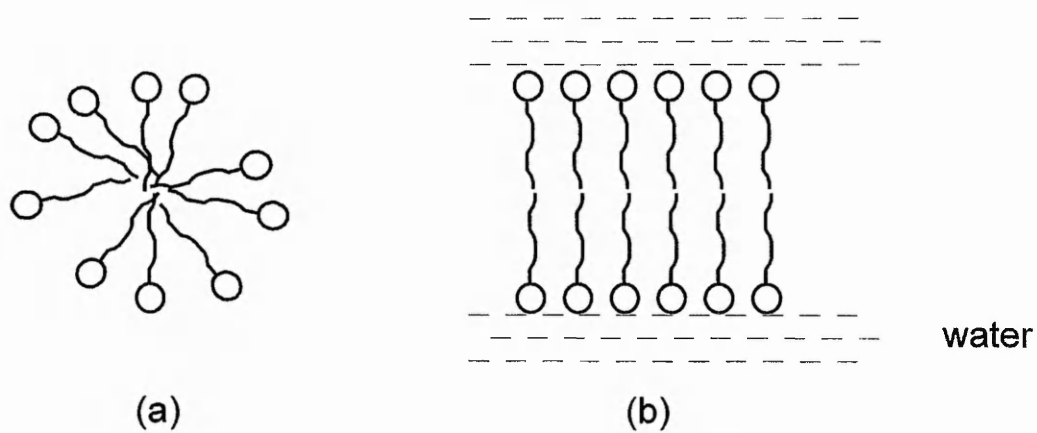
Figure 3.2. Schematic representation of micelles. (a) spherical micelle, and (b) lamellar micelle.

### 3.1.2 Adhesion and removal of soil

The adhesion and removal of soil are considered as two views of one phenomenon. Soil adhesion can be characterised by studying the force necessary to remove them from a substrate. Equivalently, the force necessary for removal can also be investigated by determining the strength of adhesion between soil and substrate. In the following pages a brief description of the adhesion and removal of oily and particulate soil is given.

### 3.1.2.1 Adhesion of oily soil on fibres

Removal of soil from surfaces requires a way to be found to overcome the adhesion forces involved in binding the dirt onto the surface. Hence, it is logical to start with an investigation of the detergency process with the forces acting on the interfaces when they approach each other.

The main oily soiling mechanism of a fabric is via capillary sorption, which is always present when a fabric is in contact with a liquid. However, when dealing with single fibres sorption can be eliminated. Therefore, a simplified soiling procedure without any sorption will be presented below. The adhesion of oily soil on surfaces can be described using the fundamental wetting properties described in Chapter 2. The deposition of a droplet of oily soil on a surface, Figure 3.3, involves a change in the surface free energy as a result of changing the area in the three interfaces. The change in total interfacial free energy $\Delta W_{adh.}$ is given by:

$$\Delta W_{adh.} = \left(A_d - A_{ow}\right)\gamma_{ow} + A_{os}\left(\gamma_{sw} - \gamma_{os}\right) \tag{3.3}$$

where $A_d$ is the droplet surface area, and the subscripts $w$, $o$, and $s$ denote aqueous, oil, and solid phase, respectively.

Using Young's equation from Chapter 2, the expression can be simplified to

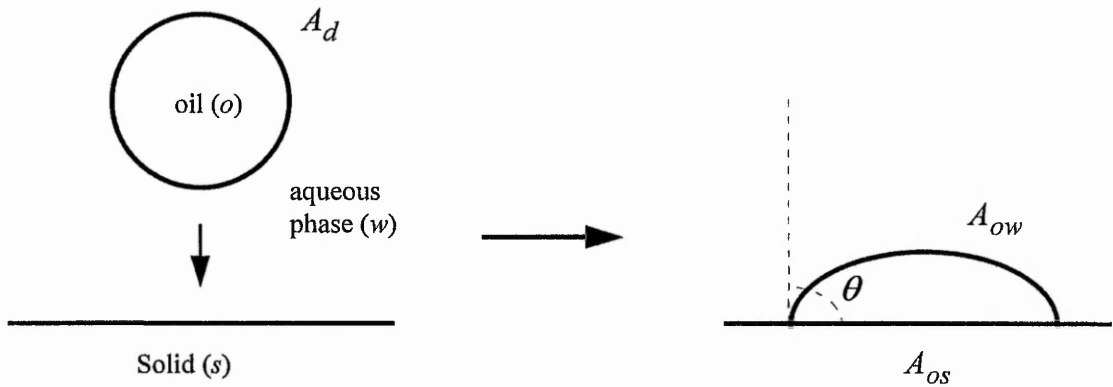$$\Delta W_{adh.} = \gamma_{ow}\left(A_d - A_{ow} + A_{os}\cos\theta\right) \tag{3.4}$$

Figure 3.3. The adhesion (or removal) of a drop of liquid on solid surface. The change in interfacial area, and therefore, in interfacial energy [4].
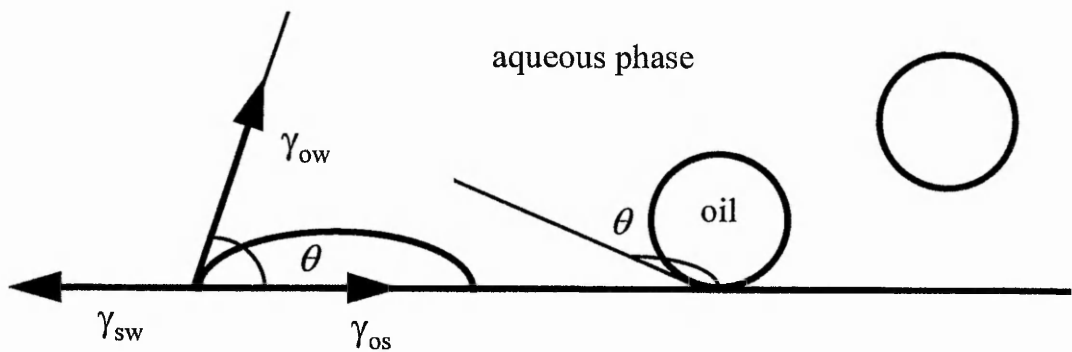


Figure 3.4. Idealised illustration of the roll-up process of a oily soil drop.

From equation (3.4) one can easily conclude that the adhesion is stronger for smaller contact angles and larger interfacial tension between oil and water $\gamma_{ow}$. Therefore, mechanisms which lower $\gamma_{ow}$ and increase $\theta$ ($\theta$ refers to the oil phase) would be beneficial for the removal process.

### 3.1.2.2 Removal of oily soil from fibres

For the removal of the oil drop from the fibre to happen spontaneously, $\Delta W_{adh.}$ in equation (3.3) has to be negative. This suggests that $\gamma_{sw}$ has to be small, $\gamma_{os}$ large, and $\gamma_{ow}$ small. Minimising the area $A_d$ would also be advantageous for the spontaneous lift off of oily soil from the surface.

In detergency, removal of oily soil normally occurs in aqueous surfactant solutions, in which the oil drop is removed wholly or in part [4]. Changing the evironment from air to water, generally lowers the adhesion energy, as can be seen in section 3.1.2.3. There are three main mechanisms for oily soil removal. The roll-up process, solubilisation and emulsification. In Figure 3.4 an illustration of an oil drop on a solid surface is given. The contact angle is given by Young's equation, eq. (3.5).

$$\gamma_{sw} = \gamma_{os} + \gamma_{ow} \cos\theta \qquad (3.5)$$

For nonpolar oil, $\gamma_{os}$ is very low, and $\gamma_{ow}$ and $\gamma_{sw}$ are often the same order, so that the contact angle $\theta$ is also very low. However, the presence of surfactants in the aqueous phase lowers the values of $\gamma_{ow}$ and $\gamma_{sw}$ [5] and if they become very low, $\theta$ can diverge and can go even above 90°. Removal of oily soil in this manner is termed as the roll-up process and is illustrated in Figure 3.4. For the roll up to occur spontaneously the resultant force $F$ of the interfacial tension has to be positive [6,7].

$$F = \gamma_{so} - \gamma_{sw} + \gamma_{ow} \cos\theta \qquad (3.6)$$

where the symbols have their usual meaning. Once the oil drop has been detached from the surface additional work is needed to remove the soil out of the vicinity of the substrate. Also other processes, like solubilisation can remove

small residual drops after the roll-up and prevent the redeposition of soil back onto the substrate.

In practice, the roll-up process is influenced by factors, such as the viscosity and buoyancy of the soil and it is considered as the main mechanism for the removal of insoluble oily soil from fibres. It will be further enhanced by a hydrophilic fibre, such as cotton, which gives rise to a lower $\gamma_{sw}$ and swelling when immersed in water.

Emulsification arises preferably in the case of hydrophobic substrates or fibre surfaces. This process can be explained that the surfactant molecules reduce the interfacial tension of the soil and water, $\gamma_{ow}$, and so allows the deformation of the soil film to form small emulsion droplets with the aqueous phase.

Finally, the combined solubilisation-emulsion process represents the dissolving of an otherwise insoluble soil by incorporating it in micelles of a surfactant solution. For micelles to exist, the critical micelle concentration (CMC) of the surfactant has to be exceeded. Therefore, this mechanism is only applicable when high surfactant concentrations are used. A five-step procedure which described the solubilisation process has been proposed by Chan *et al* and later by Schaeiwitz [8,9]:

1. A micelle diffuses to the surface of soil
2. The micelle is adsorbed at the soil/water interface
3. The soil molecules mix with the adsorbed surfactant molecules
4. The surfactant micelle is desorbed from the soil surface
5. The micelle containing solubilised soil diffuses into the bulk of the water

Solubilisation-emulsion process is considered not as the major mechanism in detergency since high concentrations of surfactant have to be used which is not always applicable and it is also slow.

### 3.1.2.3 Adhesion of particles on surfaces

The same principle of interfacial tension and surface area can be applied to the particulate case. If one considers Figure 3.5, the change in free energy $\Delta W_{adh.}$ when a particle is removed from a surface is given by:

$$\Delta W_{adh} = A_{sp}\gamma_{sp} - A_{sp}\gamma_{sw} - A_{sp}\gamma_{pw} = A_{sp}\left(\gamma_{sp} - \gamma_{sw} - \gamma_{pw}\right) \qquad (3.7)$$

where symbols have their usual meaning and the subscripts $s$, $p$, and $w$ denote the solid, particle and water phase, respectively.

However, the adhesion of particles on surfaces is more complicated than oily soil. Fortunately, due to industrial relevance and being the topic of regular research, the adhesion of particles is more fully discussed in the literature. In the following a short overview of the DLVO theory will be given, which governs the stability of colloids.

The DLVO theory postulates that the interaction between neighbouring particles can be described by three main forces: the London-van der Waals, the electrical double layer, and the Born interaction. The major contribution to the adhesion of particles on surfaces has to be the always present van der Waals force. This interaction can be described as the attraction between apolar molecules at large distances and their repulsion at contact. London managed to quantify the expressions which govern the interaction, and therefore, we should refer to the London-van der Waals interaction. The force $F_A$ of a sphere of radius $R$ acting on a flat surface at separation $H$ can be expressed as,

$$F_A = \frac{AR}{6H^2} \qquad (3.8)$$

where $A$ is the Hamaker constant of the two interacting materials [10], which can be calculated from their molecular properties. It is notable, that the Hamaker constant of a material is much smaller in water than in vacuum, hence the immersion of the soiled system in water will reduce the van der Waals attraction, in some cases considerably [11].
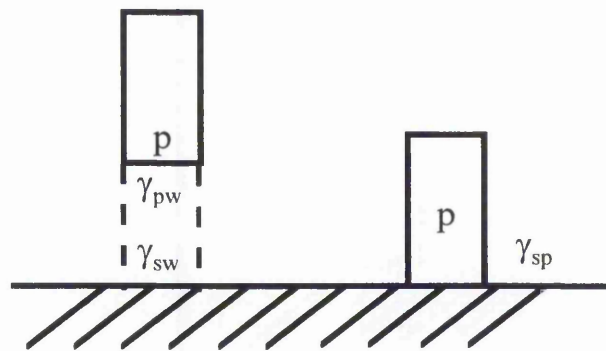
Figure 3.5. Adhesion (or removal) idealised particulate soil.
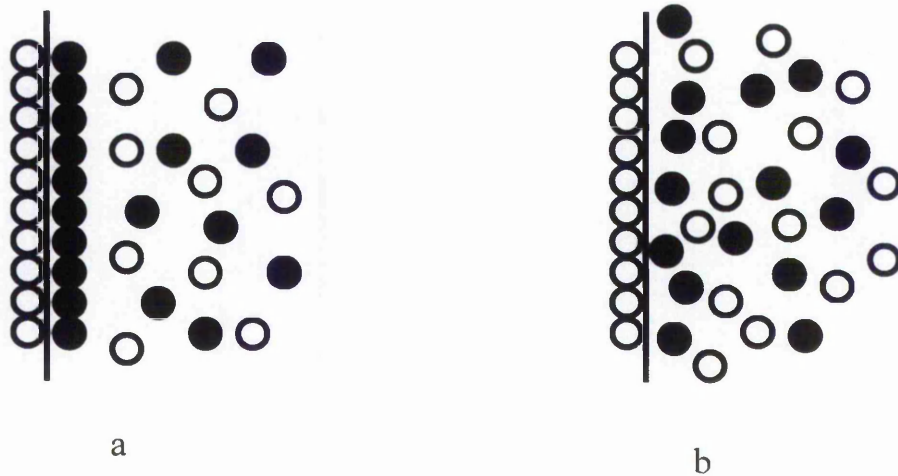


Figure 3.6. Schematic sketch of the electrical double layer, a: Helmholtz (specific adsorption) model, b: Gouy-Chapman (diffuse double layer resulting from thermal motion, no specific adsorption) model. $O$ negative, $\bullet$ positive charge.

However, the above equation is only applicable to separations of around 10 nm and less. Above the critical separation a 'retarded' form of the London-van der Waals interaction arises and the force $F_A^{'}$ between a sphere and a flat surface is

$$F_A^{'} = \frac{2\pi BR}{3H^3} \tag{3.9}$$

where $B$ is the retarded van der Waals constant. Nevertheless, since adhesion implies that the particle is in contact or at least nearly in contact with the substrate surface, e.g. fibre, only the 'unretarded' London-van der Waals interaction will be considered for further discussions.

As already mentioned in Chapter 2, the area of a particle in contact with a surface can, dependent on the material properties, deform due to the forces of adhesion. The deformation will result in an increase in contact area between the particle and the surface. Due to the increase in the actual contact area an extra term has to be included in the adhesion component of the van der Waals interaction. If the interaction force between two flat plates per unit area of surface area $P_A$ is,

$$P_A = \frac{A}{6\pi H^3} \tag{3.10}$$

then the resulting van der Waals attraction including the component due to the extended contact area of radius $z$ of the particle and the flat surface will be [11],

$$F_A = \frac{AR}{6H^2} + \frac{A}{6\pi H^3}\pi z^2 \tag{3.11}$$

In an aqueous environment another significant interaction will be present. All solids immersed in a liquid phase acquire a surface charge due to preferential adsorption of ions present in the liquid phase or due to dissociation of surface groups [11]. The corresponding surface charge is balanced by opposite charged ions and an electric double layer is so formed which ensure that the system is electrostatically neutral. This concept was introduced by Helmholtz and the electrical double layer according to this model can be seen in Figure 3.6a. Due to thermal motions of the ions the Helmholtz model will be distorted and the diffuse

electrical double layer arises which is shown in Figure 3.6b.

In the DLVO theory a full treatment of the interpenetration of the electrical double layers is given for the approach of two identical particles towards one another. Hogg *et al*, extended the theory to include the interaction of non-identical particles. The repulsive forces for a spherical particle and a flat plate according to the latter model are given in [12]. However, in this study it is sufficient to point out that the strength of the electric double layer can be influenced by electrolyte concentration, which will be used in Chapter 6.

For the sake of completeness, there is a second powerful short-range repulsive force, which prevents material in contact from penetrating each other by preventing their electron clouds from interpenetrating. This results in a minimum distance to which the materials can approach each other. The minimum distance is typically 0.4 nm and the interaction is called the Born repulsion.

An illustration of typical curves for the the London-van der Waals, electric double layer and the Born interactions is given in Figure 3.7. The resultant adhesive force of a particle on, for example a fibre is the sum of the individual interactions. A typical potential curve for the resultant force of adhesion can be seen in Figure 3.7(d).
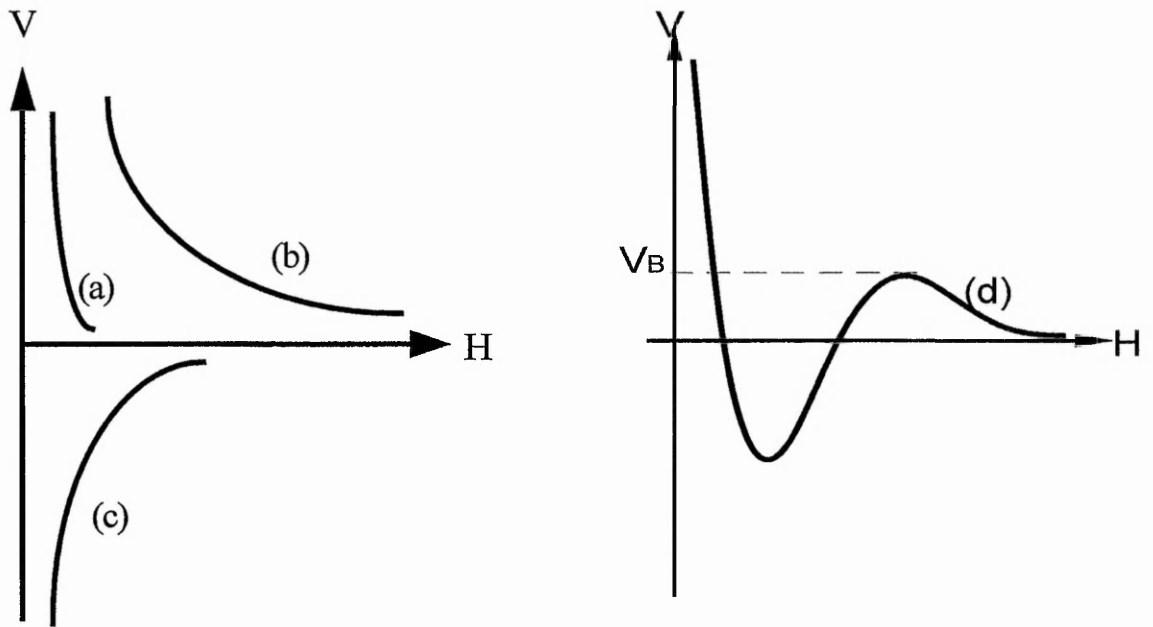
Figure 3.7. Typical potential curves for the individual interactions. (a) Born repulsion, (b) electric double layer, (c) London-van der Waals interaction, and (d) resultant curve of interaction. V is the potential and H the separation between the interacting material.
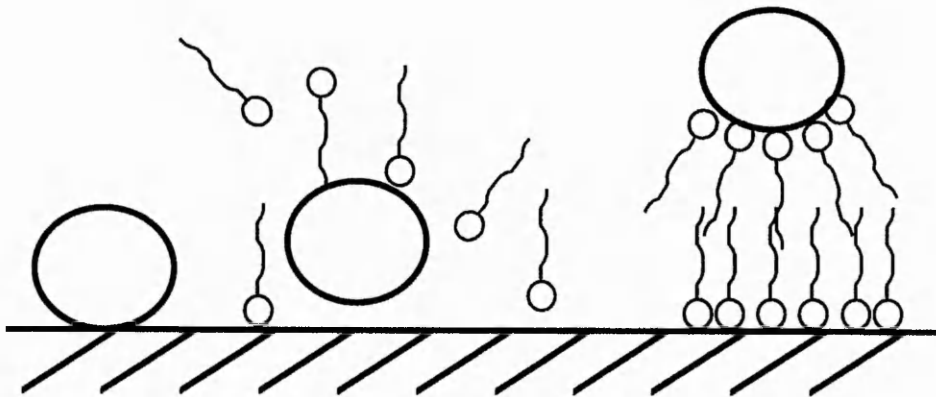


Figure 3.8. The removal of particulates. Adsorption of surfactant molecules resulted in an increase of repulsive forces

### 3.1.2.4 Removal of particles

There are many ways to achieve the removal of particles from a surface. However, all of the methods fall into two categories. The first is to reduce the adhesion force between the surfaces in contact. This can be achieved by immersion of the soiled system in an aqueous phase. As previously mentioned, the Hamaker constant will be lowered if water intervenes between the soil-substrate system, which results in a lowering of the attractive London-van der Waals force. Another possibility to reduce the adhesion is to increase the component of the repulsive electrical double layer interaction. This can be accomplished by increasing the potential of the adherents, for example by increasing the pH of the aqueous phase. In some cases this may be sufficient to cause spontaneous lift off of the particles from the surface. However, normally one needs to apply additional external force to overcome the adhesion. This, the second method, can be realised in several ways and was described in the previous chapter and can also be found in the review by Visser [11].

The removal of particulate soil in detergency is thus the combination of lowering of adhesion forces and application of external force to remove the particles. Surfactant - especially anionics and nonionics are favourable in particle removal. Due to their chemical configuration they are very efficient in giving rise to the repulsive double layer force. The surfactant molecules adsorb themselves to both the particles and the substrate surface in such a way that their hydrophilic tail orients into the aqueous solution. The adhered surfactant layer gives rise to an extra term in the repulsive double layer interaction. Combined with the hydrodynamic flow the particles can be lifted off from the fabric and eventually removed as illustrated in Figure 3.8.

A quantitative description of the removal of particulates from surfaces was given by Lange [13]. According to that investigation the removal process can be divided into two steps. Step 1 represents the penetration of the aqueous phase between the soil and the substrate surface via capillary forces. This causes a displacement of the particle from the surface allowing surfactant molecules to

adsorb themselves at the particle and substrate surfaces, resulting in a larger displacement of the soil from the substrate. At this distance, where the interaction of soil and substrate is insignificant, it can be easily removed by external forces, which constitute step 2.

It is known that in most cases soil removal is seldom complete. The rate of soil removal often decreases the longer the wash cycle lasts. Additionally, the problem of redeposition of already removed dirt back onto the fibre surfaces increases with increase in washing time. Redeposition can be observed as greying of garments over several laundering cycles.

### 3.1.2.5 Redeposition

Redeposition is not very well understood and it is very difficult to characterise. Not only is the deposition of soil back onto the fibre dependent on the washing conditions but also on the temperature, type of detergent, soil, and finally on the textile itself. This fact makes it difficult to design suitable testing methods to help in finding a general view of the redeposition of soil. However, let us consider the theoretical aspects of the redeposition problem.

The theory for colloid stability governs the redeposition process. Redeposition normally involves already removed soil which is in the form of a dispersion for particulate soil and an emulsion for oily soil, respectively. The stability of these colloids can be found within the DLVO theory which states that the two most important interactions for stability are the attractive London-van der Waals and the repulsive double layer force. Similar to Figure 3.9 a double layer will form if a negatively charged particle or an oil drop is immersed in an aqueous phase and the charge is symmetrically distributed over the particle.
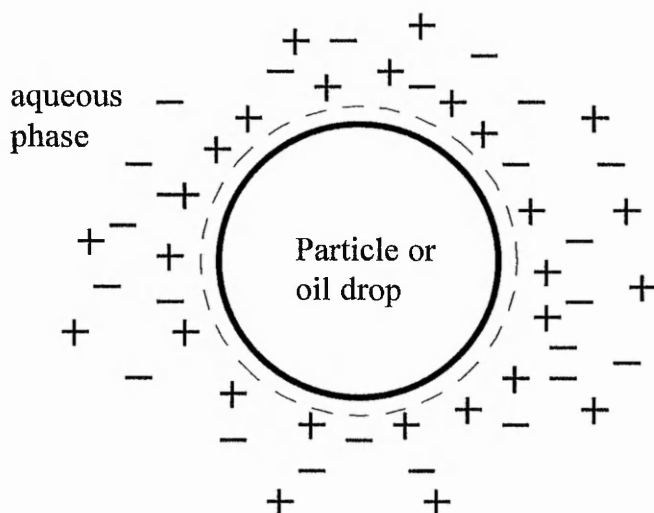
Figure 3.9. Electric double layer around an oil drop or a particle immersed in an aqueous phase.

The interactions of the double layers of neighbouring particles or drops prevents them from approaching each other. Therefore, the barrier for coalesce of emulsion drops or the flocculation of particles is set by the strength of the double layer interaction. An important quantity is the energy barrier in the total potential energy curve $V_B$, shown in Figure 3.7(d). The higher the potential barrier $V_B$ the greater the resistance to coalescence and therefore, the redeposition of soil back onto the fibres is less likely to happen.

## 3.2 Light guiding in fibres

The method developed in this thesis to investigate the detergency process is a single fibre light transmission technique, the probe being a textile like fibre which is of relevance to the detergency industry. Light guiding in the fibre is obtained via total internal reflection (TIR) with the intensity of the transmitted light depending on the refractive indices of the fibre and that of its environment.

Light transmission in this manner experiences a variety of attenuation coefficients. The first coefficient is the coupling loss which arises when light is coupled from air into the fibre. Due to the difference in the refractive indices between the fibre endface and air some of the light will be reflected back when incident on the fibre. This coupling efficiency is higher the smaller the difference of the refractive indices. Once light is within the fibre, the rays which fulfil the condition for TIR will be reflected repeatedly at the fibre wall and the efficiency of this reflection is also dependent on the refractive indices at the fibre-outer medium interface and it is called the Fresnel reflection coefficient. It has to be combined with the number of reflections needed to travel along the fibre to give the overall loss due to reflection along the fibre. Light rays that do not fulfil the condition for TIR will be lost into the surroundings of the fibre. Before the transmitted light emerges from the other end of the fibre it passes through another fibre-air interface and experiences a second coupling loss factor. For simplicity and if one only looks at the intensity of the light then it is valid to assume that the coupling loss is the same for entry and exit into and out of the fibre. Finally, however in this case a quite considerable loss coefficient is the

attenuation due to intrinsic light absorption of the textile fibre material. All these loss coefficients have to be combined to give the total transmitted light intensity of the fibre. A quantitative description of the several loss factors will be given in section 3.2.2 preceded by some general consideration of light guiding in fibres.

### 3.2.1 General parameters

In the following a closer look will be taken at the mechanism of the TIR and the light guiding will be described in terms of a model developed to discuss quantitatively the experimental results. In addition, the loss coefficients mentioned previously will be expressed quantitatively. All calculations have been implemented using Mathematica. The model is limited to meridional rays and multimode fibres.

An important characteristic of light guiding in fibres is the fibre parameter V which gives the number of modes supported by the fibre, and it is defined as,

$$V = \frac{2\pi r}{\lambda}\sqrt{n_f^2 - n_0^2} \tag{3.12}$$

where $r$ is the fibre radius and $\lambda$ the wavelength of light used. $n_f$ and $n_0$ are the refractive indices of the fibre and the surrounding medium respectively. In this case where the refractive index of polyester is 1.55 to 1.70, the fibre parameter in air is 4840 to 5618. Therefore, the assumption of a multimode fibre is satisfied. The fibre parameter for the PMMA optical fibre used in the immersion experiments was 625.

Figure 3.10 shows the light guiding for meridional rays in a straight cylindrical fibre. Meridional rays are rays which pass through the fibre axis and travel in one plane only. Below a more detailed description of the light transmission in a fibre via TIR is given.
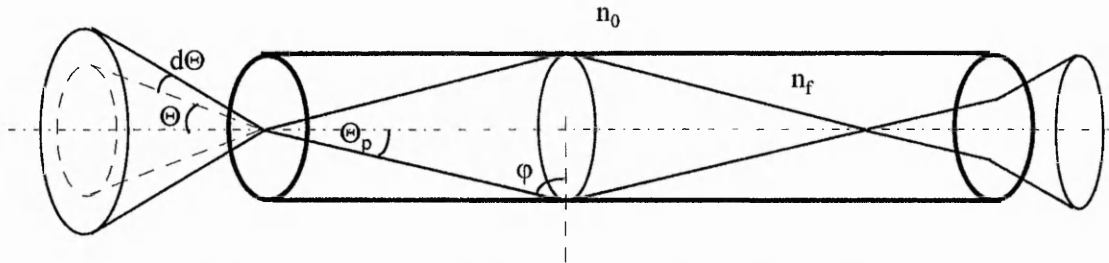
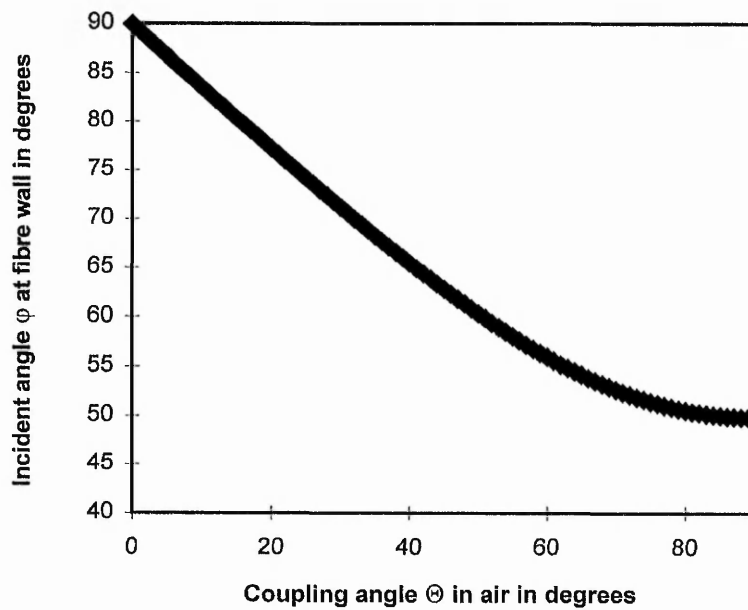Figure 3.10. Illustration of light transmission in a cylindrical straight fibre.

Figure 3.11. The relationship of the coupling angle in air $\Theta$ and the incident angle $\varphi$ within the fibre, see Figure 3.10. Note that the critical incident angle $\varphi_{crit} = 48.8°$ for fibre/air and $\varphi_{crit} = 59.0°$ for fibre/water system, respectively.

Light incident on a plane interface between two dielectric media with different refractive indices, such as fibre-air interface, can be reflected back into the originating medium. This fact is governed by Snell's law which says that light incident at angles greater than the critical angle $\varphi_{crit}$ will undergo total internal reflection, where $\varphi_{crit}$ is defined as follows,

$$\sin\varphi_{crit} = \frac{n_0}{n_f} ; \qquad\qquad \text{with } n_f > n_0 \qquad\qquad (3.13)$$

This means that if $\varphi > \varphi_{crit}$ the light rays will be trapped within the fibre and transmitted as seen in Figure 3.10. An important quantity in light guiding in fibre is the acceptance angle or the numerical aperture ($NA$). The acceptance angle represents the maximum cone angle of light rays in air that will be totally internally reflected once entering the fibre. Light rays which strike the fibre entrance with a higher angle will be refracted out of the fibre because the condition for TIR will not be fulfilled. The numerical aperture and the acceptance angle in air ($n_{air}$= 1) are defined as,

$$NA = n\sin\Theta_{accept.} = \sqrt{n_f^{\,2} - n_0^{\,2}} \qquad\qquad (3.14)$$

and

$$\Theta_{accept.} = \arcsin NA \qquad\qquad (3.15)$$

To give a quantitative idea of the coupling of light into a fibre a plot which shows the relationship between $\Theta$ and $\varphi$ is given in Figure 3.11 according to Snell's law of refraction, eq. (2.15)

Comparing the critical angle for TIR and the relationship between $\Theta$ and $\varphi$ one can claim that all light coupled into the fibre will be totally internally reflected when the fibre is in air. If the fibre is immersed in water, the critical angle for TIR moves from 48.8° to 59.0° and hence an attenuation in the transmitted intensity occurs. The next section gives a more theoretical view of this loss mechanism.

### 3.2.2 Transmission loss coefficients

The condition for TIR is dependent on the refractive indices of the media and the incident angle, according to Snell's law, equation (2.15). A more general description of the intensity of the reflected light dependent on the angle of incidence is given by the Fresnel equations of reflection according to their polarisation. For polarisation perpendicular to the plane of incidence [14],

$$R_\perp = \left[ \frac{\sqrt{(n_0 - ik)^2 - n_f^2 \sin^2 \varphi} - n_f \cos\varphi}{\sqrt{(n_0 - ik)^2 - n_f^2 \sin^2 \varphi} + n_f \cos\varphi} \right]^2 \tag{3.16}$$

and, for polarisation parallel to the plane of incidence,

$$R_\parallel = \left[ \frac{n_f \sqrt{(n_0 - ik)^2 - n_f^2 \sin^2 \varphi} - (n_0 - ik)^2 \cos\varphi}{n_f \sqrt{(n_0 - ik)^2 - n_f^2 \sin^2 \varphi} + (n_0 - ik)^2 \cos\varphi} \right]^2 \tag{3.17}$$

where $(n_0 - ik)$ is the refractive index of the outer medium with an absorption coefficient $k$, and $\varphi$ is the angle of incidence at the fibre interface.

The total reflected light coefficient is therefore:

$$R(\varphi) = \frac{1}{2}\left(R_\perp + R_\parallel\right) \tag{3.18}$$

The above equation gives the reflection coefficient for one reflection at the fibre interface. Figure 3.12 shows a typical plot of the Fresnel reflection for polyester $n_f$=1.55 and air $n$=1. Note that a more detailed description of the theory can be found in the Appendix section. In the following, several diagrams of particular relevance for interpretation of data in the results chapters, will be given.

The data in Figure 3.12 show that for low angles there is no reflectance of light at the fibre wall indicating that all light will pass through the fibre-air interface. At around 40 degrees, the reflectance increases sharply and virtually reaches 100 % efficiency. In this region the fibre wall acts as a mirror reflecting virtually all incident light; the TIR region.
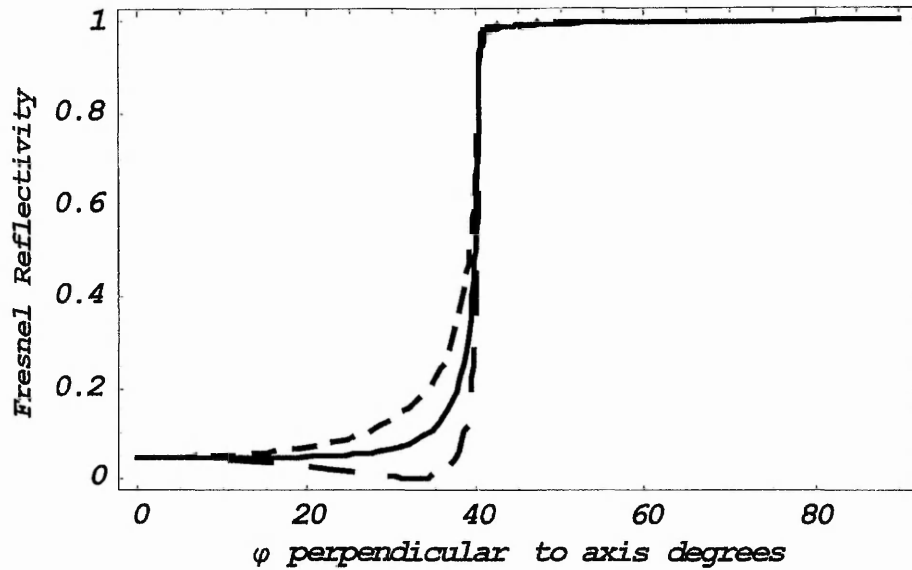
Figure 3.12 Plot of Fresnel reflectance coefficient for one reflection for the case of polyester fibre ($n_f$=1.55) and air ($n$=1). The dashed lines are the perpendicular and parallel components where the solid line is the total reflection coefficient.



Figure 3.13 Plot of reflectivity in a fibre with a refractive index of $n_f$ =1.55 immersed in liquid with refractive index of $n_o$ =1.33 (water), $n_o$ =1.4 (oil), (and for comparison, $n_o$ =1.55 (particles)) from left to right.

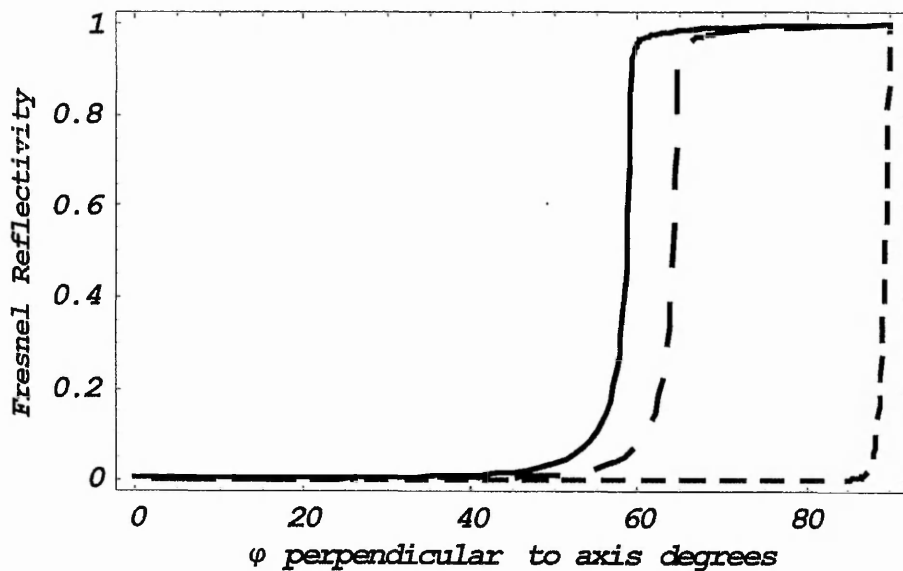In Chapter 5 experiments will be performed where the fibre is immersed in liquids with a range of refractive indices. The relationship of the reflection coefficient and the incident angle $\varphi$ can be illustrated which can be used to interpret the results. To model the immersion of the fibre, the air surrounding the fibre is replaced by liquids with a range of refractive indices. The immersion of a fibre of the refractive index of $n_f$ in a liquid of a refractive index of $n_o$ can be visualised below, where a fibre with a refractive index $n_f$=1.55 is immersed in a liquid with a refractive index of $n_o$, for a single reflection.

Figure 3.13 illustrates that the cone angle for total internal reflection is highly sensitive to the refractive index of the surrounding medium, for any one reflection. Moreover, even light rays that satisfy the condition for TIR are not all reflected with 100% efficiency.

Thus, since the total internal reflected rays experience the reflectance coefficient every time they strike the fibre wall one has to consider the total number of reflections within the fibre to obtain a realistic model of light transmission. From Figure 3.10 it can be shown that the number of reflections per unit length of fibre is given by,

$$\eta_{pul} = \frac{\tan\Theta_p}{d}$$  (3.19)

and the total number of reflections is then,

$$\eta = L * \eta_{pul}$$  (3.20)

where $L$, and $d$ are the fibre length and diameter, respectively. The transmittance coefficient combined with the number of reflections is therefore,

$$T_{refl} = R(\varphi)^{\eta}$$  (3.21)

Below a plot for the Fresnel reflection coefficient combined with the number of reflections necessary to travel along the fibre, equation (3.24), is shown for the system defined in Figure 3.13. In Figure 3.14, the x-axis angle $\Theta_{cone}$ is the ray's angle to the axis prior to entering the fibre from air (see Figure 3.10).
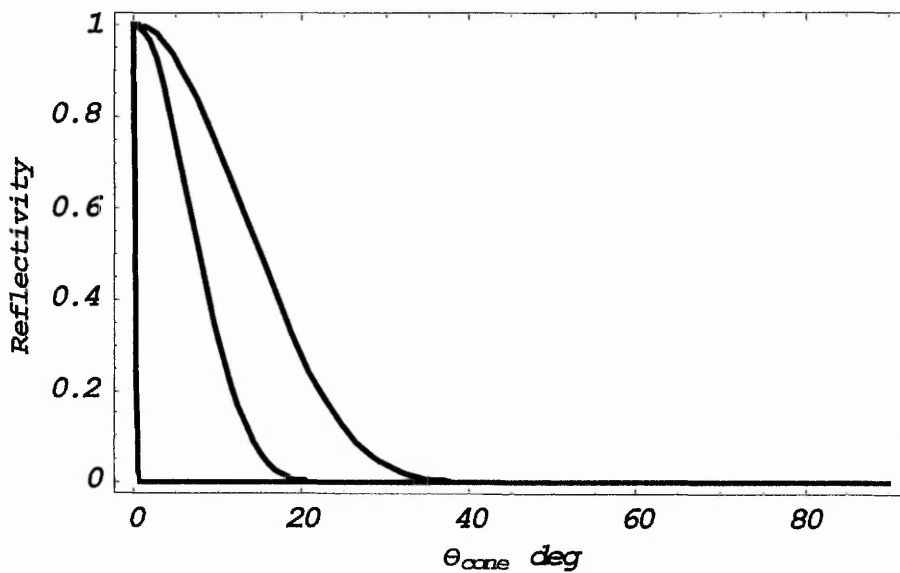
Figure 3.14 Fresnel reflection coefficient combined with the number of reflections needed to cover the length of the fibre. Plot for a range of refractive indices, from left to right, $n_O$ =1.55 (particles), $n_O$ =1.4 (oil), and $n_O$ =1.33 (water), fibre length was 10cm.

Figure 3.14 illustrates that the cone angle of light which will undergo TIR in air prior to coupling into the fibre is strongly related to the refractive index of the medium around the fibre. Furthermore, once the refractive index of the surrounding medium is equal to that of the fibre, no light will be guided via TIR. Only light launched at $\Theta_{cone} = 0°$, parallel to the fibre axis, will emerge from the opposite end of the fibre.

The equations of reflection above strictly only apply for the reflections at the fibre-air or fibre-outer medium interface. However, with a slight modification in changing the refractive index $n_f$ to that of air ($n_{air}$ =1), one can obtain the loss due to coupling of light into the fibre entrance from air. One has also to consider the coupling of light out of the fibre at the other end, therefore the transmission coefficient due to coupling is according to,

$$T_{ends} = \left[1 - R_{entry}\left(n_{air}, n_f, \varphi\right)\right] \times \left[1 - R_{exit}\left(n_f, n_{air}, \varphi'\right)\right] \qquad (3.22)$$

However, the equation can be simplified to,

$$T_{ends} = \left[1 - R_{entry}\left(n_{air}, n_f, \varphi\right)\right]^2 \qquad (3.23)$$

An additional effect of the transition of light from air into the fibre medium is the refraction. The cone angle $\Theta$ of the incident light will therefore change according to equation (3.24) at the entry of the fibre, see Figure 3.10.

$$\Theta_p = \arcsin\left(\frac{n_0}{n_f}\sin\Theta\right) \qquad (3.24)$$

Of course one should also consider the material absorption coefficient $\alpha$ in this model. The intrinsic absorption coefficient in optical fibres is very small. However, in this case where textile-like fibres are used they can be considerably higher dependent on the material absorption spectrum and the light used. The loss due to material absorption is defined as

$$e^{-\alpha L_{optical}} \qquad (3.25)$$

where $L_{optical}$ is the optical path in the fibre and it is given by

$$L_{optical} = \frac{L}{\cos\Theta_p} \qquad (3.26)$$

To obtain the overall transmission of light travelling through the fibre all partial transmission coefficients have to combined and this is shown below in equation (3.27). After transforming all attenuation coefficients to cone angle $\Theta$ of light incident on the fibre entrance.

$$T_{total} = 2\pi K \int_0^{\Theta_{cone}} F(\Theta)[1-R(\Theta)]^2 [R(\Theta)]^{\eta(\Theta)} e^{-\alpha L_{optical}(\Theta)} \sin\Theta \, d\Theta \qquad (3.27)$$

where the $2\pi K$ is the normalisation factor, and the $F(\Theta)$ is the angular distribution of angles in the cone. For simplicity, $F(\Theta)$ was set to 1 implying a uniform distribution of all angles.

On the next few pages it will be shown how the model described above can be applied to some of the experiments carried out in this investigation. The emphasis will be on the application of the theory, therefore no parameters will be given at this stage.

### 3.2.3 Immersion of fibres

To illustrate the transmission in fibres according to equation (3.27) several diagrams will be presented. In Chapters 5 and 6 this theory will be used to interpret experiments, including the immersion of fibres in a range of liquids with different refractive indices. This study was to investigate the relationship between the light attenuation and the refractive index of the outer medium, $n_0$. Figure 3.15 is an example for the modelling of the immersion experiments carried out with polyester fibre of refractive index of $n_f$=1.55.
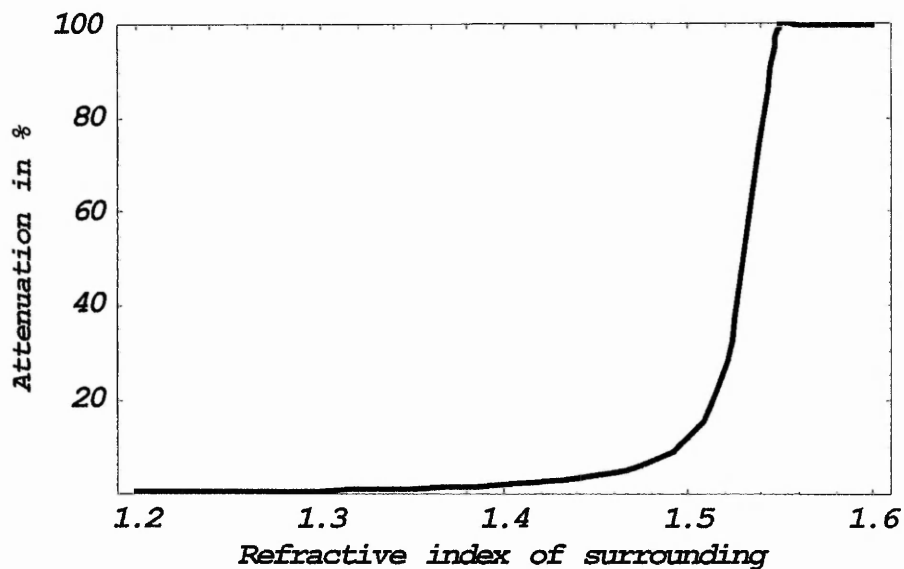
Figure 3.15. Plot of the attenuation of transmitted light in polyester fibre when the latter is immersed in liquids with a range of refractive indices.
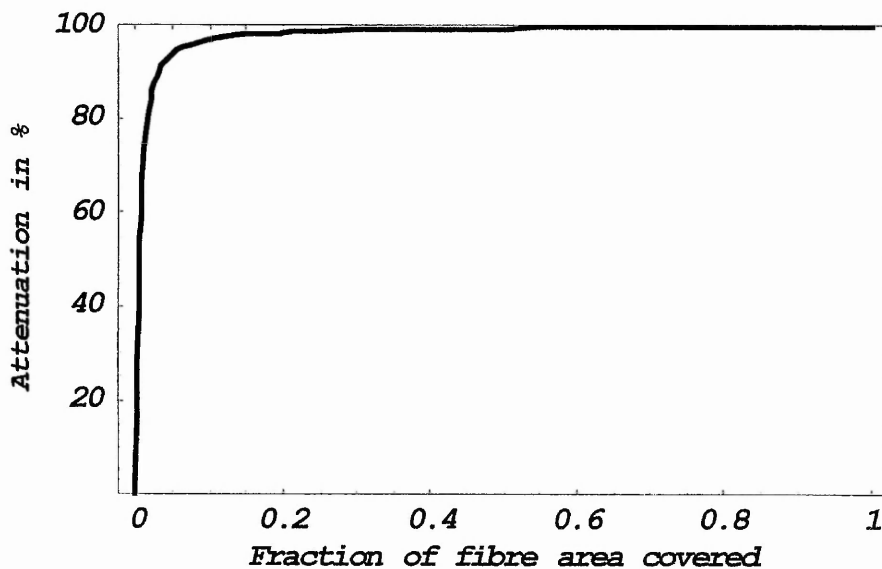


Figure 3.16 Plot of the attenuation of transmitted light vs. the area covered by latex particles. 800 μm polyester fibre

Figure 3.15 shows that as soon as the surrounding medium possesses a refractive index equal to that of the fibre $n_f$=1.55, all light will be lost. The graph was obtained by solving equation (3.27) for different $n_o$'s according to the alkanes. By looking at the transmission coefficients it becomes clear that only the Fresnel reflection coefficient changes while all others remain constant in this type of experiment. Increasing the refractive index of the outer medium decreases the cone angle for TIR, equation (3.13), and so increases the attenuation, until TIR ceases to exist when $n_0 \geq n_f$ and all light will be lost. The plot is to illustrate the problem and therefore, no parameters are given here. Fitting of the parameters will be carried out in later chapters where the experimental data and that of the theory are plotted together.

### 3.2.4 Deposition of particles

Another experiment in this thesis is the deposition of particles onto the surface of polyester fibre via the evaporation of particle suspension drops, Chapter 6. Such deposition experiments can also be modelled with the light guiding theory. Unlike the immersion experiments where the light attenuation is affected by the refractive index of each individual liquid, the particles deposition study concerns the amount of the fibre area covered by the particles and its effect on the light transmission. The latex particles used have a refractive index of $n$=1.59 and a plot of the light attenuation versus the fraction of the fibre covered is shown in Figure 3.16.

Similar to the immersion study, the only component that is affected in equation (3.27) is the Fresnel reflection coefficient, to the first approximation. Realistically, the number of the reflection would also be affected since $\varphi_{crit}$ changes and hence the optical path length. The Fresnel reflection coefficient in this case can be expressed as,

$$R = \left[ R_1\left(n_f; n_{part.}; \varphi\right)^X \times R_2\left(n_f; n_{air}; \varphi\right)^{(1-X)} \right]^{\eta} \tag{3.28}$$

where $R_1\left(n_f; n_{part.}; \varphi\right)$ and $R_2\left(n_f; n_{air}; \varphi\right)$ represents the Fresnel reflection

coefficient for fibre-particle (fraction of fibre covered by particles) and fibre-air (fraction of fibre uncovered) systems, respectively, $X$ is the fractional length or area of the fibre covered by particles, and $\eta$ is the total number of reflections within the fibre.

As expected, due to the high refractive index of the latex particles virtually all light is lost when 20 % of the fibre is covered. This shows that the particles act as very efficient windows, through which light can be leaked out of the fibre; one reason why they were chosen as a model system.

In Chapter 6 the deposition of particles is achieved by evaporation of particle suspensions. Therefore, the next section considers the processes governing the evaporation of a particle suspension on a substrate.

## 3.3 Evaporation of particle suspension

The evaporation of particle suspension drops on flat surfaces leaves a non-uniform particle pattern on the surface. This pattern can be observed, for example, with coffee stains on fabrics showing a ring-like formation. The ring-like deposit can be explained through the contact line pinning (CLP) of the suspension drop while it evaporates [15-17]. It is known that the pinning of the contact line can be caused by irregularities, such as, surface roughness or chemical heterogeneity of the surface. This will be further enhanced by the presence of particles in the evaporating drops. Deegan claims one particle is sufficient to cause contact line pinning [17]. The fact that the contact line is pinned throughout the course of the evaporation process means that there must be a continuous flow of liquid towards the contact line, as illustrated in Figure 3.17. This flow drags the suspended particles toward the contact line, thus accounting for the strong perimeter concentration of the stains, that is observed following complete evaporation.
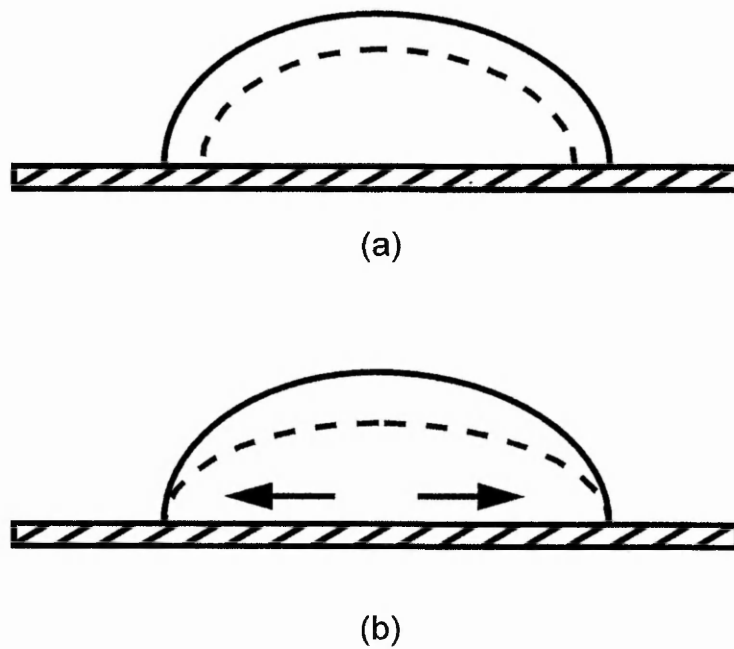
(a)

(b)

Figure 3.17. Illustration of the evaporation process. (a) contact line is not pinned, retreat of the contact line from the solid to the dash line during the evaporation; (b) contact line pinning, the drop profile moves from the solid to dash line. Therefore, an outward flow is necessary to keep the foot of the contact line pinned.

This flow causes the transport of particles from the centre to the contact line and eventually causes a ring-like deposit. Therefore, the two conditions for the ring-like formation are contact line pinning and evaporation. In fact, it was found that the evaporation of particle suspension drops when either a smooth mica surface is used or when the evaporation is limited does not give the ring like deposit [17]. A theoretical treatment of the flow profile and the rate of particle deposition can be found in the same literature.

## 3.4 Quartz crystal microbalance

The evaporation of particle suspensions was not only studied with the light transmission method but also with the quartz crystal microbalance (QCM) to offer a complementary view. Hence in the following a very brief account of the relevant basics of the QCM technique will be given.

The QCM is a very sensitive technique frequently used to detect mass deposition in the range of nanograms. Due to its high sensitivity it has been exploited extensively in research not only to detect mass deposition but also to study interactions of liquids [18,19]. In Chapter 2 it was reported that QCM has been employed to investigate the removal of soil from hard surfaces. In this thesis the technique was used to complement the light transmission method and verify the results of the latter method. The QCM comprises an AT-cut quartz crystal sandwiched between two gold electrodes that are used to provide an alternating electric field which induces shear vibration of the quartz crystal at frequencies in the megahertz region [20]. Below a short summary of the theory of the QCM method relevant to the investigation reported in this thesis is given.

### 3.4.1 Rigid mass

If a rigidly bound uniform mass layer is deposited onto the crystal surface then the downward shift in resonance frequency $f_0$ provides a direct measurement of the mass changes according to the Sauerbrey equation [21],

$$\Delta f = -\frac{2f_0^2 \Delta m}{A\sqrt{\rho_q \mu_q}} \qquad (3.29)$$

where $\Delta f$ is the measured frequency shift, $f_0$ resonance frequency of the quartz crystal, $\Delta m$ the mass change, $A$ the piezoelectrically active area defined by two gold excitation electrodes, $\rho_q$ the density of quartz (*2648 kg m$^{-3}$*), and $\mu_q$ the shear modulus (*2.947×10$^{10}$ kg m$^{-1}$ s$^{-2}$ for AT-cut quartz*) [19]. An AT-cut quartz crystal is a quartz crystal which is cut at a specified angle to the crystallographic axes so that it has small or vanishing dependence of wave velocity upon temperature [22]. Another feature of the rigid mass view is that for a uniform rigid mass layer deposited onto the crystal no absorption of the crystal energy occurs and therefore no dissipation ($\Delta D$) of the crystal energy is caused by the mass.

### 3.4.2 Newtonian liquid

Studies employing the QCM to investigate interactions with liquids show that the behaviour differs from the rigid mass case. For example, when the crystal is immersed or covered with water, a shear wave is generated by the vibration of the crystal and radiates energy into the liquid. The amplitude of the shear wave in a Newtonian liquid is described by an exponentially damped cosine function, decaying to 1/e of its original amplitude at the decay length or penetration depth $\delta$, which is given by:

$$\delta = \sqrt{\frac{\eta_L}{\pi f_0 \rho_L}} \qquad (3.30)$$

and the frequency shift experienced by the QCM upon immersion in a liquid is according to [21]:

$$\Delta f = -f_0^{3/2}\sqrt{\frac{\rho_L \eta_L}{\pi \rho_q \mu_q}} \qquad (3.31)$$

where $\eta_L$, $\rho_L$ are the viscosity and density of the liquid, respectively. The penetration depth of a 5 MHz shear wave in water is typically $\delta = 0.25$ μm. Upon immersion of the crystal in a Newtonian liquid a frequency shift according to

equation (3.31) arises as well as a dissipation of the crystal shear wave energy which is dependent on the viscosity-density product of the liquid according to [23],

$$\Delta D = 2Q_0{}^2 \sqrt{\frac{f_0 \rho_L \eta_L}{\pi \rho_q \mu_q}} \tag{3.32}$$

where $Q_0$ is the quality factor of the resonator. Note that here, the frequency shift $\Delta f$ as well as the dissipation $\Delta D$ are dependent on the square root of the viscosity-density product of the liquid

Finally, it is to be noted that the mass sensitivity is not uniform across the crystal surface. It has more of a Gaussian profile with the highest sensitivity at the centre of the crystal [24]. However, in this investigation where small droplets are deposited in the centre of the crystal the sensitivity profile is not expected to have a large effect on the results.

**References**


[1] M.F.Cox, JAOCS, **63**, (1986), 559

[2] C.A.Miller, K.H.Raney, Collois and Surfaces A, **74**, (1993), 169

[3] J.Bibette, F.Leal Calderon, P.Poulin, *Emulsions: basic principles*, Rep. Prog. Phys., **62**, (1999), 969

[4] B.J.Carroll, Colloids and Surfaces A, **74**, (1993), 131

[5] R.J.Taylor, *Theory of detergency*, A Unilever Educational Booklet, Advanced series, no.7

[6] N.K.Adam, J. Soc. Dyers Colour., **53**, (1937), 121

[7] W.Kling, Kolloid Z., **115**, (1949), 37

[8] A.F.Chan, D.F.Evans, E.L.Cussler, Amer. Ind. Chem. Eng. J., **22**, (1976), 1006

[9] J.A.Shaeiwitz, A.F.-C.Chan, E.L.Cussler, D.F.Evans, J. Colloid Interface Sci., **84**, (1981), 47

[10] H.C.Hamaker, Physica (Utrecht), **4**, (1937), 1058

[11] J.Visser, *Particle adhesion and removal: a review*, Particulate Science and Technology, **13**, (1995), 169

[12] R.Hogg, T.W.Healey, D.W.Fuerstenau, Trans. Faraday Soc., **62**, (1966), 1638

[13] H.Lange, *Solvent properties of surfactant solutions*, (K.Shinoda, Ed.), Dekker, New York, 1967

[14] N.S.Kapany, *Fiber optics, principles and applications*, Academic Press, New York, 1967

[15] R.D.Deegan, O.Bakajin, T.F.Dupont, G.Huber, S.R.Nagel, T.A.Witten, *Capillary flow as the cause of ring stains from dried liquid drops*, Nature, **389**, (1997), 827

[16] R.D.Deegan, *Pattern formation in drying drops*, Physical Review E, **61**, (2000), 475

[17] R.D.Deegan, O.Bakajin, T.F.Dupont, G.Huber, S.R.Nagel, T.A.Witten, *Contact line deposits in an evaporating drop*, Physical Review E, **62**, (2000), 756

[18] S.Bruckenstein, M.Shay, *Experimental aspects of use of the quartz crystal microbalance in solution*, Electrochimica Acta., **30**, (1985), 1295

[19] Z.Lin, R.M.Hill, H.T.Davis, M.D.Ward, *Determination of wetting velocities of surfactant superspreaders with the quartz crystal microbalance*, Langmuir, **10**, (1994), 4060

[20] M.D.Ward, D.A.Buttry, Science, **249**, (1990), 1000

[21] K.K.Kanazawa, J.G.Gordon, II. Anal. Chim. Acta., **175**, (1985), 99

[22 R.Stern, M.Levy, (Ed.), *Acoustic wave sensors, theory, design, and physio-chemical applications*, Academic Press, San Diego, 1997

[23] M.Kaspar, H.Stadler, T.Weiss, Ch.Ziegler, *Thickness shear mode resonators ("mass-sensitive devices") in bioanalysis*, Fresenius J. Anal. Chem., **366**, (2000), 602

[24] L.McKenna, M.I.Newton, G.McHale, R.Lucklum, J.Schroeder, *Compressional acoustic wave generation in microdroplets of water in contact with quartz crystal resonators*, Journal of Applied Physics, **89**, (2001), 676

# Chapter 4: Experimental Development and Apparatus

This chapter describes the development of the equipment used in this work. It was necessary to use several experimental arrangements for this investigation and all of them will be covered in this chapter. However, the light guiding apparatus will be treated in more detail presenting its chronological progress from a simple idea to fully operating experimental arrangement and its testing will be the main subject of the chapter.

The first section deals with the preliminary work in obtaining light guiding in optical and textile fibres. An inventory of requirements which the experimental arrangement has to fulfil will be given. Finally, the experimental apparatus will be presented and explained in detail. To conclude this part of the chapter preliminary experiments with their results will be presented; these will be fundamental for the interpretations later in this thesis.

The second part of the chapter describes other equipment, such as the videomicroscopy used to visualise processes which could not be captured by the light transmission technique. Besides, the video observations offer a basis for the interpretation of the light transmission signal. Finally, the quartz crystal microbalance (QCM) will be briefly outlined combined with some experiments developed to test its arrangement. In addition, some preliminary experiments to study the feasibility of the experimental arrangements will be described. These experiments were undertaken to characterise the systems and to find out their limits.

## 4.1 Light guiding experimental arrangement

The preliminary work was based on optimising the coupling of light into an optical fibre, and investigating whether it was feasible to use textile fibres instead of optical fibre for the second part of the project. Optical fibres are very efficient in guiding light, however, in this study a textile like fibre will be used as the light

guide as it is of relevance to the study to the detergency process. Textile fibres are not made for guiding light, (see Figure 2.6 and 2.8), and one would expect very high intrinsic light absorption and scattering coefficients. To illustrate this, experiments were carried out using an arrangement comprising of a 4 mW Helium-Neon (HeNe) laser with a wavelength of 633 nm, fibre optics holders and positioners, and a semiconductor optical detector. The obtained optical data for a large size (800 $\mu$m), polyester fibre is shown in Figure 4.1.

From Figure 4.1, one can estimate the attenuation caused by material absorption of the polyester fibre, which is around 49 dB/m. By comparing the data of polyester to a commercially used plastic optical fibre it is obvious to see the difficulties that arise when using textile fibres for light guiding. Not only is the light absorption coefficient of the textile material much higher than that of the optical fibres (0.2 dB/m) [1], but also the preparation of the endfaces for efficient coupling is an additional problem. In the optical fibre industry the endfaces of light guides are often nicely cleaved using a very sharp diamond cleaver or/and polished with very fine polish paper to smooth the surfaces for optimum coupling. Since textile fibres are of different material their properties, such as elasticity, are different and therefore it is very hard to obtain a nicely cleaved endface. Textile fibres are not polishable without care, the polymer molecules will be broken up in the process and the endface becomes milky thus degrading the light transmission properties. In this work non-abrasive polish papers from 3M with different grain sizes were used to polish the larger polyester fibre.
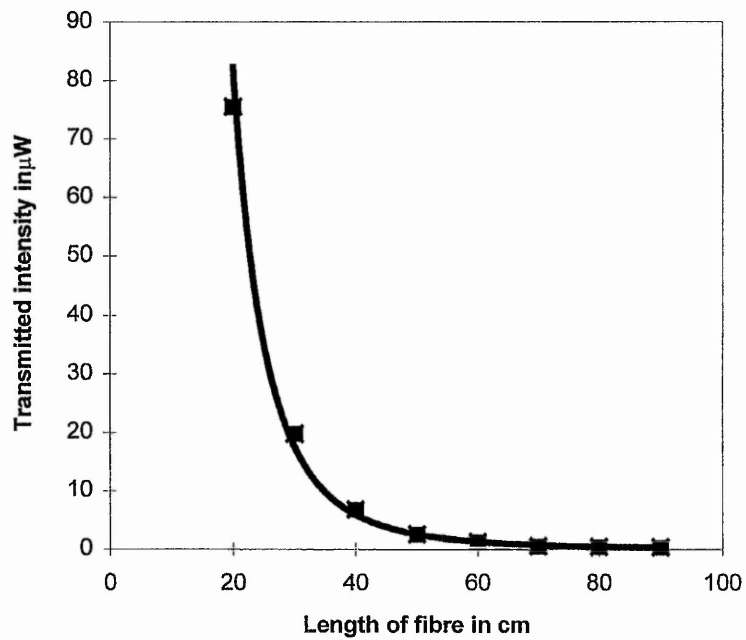
Figure 4.1. The effects of material absorption of light in relation to fibre length. Polyester fibre of 800µm in diameter.

### 4.1.1 Description of components

The possible requirement of using smaller fibres in future meant that the light coupling deserved particularly detailed considerations. Since the material absorption coefficient of polyester is quite high the length of fibre in use has to be kept as short as possible. Furthermore, it was expected that the light intensity of the output of the fibre would be very low and one might need to amplify the signal considerably. Therefore, a lock-in technique was used for the detection of the signal. Not only does the lock-in amplify the signal it is also highly effective at filtering out signal noise. In Figure 4.2 a schematic view of the basic experimental arrangement is given. A detailed description of each individual component of the arrangement is given below.

A single mode fibre coupler from Thorlabs was used as the laser diode stage, with the fibre optic translation mount removed. The laser was mounted on a manual x-y translator stage to provide precise adjustment of the focus point of the laser. In addition, the fibre coupler consisted of an optical system which was required due to the highly divergent beam of the diode laser. A collimating and a focusing lens, also from Thorlabs, were used to focus the laser beam onto the fibre end. The lenses possessed anti-reflection coatings to reduce reflection to below 1 % and their numerical apertures (NA) are 0.55 and 0.25 for the focusing and the collimating lens, respectively. A laser focus point of 20 μm could be obtained with this arrangement.

The light source was a AlGaInP index-guided laser diode with a double heterostructure. The wavelength of the light is around 670 nm and the laser provided 5 mW power in continuous wave mode, although, in this project it was used in pulse mode. A disadvantage of the laser diode was its highly divergent beam which is 10° parallel and 30° perpendicular to the beam axis. This fact made the optical fibre coupler with the combination of lenses described above necessary. However, laser diodes are widely used and they are cheaply and readily obtainable. The output of the laser diode was controlled via a laser diode controller.

A laser diode controller unit LDC 500, from Thorlabs was used to operate the laser. It is able to drive the laser diode in constant laser current or constant power mode. The maximum laser current could be set so that accidentally exceeding the current, which leads to a damage of the diode, could be avoided. In addition, the unit allowed a modulation of the laser current by an external pulse generator. Throughout this investigation the laser was set to constant current mode and it was driven by a signal generator to control the frequency of the pulsed laser output.

A pulse generator from Thurlby Thandar Instruments supplied the pulse for activating the laser. The frequency of the pulsed signal was around 500 Hz and the magnitude of the signal could be adjusted with the generator. It was set to optimise the performance of the photodiode, which has an offset in rise and fall time.

The flow cell, Figure 4.2 and Appendix 1, which is basically a glass cell of around 50 ml in volume, incorporated a jacket for thermostatting with ports for the introduction and extraction of test liquid. The cell had flanges on both ends for the introduction of the fibre. Once the fibre is mounted within, the cell becomes water-tight.
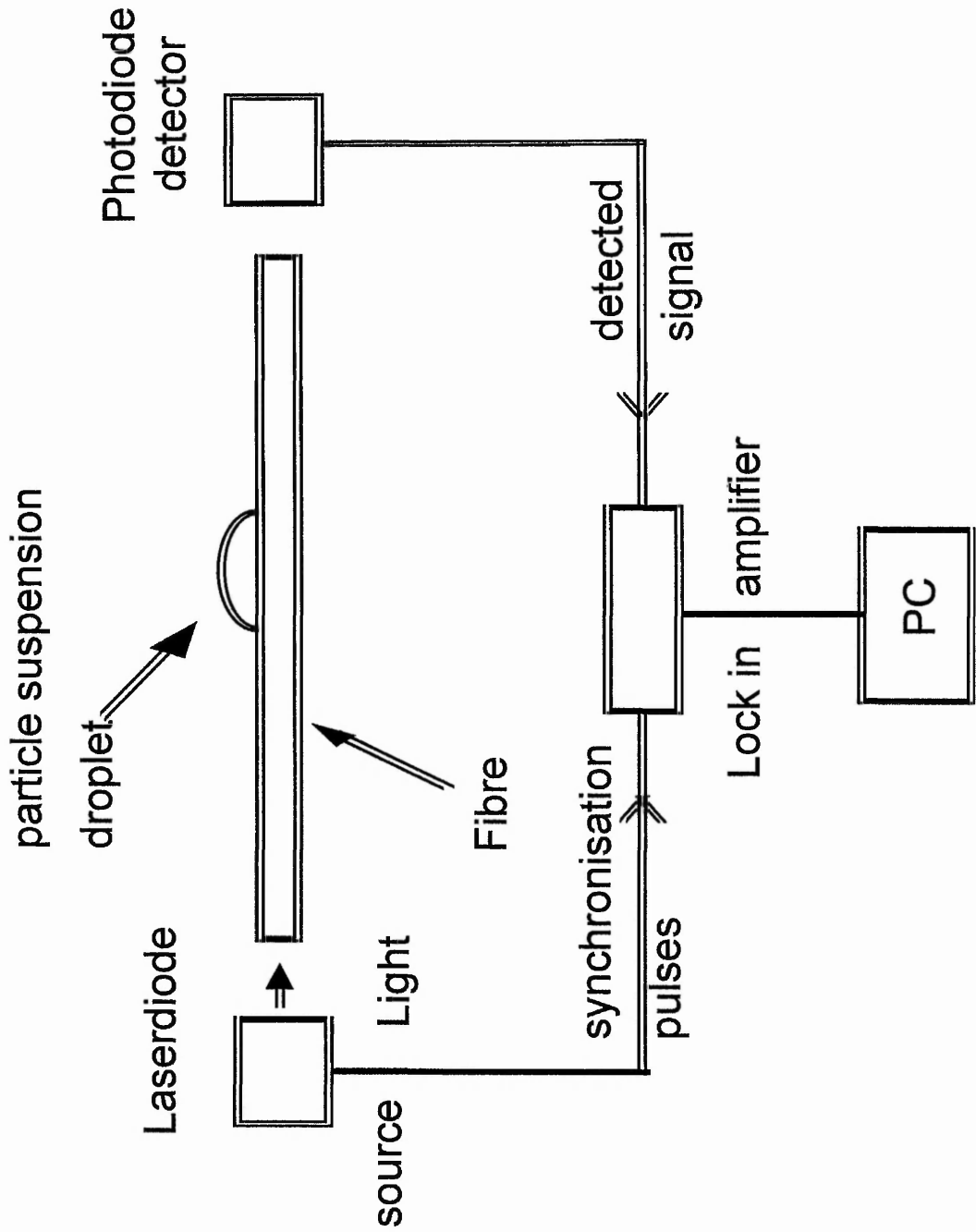
Figure 4.2. A schematic view of the basic experimental arrangement for the transmission experiments.

The detector used was a RS 308-067 high performance silicon photodiode combined with a high gain, low noise amplifier. The spectral response of the diode is shown in [2] and for a wavelength of around 650 nm, a response of 0.35 A W$^{-1}$ was obtained. A light-tight box was used to incorporate the photodiode as well as some additional electronics. The electronics consisted of an amplification circuit with adjustable gain and a low pass filter for further noise rejection of the signal before it was fed into the lock-in amplifier.

Lock-in amplifiers are used to measure the amplitude and phase of signals buried in noise. They act as a narrow bandpass filter which removes much of the unwanted noise while allowing through the signal which is to be measured. The frequency of the signal to be measured and hence the passband region of the filter is set by a reference signal, which has to be supplied to the lock-in amplifier along with the signal to be measured. A time constant function on the lock-in allows the pass-band frequency width to be set.

In this investigation a lock-in amplifier by Scitec Instruments, model 500mc, was used. The reference signal was supplied directly from the signal generator which had a frequency of 500 Hz. This choice was high enough not to be influenced by surrounding frequencies (i.e. background lights) but still low enough that it would not be distorted due to the rise and fall time constants of the photodiode. The output signal (the actual signal) of the photodiode was connected to the signal input of the lock-in. A minimum time constant of 300 ms was found to give a stable output signal from the lock-in. A time constant of 1 s was used for all measurements.

The output of the lock-in amplifier was connected to a Keithley digital voltmeter (DVM). A C-program was written for data acquisition and the computer was connected to the DVM via an IEEE 488 interface. The time constant for the recording of the data in the program could be set so that multiple measurements per second could be realised. However, it was found that one measurement per second was sufficient.

### 4.1.2 Basic light transmission in fibres

The light guiding system in section 4.1.1 acted as the basic arrangement for the light transmission study. Modifications of this basic system required for individual experiments will be mentioned later in this report. Having described the basic experimental system, some of the preliminary investigations to illustrate the feasibility of the light guiding principle will be given.

### 4.1.2.1 Small diameter polyester and Tencel fibres

As Figure 4.1 shows, light travelling through a section of polyester fibre suffers very high attenuation due to intrinsic absorption or scattering caused by the fibre material. However, in the case of very large polyester fibres the amount of light coupled into the fibre exceeds the amount of light absorbed and a reasonable fraction of light is detectable at the other end of the fibre. The smaller the fibre diameter the harder it is to couple light efficiently. Therefore, it was expected that the coupling of light into polyester fibre of 80 $\mu$m diameter and Tencel of 57 $\mu$m would give some difficulties. In fact, the first experiments carried out using the same equipment as in the case of the 800 $\mu$m polyester fibre did not indicate any light transmission in the smaller fibres at all. Two possible reasons were considered. First, the coupling of light was inefficient or second, the attenuation was too high so that all light was absorbed while travelling through the fibre. It was impossible to change the intrinsic properties of the fibre, therefore, the work was concentrated on the efficient coupling of light into the fibre. Undoubtedly, this means that the endfaces of the fibre have to be uniform and smooth to avoid any scattering effects.
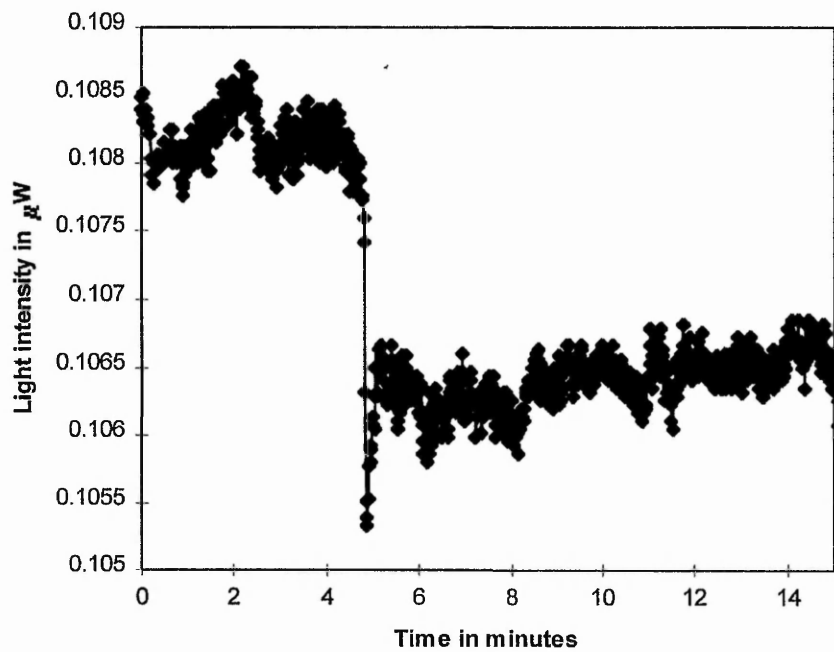
Figure 4.3. The deposition of a 0.5μl drop of myrrh oil (n=1.52) onto an 80 μm diameter polyester fibre while immersed in water. Fibre length is 8 cm.

Several approaches were attempted, such as the cleaving of the ends by a very sharp steel blade, or by a diamond cutter. In the end it was found that the combined cooling of the fibre by liquid nitrogen for a couple of minutes, and cutting the ends by a sharp pair of scissors gave the best transmission results. The ends were then observed under a microscope to ensure the cut end was smooth. If this was not the case the procedure was repeated until it was successful. With this method, transmission in 80 $\mu$m diameter polyester fibres of lengths of 10 cm and in 57 $\mu$m diameter Tencel fibres with lengths of 7 cm were achieved, despite the high intrinsic attenuation by the fibre material. A short section of 80 $\mu$m diameter polyester was mounted in a small PTFE cell. The fibre was equilibrated in water before a droplet of myrrh oil, which has a refractive index of n=1.52, was deposited onto the fibre surface. The results are shown in Figure 4.3.

The first part of the graph (from 0 up to 5 minutes) shows the period during which the fibre was fully immersed in distilled water. It is well established that highly birefringent fibres react very sensitively towards different measurands, such as temperature [3]. Immersion of the fibre in a water bath helps to keep the temperature fluctuations around the fibre to a minimum. Furthermore, sagging of the fibre when the oil drop is deposited is minimised by immersion. At around 5 minutes a 0.5 $\mu$l volume drop of myrrh oil (density = 0.998 - 1.022 g ml$^{-1}$) was deposited onto the fibre and this causes a sudden decrease in the transmission signal. This fall in intensity can be explained by the replacement of fibre-water interface by fibre-oil interface, and since the oil has a higher refractive index than water, it causes light to be leaked out of the fibre. After the decrease in intensity the signal stabilises, although very high fluctuations can be observed.

A second type of experiment was carried out to investigate the relationship of the wetted area and the attenuation in transmission intensity. Figure 4.4 shows schematically the arrangement used in this investigation. A section of 800 $\mu$m polyester fibre was mounted in a glass tube that was sealed at the bottom using a rubber bung. The laser diode was positioned below the glass tube and focused

onto the fibre. The other end of the fibre was mounted in the detector box. Bending the fibre was necessary for ease of handling and operating the system, i.e. filling and emptying the glass tube. A ml syringe was used to introduce the liquid into the glass tube. The level of water was then periodically increased by the addition of 100 $\mu$l of water every 100 seconds (from 300 seconds onwards); each addition corresponded to an increase in wetted length of 1.66 mm. A typical response of the light signal is shown in Figure 4.5.

One can clearly see that the transmission decreases every time water was introduced and an increase in immersed length of the fibre occurred. The immersed length of the fibre is known and the percentage attenuation, as a function of wetted area of fibre can therefore be determined and is shown in Figure 4.6.

Figure 4.6 shows the relationship between the wetted area and the attenuation of transmitted light. The 80 $\mu$m diameter polyester fibre system possesses a very high sensitivity since very small area coverage causes significant attenuation of the transmission. It should be noted that the results presented for the 80 $\mu$m fibre should be considered only as an illustration of the capability of the experimental equipment. Further investigation into this small type of polyester fibre was not pursued. Nevertheless, the light transmission technique and the experimental apparatus are able to give representative results for small sizes of textile fibres.
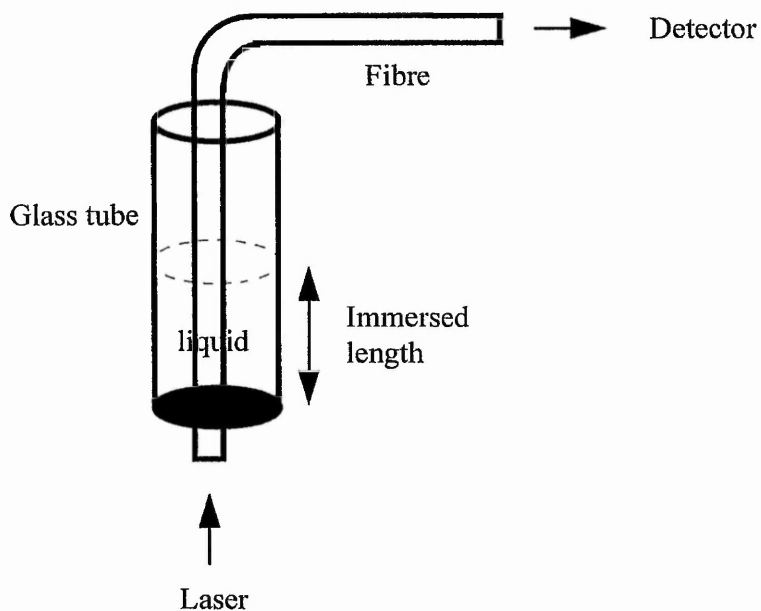
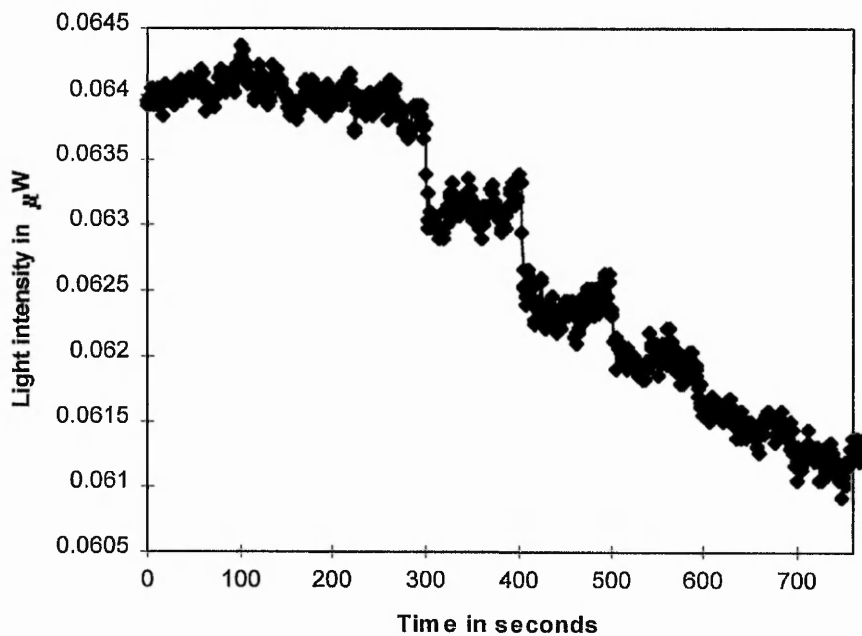Figure 4.4. Arrangement for partial immersion experiments



Figure 4.5. The effect of immersion of an 80 μm polyester fibre in water on the light transmission. 100 μl of water has been introduced into the glass tube every 100 seconds. Fibre length was around 8 cm.
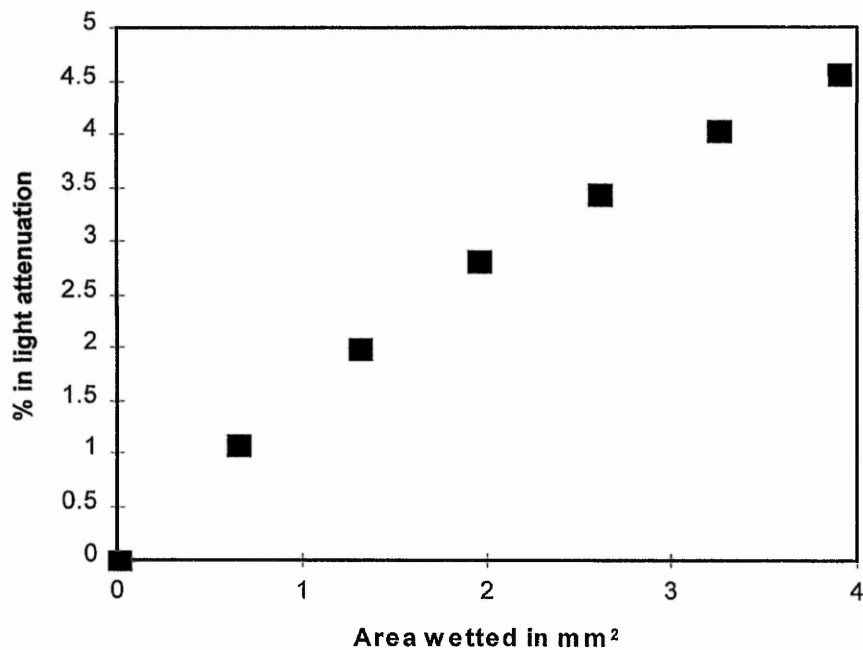
Figure 4.6. The effect of immersed area on the attenuation of transmitted light. Partial immersion of 80 μm polyester fibre in water using experimental arrangement shown in Figure 4.4.

### 4.1.2.2 Large diameter polyester fibre

The main fibre used in this investigation was a larger textile-like polyester fibre with a diameter of 800 $\mu$m. This fibre has the same material properties as the 80 $\mu$m diameter fibre, but was much easier to work with. Figure 4.7 shows a typical result of an experiment where a droplet of distilled water was deposited onto the surface of the fibre and was then left to evaporate. The water drop had a volume of 0.3 $\mu$l and it was deposited with a syringe on the top surface of the fibre.

The horizontal part (the first 4 minutes) of the signal in Figure 4.7 represents the light transmission of the polyester fibre in air. As soon as the water droplet was deposited the transmission decreased. This fall in signal is caused by the part of air-fibre interface being replaced by a water-fibre interface. Due to the higher refractive index of water compared to that of air, light will escape out of the fibre when it hits the water-fibre interface. After the initial fall, the light intensity stays constant for a period of 2 - 3 minutes. This phase corresponds to the pinning of the contact line of the water droplet that was also observed via videomicroscopy. Due to the pinning of the contact line, the evaporation is primarily by reducing the droplet height, whereas the drop-fibre contact area remains constant. Contact line pinning lasts until a critical value for the contact angle is reached after which the contact line starts to recede, thus decreasing the drop-fibre contact area. This fact is shown by the increase in the transmission signal, since the "window" through which light is leaking out of the fibre is progressively receding. Finally, when all water has evaporated, the signal reaches its original level prior to the deposition of the water drop.
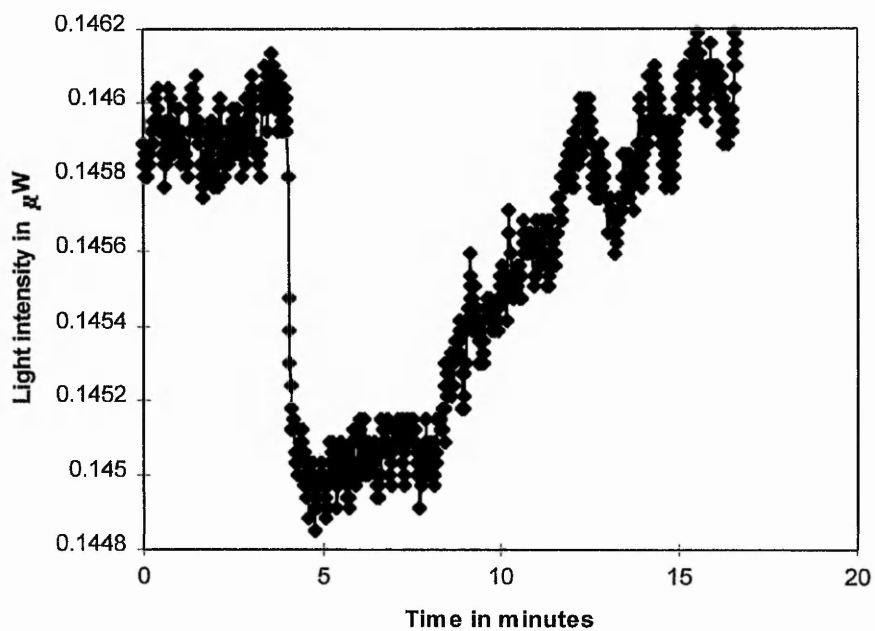
Figure 4.7. Evaporation of a droplet of distilled water of volume of 0.4 μl on a 800 μm diameter polyester fibre.

The investigation of the relationship between the wetted length of the fibre and the attenuation of the transmitted light can be studied with minor modifications of the arrangement. By removing the glass cell the fibre surface can be made accessible and simple deposition experiments of drops of liquid can be realised. Complete immersion of the fibre in a series of alkane and the deposition of oil drops from an emulsion can be investigated by using the glass cell as a part of a closed pump circuit.

| Chemicals | Refractive index n |
|-----------|--------------------|
| pentane | 1.358 |
| hexane | 1.375 |
| heptane | 1.387 |
| octane | 1.398 |
| nonane | 1.405 |
| decane | 1.411 |
| undecane | 1.417 |
| dodecane | 1.422 |
| cyclohexane | 1.426 |
| hexadecane | 1.434 |

Table 4.1. List of the series of alkanes used in the immersion experiments.

The complete immersion experiments were carried out using a series of alkanes, as shown in Table 4.1. The same series of alkanes were used in a previously published investigation which therefore offers a basis for the comparison of the two sets of results [4]. All chemicals were obtained from Aldrich and were of analytical grade purity.

After the immersion of the fibre in one pure phase (alkane), it was relevant to see whether this method was feasible for the interaction of the fibre with two phases. An experiment was performed where the fibre was immersed in a first phase, but then where a second phase deposits onto the fibre replacing the first. The

experiment chosen was the deposition of oil drops from an emulsion. The experimental method including the preparation and the use of the emulsion in this study will be described below, whereas the results will be presented in Chapter 5.

### 4.1.3 Emulsion systems

The emulsion used for the oil droplet deposition experiments was prepared shortly before the start of the measurements. This is necessary due to the short period of stability of the emulsion, after which the single oil drops start to coalesce, the emulsion will eventually separate itself into the two immiscible - water and oil - phases. The emulsion consisted of n-decane dispersed in 10 mM dodecyltrimethylammonium bromide (DTAB). To disperse the oil phase, a Silverson Laboratory Mixer was used. This machine forces the oil-water solution through an emulsor screen and therefore, promotes the breakdown of the oil phase, in this case decane, into small drops. It was observed under the microscope that the average droplet size was around 4-8 $\mu$m (see Figure 5.10).

So far, only the interactions of the textile-like fibre with liquids have been presented. As a model particulate system, a monodisperse latex suspension, with almost perfectly sphere like particles, was used. Later in the investigation a clay suspension with a particle size distribution, which represents a possible industrial application, was investigated. In both cases evaporation of suspension drops was used to force deposition of a controlled amount of particles onto the fibre. In the following, details of the particle suspension used in the investigation will be given and the results will be shown in Chapter 6.

### 4.1.4 Particle suspension

The latex polystyrene particle suspensions were all obtained from Duke Scientific Corporation with particle size ranges from 1.9 $\mu$m, 3.15 $\mu$m, 5 $\mu$m, and 10 $\mu$m in diameter. They were all monodisperse and fluorescent green except the 3.15 $\mu$m particles. The stability of the suspension is very high since the difference in density of the polymer and the water phase, in which the polymer is dispersed, is

minimal. The density of the latex particles is 1.05 g cm$^{-3}$ compared to that of water of 1.0 g cm$^{-3}$. All suspensions came with a stock concentration of 1 % except the 3.15 $\mu$m size which came with a concentration of 10 % solids.

The clay particle suspension was obtained by dispersion of montmorillonite clay particles in water with 0.2 % w/w NaCl. Figure 4.8 illustrates the size distribution of the clay particles. The small amount of salt was used to force the separation of the particles when added to water. During the dispersion process, the system was kept under constant stirring for a period of several minutes before it was placed in a ultrasonic bath to further enhance the separation process. With this method relatively stable clay suspensions were obtained with lifetimes easily exceeding a day. The refractive index of montmorillonite ranges from 1.55 to 1.57 dependent on crystal orientation and the density is 2.5 g cm$^{-3}$ [5].

With the light transmission method one can display the process occurring on the fibre surface from within the fibre. However, it was not known how sensitive this method would be and hence a second complementary technique to look from the outside of the fibre on its surface was sought.
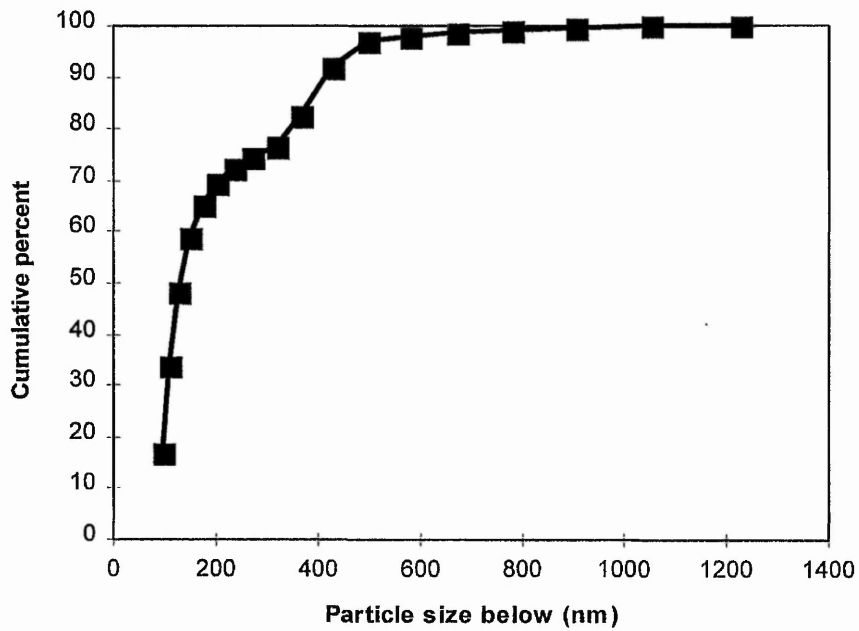
Figure 4.8. Size distribution of montmorillonite clay particles obtained by Zeta Sizer. (with permission of Unilever plc.)

## 4.2 Video imaging arrangement

With light transmission one can characterise the interaction of the liquid with the fibre via the contact area and the refractive index of the liquid. Video-microscopy provides a complementary technique giving direct visual observation of changes at the fibre surface. The system enabled the processes involved when a droplet of emulsion or a droplet of particle suspension was placed onto the fibre to be directly observed. This system was also used for the liquid case, for example, to determine the contact angle and area of liquid on fibres or flat surfaces. The results of the observations formed the basis for the discussion of the transmission signal. It was also interesting to compare the transmission signal that was obtained from the inside of the fibre and the imaging taken from the outside.

In this experimental arrangement two video cameras were used. One camera was used for the top view and one for the side view. The top view camera was mounted on an x-y-z translator for precise positioning while the side view camera was fixed to an x translator. The image sensor of the cameras is an interline-transfer CCD chip that enables receipt of good quality pictures with high sensitivity. The image quality does not suffer even if a backlight is used. A range of objectives (x4 - x40) have been used to display the pictures. The signal video output of the cameras were connected to two video cassette recorders and a picture was displayed on a monitor, which can be switched between the two views.

An xyz adjustable stage was used as the sample holder. The table where the sample can be placed is made of Perspex which is transparent, so that a backlight can be used to improve the contrast of the pictures. Fibres as well as flat surfaces, such as microscope slides, can be used with the sample stage.
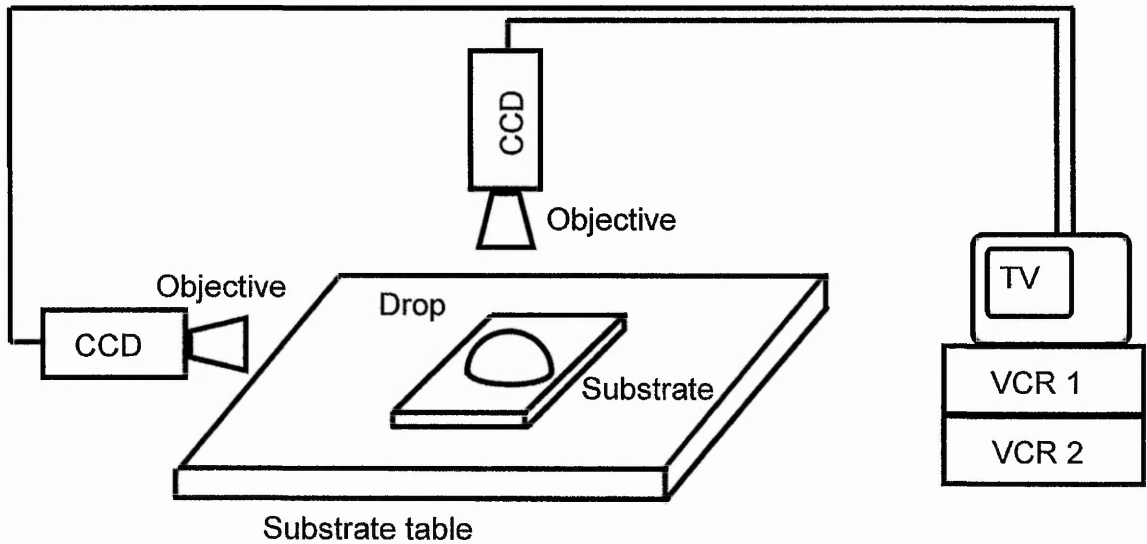
Figure 4.9 Schematic of the videomicroscopy arrangement. The substrate table could be positioned in the x-y-z direction and the two video cameras (CCDs) were connected to the video recorders and TV.

With the equipment described above it was possible to view pictures of drop-on-fibre systems. However, as described later, it was found very difficult to visualise directly polystyrene latex particles with a diameter of 1.9 μm. Therefore, a dark field illumination (DFI) method was introduced. DFI can be described as the illumination from a light, such that no light other than that scattered by the particles will be detected by the objective, thus causing the particles to appear as bright specks in a dark background. With this method details could be seen that are normally not resolved by the microscope objective. If used correctly this method would illuminate the green fluorescent particles whereas the background is kept dark, which makes the identification of the latex particle much easier. The DFI source was a ring-like light source that was powered by a light source in the controller unit. An optical fibre served as the connection of the ring-like light source and the controller unit. Both items were obtained from RAM Optical Instrumentations.

The video imaging arrangement enables one to record the drop-fibre system on a video tape. The pictures were then used to determine the contact angle between the fluid and the fibre. A software package, Image Tool, was used to playback the video tape and single pictures of the drop on fibre system could be frozen or captured. Some of these images are shown in Chapters 5 and 6.

The determination of the contact angle between a fluid and a substrate can be performed by measuring the angle from the drop on substrate (fibre) profile. An accuracy of ±2° could be obtained for large contact angles (>50°), but the accuracy decreases for smaller contact angles. The area wetted by a liquid drop or the covered area by particles on flat surfaces could also be worked out by measuring the area in pixels and converting it with a calibration into real areas. Determination of the contact area or covered area on fibre surfaces is more complicated due to the surface curvature. To overcome this problem a C-program was written to estimate the contact area on the curved fibre surface. Figure 4.10 (a) shows an illustration of one half of the cross-section of the fibre. At any point on the fibre surface the following equations are valid,

$$\sin\omega = \frac{\Delta x}{\Delta l} = \frac{y}{r_f} = \frac{\sqrt{r_f^2 - x^2}}{r_f} = \sqrt{1 - \left(\frac{x}{r_f}\right)^2} \qquad (4.1)$$

Hence,

$$\Delta l = \frac{\Delta x}{\sqrt{1 - \left(\frac{x}{r_f}\right)^2}} \qquad (4.2)$$

Figure 4.10 (b) shows the plane view of the fibre-drop system. The drop outline can be manipulated with the imaging software so that it appears as a white line in the pictures. This is recognised by the C-program and it sums over all columns and rows while weighting the planar projected length by $\sqrt{1 - (x/r_f)^2}$ to include the curvature of the fibre [6]. A listing of the program is given in Appendix 2.

With the described videomicroscopy arrangement, it was possible to verify the contact line pinning process observed in Figure 4.7. An experiment was carried out where the evaporation of a water drop on an 800 μm polyester fibre has been recorded. After analysing the recording data the droplet length and evaporation time were obtained. The results are given in Figure 4.11. It can be seen that in the first few minutes after the deposition of the water drop hardly any change in the contact diameter of the drop was observed, indicating that the evaporation is mainly in reducing the droplet height rather than the contact area of the drop with the fibre. After 5 minutes, however an increase in receding of the contact area was recorded.
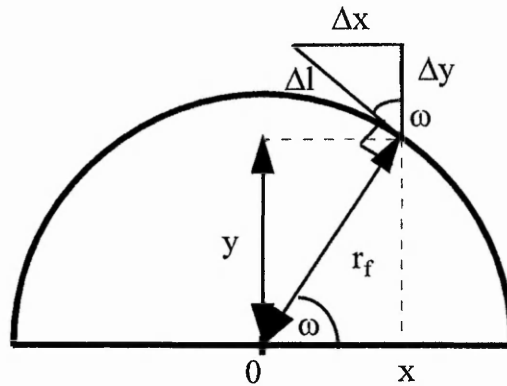
Figure 4.10 (a). Top half of cross-sectional area of fibre with radius of $r_f$ showing the relationship between a small change of planar length $\Delta x$ and the change in curved length $\Delta l$.
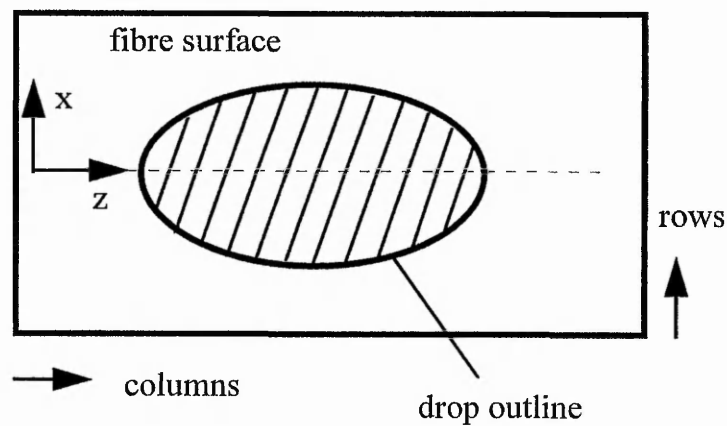


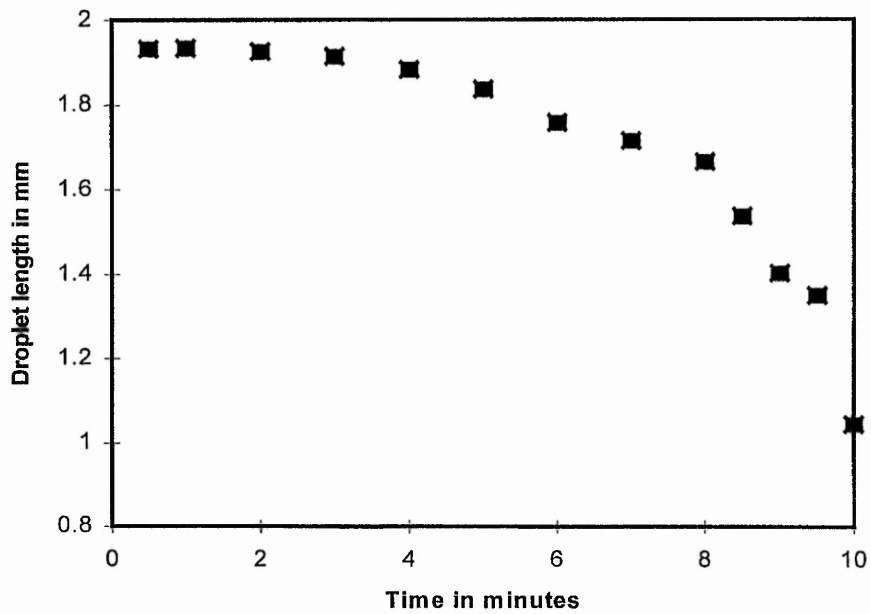Figure 4.10 (b). Plane view of drop-fibre system.

Figure 4.11. Illustration of the contact line pinning process via videomicroscopy. Graph shows the water droplet length variation with time of evaporation. Drop volume was 1 μl.

## 4.3 Quartz crystal microbalance

As mentioned in the literature review chapter, QCMs have been reported to investigate the detergency process. QCM techniques showed promising characteristics for the study of the removal of soil from hard solid surfaces. In this study a QCM system from Maxtek was used to investigate the evaporation of particle suspensions. It was believed that the QCM results would lead to a better understanding of the transmission signals obtained from the fibre arrangement, because the crystal response gives a direct relationship between the deposited mass and the frequency shift, assuming a rigid mass interpretation. This complements the fibre transmission data which give indirectly the relationship between the light attenuation and the contact area and refractive index of the deposited material. The component parts in the QCM arrangement are detailed in the following.

The heart of the arrangement is the AT-cut quartz sensor crystal. The crystal had a gold electrode on either side and its resonance frequency was 5 MHz. Two types of crystal were looked at in this study: a polished and an unpolished crystal. STM images of the gold electrode surface of both crystals are shown; polished 4.12(a), and unpolished 4.12(b).
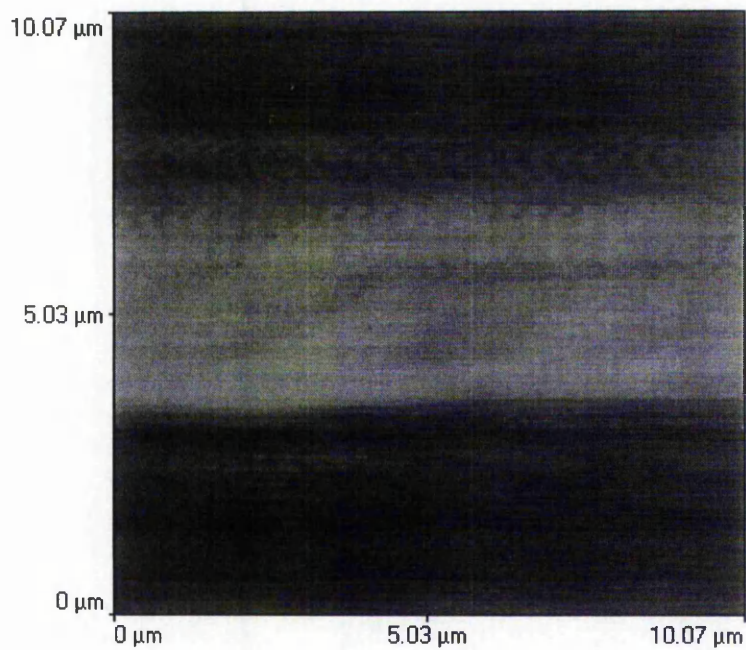
(a)
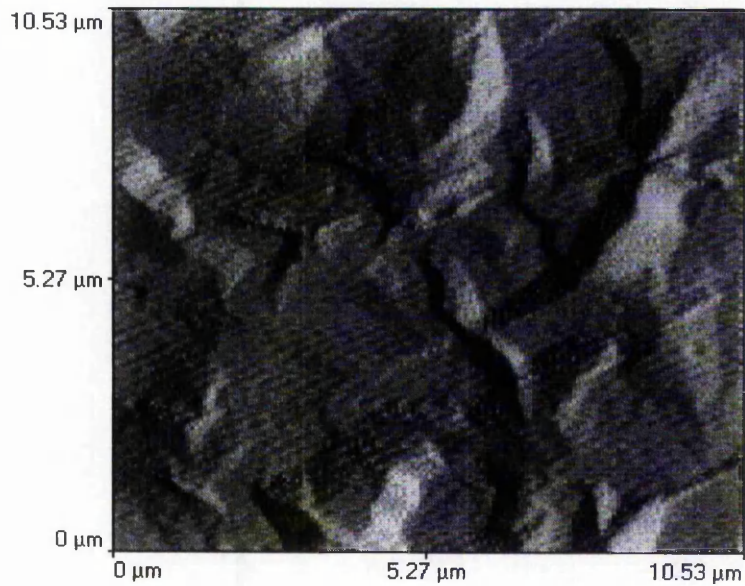


(b)

Figure 4.12. STM images of gold electrodes. Surface roughness of polished (a) and unpolished (b) gold electrodes on quartz crystal.

It can be seen from Figure 4.12, the surface of the unpolished crystal is scattered with troughs which could receive particles which have the right sizes to fill up these craters. These particles are then more rigidly bound to the surface of the gold electrode. The polished surface shows no indication of any visible roughness, although, some scratches which were caused by earlier experiments could be seen.

The crystal is mounted in a plastic holder. Integrated into the holder are the contacts for the electrical signals. The housing of the holder is sealed so that it can be used in gas or liquid environments. The holder CHC-100 is terminated with a standard female BNC connector which is connected to a phase lock oscillator (PLO).

The phase lock oscillator or resonator (PLO) generates outputs for the crystal frequency and conductance. Both signals were measured using a HP frequency counter and a Keithley DVM, respectively. Both the frequency counter and the DVM were connected to a personal computer via an IEEE interface.

A Labview program was written to deal with the data obtained from the PLO. The program was able to show the frequency curve and the crystal conductance in real time on screen. It should be noted that the conductance is presented in units of voltage in this system (see eq. 4.3).

particle suspension
drop

Computer

Frequency
counter

Voltmeter

Oscillator

Power
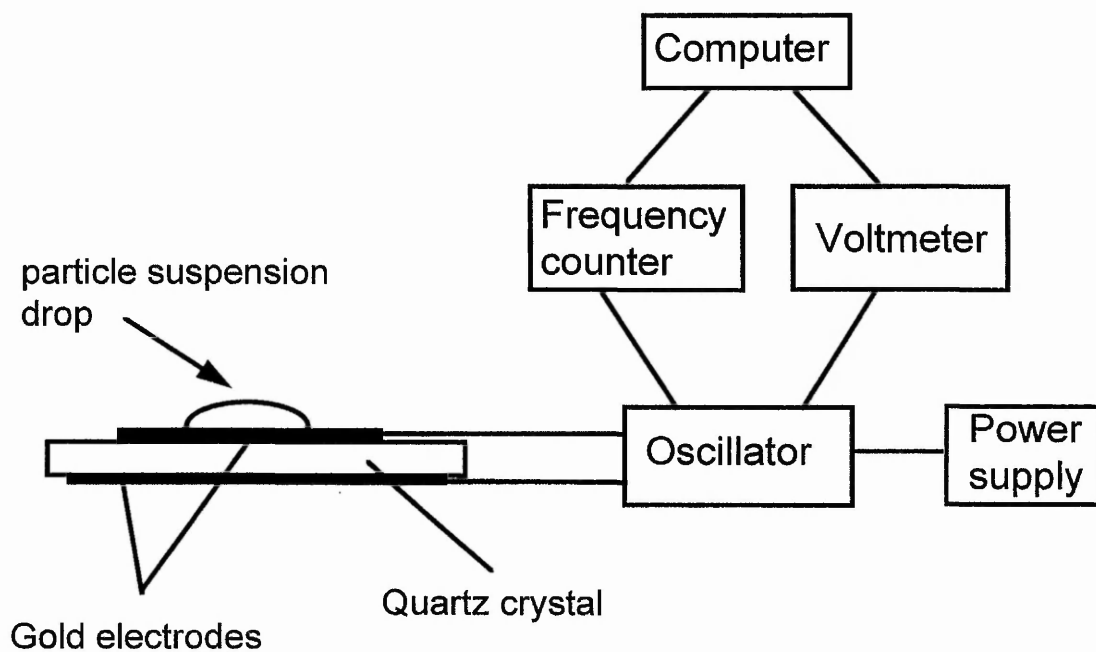supply

Gold electrodes

Quartz crystal

Figure 4.13 Schematic illustration of the QCM set-up used for the deposition experiments.

Figure 4.13 illustrates the QCM arrangement used for this investigation. It was found logical to start the study with the QCM with simple experiments which are already documented in the literature to ensure that the system was able to produce reproducible results. Water droplet evaporation was found to be suitable for this purpose and provided a simple way to compare the QCM data with that of the light transmission. The QCM equipment was set up and the phase lock oscillator adjusted to give a stable signal of the crystal resonance frequency. After the frequency signal was stable for a period of time, typically 15 minutes, the suspension drop was deposited using a syringe. It was ensured that the drops were deposited in the centre of the electrode, to take into account the Gaussian radial sensitivity of the crystal. Both a rough and a polished crystal were used to investigate the effect of surface roughness of the gold electrode on the frequency and dissipation signals. The PLO gives a voltage which is proportional to the crystal conductance (see graphs of crystal response) and the crystal dissipation is defined by the system used as,

$$\Delta D \,(\text{in } \Omega) = \frac{100}{\text{conductance (in Volt)}} - 20 \tag{4.3}$$

The QCM method will be used for the investigation into the evaporation of particle suspensions in Chapter 6. Below, the evaporation of distilled water on the quartz crystal is shown, which will form the basis of the interpretation of the particle experiments. The difference in signals will then be due to the presence of the particles in suspension.

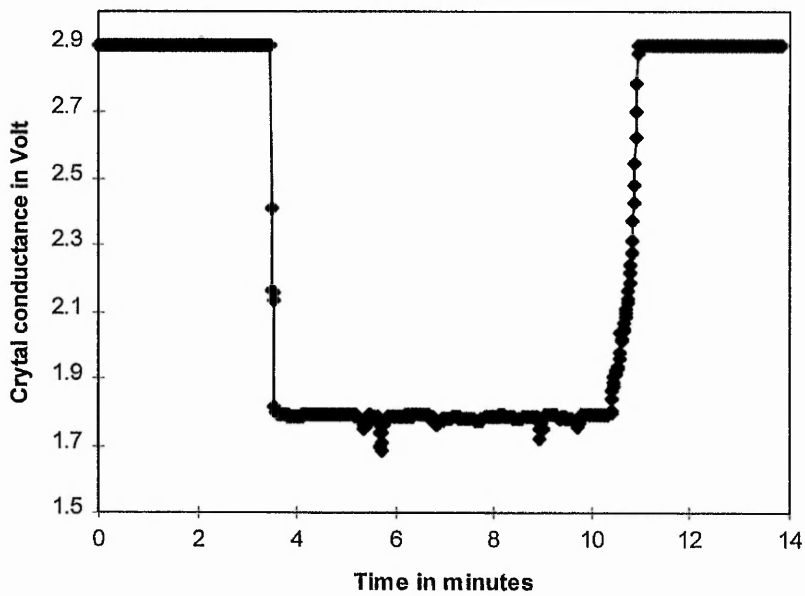### 4.3.1 Evaporation of distilled water on rough crystals

An unpolished quartz crystal was used for the initial evaporation experiments. Typical frequency and conductance responses of the quartz crystal during the evaporation of a drop of distilled water are given in Figure 4.14. The frequency signal (4.14 a) of the crystal shows a sudden decrease when the water drop is deposited onto the electrode. After that the signal stabilises and remains constant for a long period of time until, in the final stages of evaporation, it recovers rapidly back to the level prior to the deposition of the water drop. The

conductance signal (4.14 b) shows a similar pattern. It decreases suddenly when the water drop is deposited stabilises and recovers to its previous level before the deposition.

The two patterns can be explained as followed. Deposition of the water drop causes the frequency to fall because an additional mass has been placed onto the crystal. Due to the liquid phase (Newtonian liquid) the crystal experiences a damping of the shear wave, which is shown in Figure 4.14 (b). Both signals depend on the square root of the viscosity-density product. The roughness of the gold electrode encourages contact line pinning of the water drop and the evaporative effect is to mainly reduce the droplet height instead of the contact area of the drop with the electrode. The mechanism of contact line pinning during evaporation is well known and has been reported in the literature [7-9]. This causes the frequency and the conductance signal to remain constant, since the penetration depth $\delta$ of the shear wave into the liquid is much less then the drop height. Joyce *et al* also reported that mass loss from a droplet surface does not affect the effectively coupled surface layer until the fluid height is less than $0.5\delta$, where $\delta$ is the shear wave penetration depth defined in equation (3.30) [10]. Contact line pinning remains until the final stages of evaporation when the drop depins and reduces its contact area with the gold electrode until all the water has fully evaporated. At this stage both signals recover to their original level.
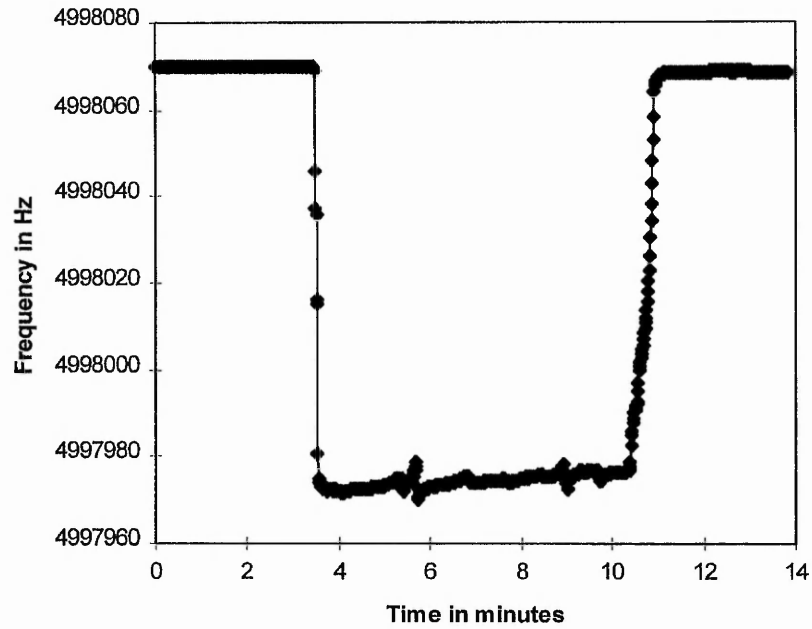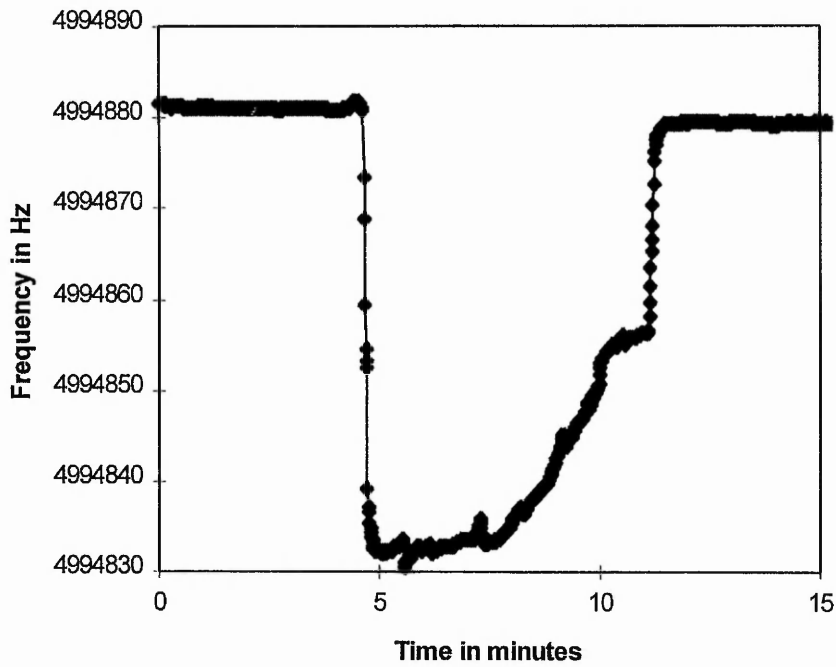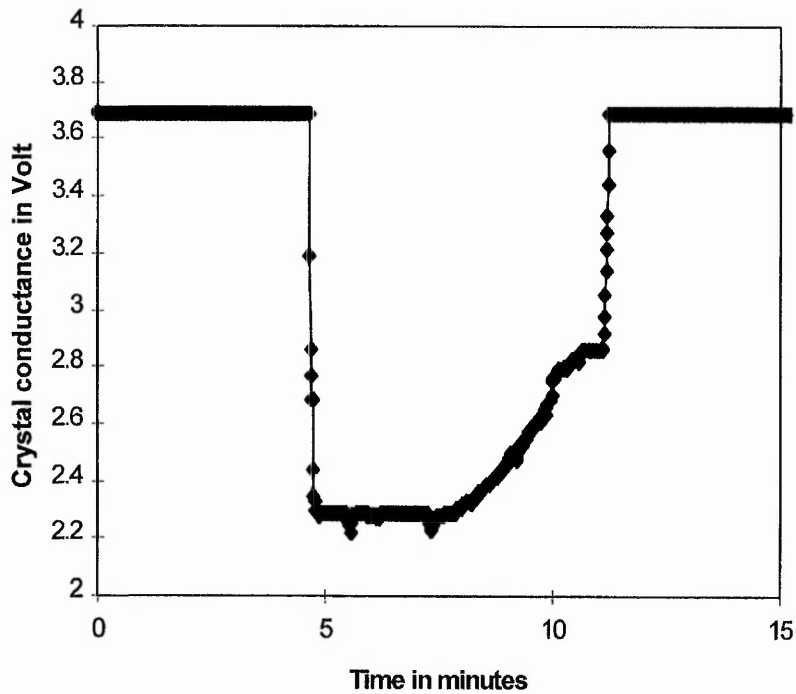
(a)



(b)

Figure 4.14. The evaporation of a droplet of distilled water, volume 0.5μl, on rough quartz crystal. (a) frequency signal, and (b) crystal conductance signal.

### 4.3.2 Evaporation of distilled water on polished crystals

The same experiment was carried out using a polished quartz crystal. A typical result of the evaporation of a droplet of 0.5 $\mu$l volume is shown in Figure 4.15. The first part of the two diagrams look similar to that of the rough crystal. However, the second part, between 7 and 10 minutes, is significantly different. Both signals, the frequency and the crystal conductance, decrease when the droplet is deposited. After a period where both signals seem to be stable they increase steadily before they "jump" back to their level prior to the deposition of the water drop. The evaporation of the water drop on the polished crystal started off in a manner similar to the rough crystal with a reducing droplet height and a pinned contact area. This process lasts until a critical value for the contact angle is reached, after which the contact line starts to recede. This can be clearly seen in the rise of the signals caused by the reduction in the wetted area. The polished surface does not give rise to as much pinning of the contact line as the rough crystal surface. In the final stage of the evaporation the signal rises back rapidly to its previous value since all the water is removed from the quartz by evaporation. The polished crystal shows that complete contact line pinning occurs during a much shorter duration; this is consistent with reports in the literature [11]. Comparing Figure 4.7 for the light transmission down a fibre and 4.15 for the QCM one can see some similarities in the signals as a droplet of distilled water evaporates. Both signals experienced a decrease when the water drop was deposited followed by a constant part and finally a recovering back to the initially level after complete evaporation. From this comparison, a possible interpretation is that the polyester fibre possesses a smooth surface which reduces the period of contact line pinning. A smooth surface is consistent with the SEM pictures in Figure 2.6 (a) and (b).

(a)



(b)

Figure 4.15. The evaporation of a droplet of 0.5µl of distilled water on a polished crystal. (a) frequency signal, and (b) crystal conductance signal.

This chapter has described the experimental arrangements used in the investigations in this thesis. It has also stressed the differences in using textile like fibres instead of conventional optical fibres for light guiding purposes. Furthermore, some preliminary experiments have been shown in this chapter to demonstrate the feasibility of the measurement techniques. It has also been shown that small textile like fibres, such as 80 $\mu$m, can be used with the light transmission arrangement, and do provide reproducible results. The characterisation of the QCM arrangement has been undertaken with the evaporation of a droplet of water on the crystal surface and the results are in agreement with those found in the literature. Observations by the video microscopy technique provide a direct aid to interpretation of the signals obtained from the other two techniques.

# References

[1] Mitsubishi Rayon Co., LTD. Eska, *High performance plastic fiber optics*, datasheet.

[2] RS Data Library sheet, *Photodiodes*, Issued March 1993, F14784, p.15

[3] W.J.Bock, W.Urbanczyk, R.Buczynski, A.W.Domanski, *Cross-sensitivity effect in temperature-compensated sensors based on highly birefringent fibers*, Aplied Optics, **33**, (1994), 6078

[4] B.J.Carroll, *Droplet deposition effects on light transmission by an optical fibre*, Colloids and Surfaces, **58**, (1991), 303

[5] D.Lide (Ed.), *CRC handbook of chemistry and physics: a ready-reference book of chemical and physical data*, CRC Press, London, 1995, 76th. Ed.

[6] N.T.Pham, G.McHale, M.I.Newton, B.J.Carroll, S.M.Rowan, *Investigation of deposition of monodisperse particles on fibers*, submitted to Langmuir,

[7] R.G.Picknett, R.Bexon, *The evaporation of sessile or pendant drops in still air*, Journal of Colloid and Interface Science, **61**, (1977), 336

[8] K.S.Birdi, D.T.Vu, A.Winter, *A study of the evaporation rates of small water drops placed on a solid surface*, J. Phys. Chem., **93**, (1989), 3702

[9] C.Bourges-Monnier, M.E.R.Shanahan, *Influence of evaporation on contact angle*, Langmuir, **11**, (1995), 2820

[10] M.J.Joyce, P.Todaro, R.Penfold, S.N.Port, J.A.W.May, C.Barnes, A.J.Peyton, *Evaporation of sessile drops: application of the quartz crystal microbalance*, Langmuir, **16**, (2000), 4024

[11] L.McKenna, M.I.Newton, G.McHale, R.Lucklum, J.Schroeder, *Compressional acoustic wave generation in microdroplets of water in contact with quartz crystal resonators*, Journal of Applied Physics, **89**, (2001), 676

# Chapter 5: Liquid Soiling of Fibres

The first part of this chapter marks the preliminary experimental work which was performed to characterise the fibre light guiding system. Most of the early work was concerned with liquid soil. The chapter starts by describing a range of deposition experiments with a range of liquids that were conducted to ensure the system was giving reproducible results before more complex experiments were performed. Partial immersion experiments with polyester fibre were carried out to test the feasibility of the method for textile-like fibres. The results from the measurements show the relationship between the immersed length or area of the fibre and the light attenuation. Complete immersion experiments in a variety of liquids - a series of alkanes - was the next step to investigate the relationship of refractive indices and the intensity of the transmitted light. Finally, the deposition of polydispersed oil drops from an emulsion was investigated. This experiment combines the immersion and the deposition of single drops onto the fibre surface. The discussion in this chapter is based on the few published pieces of work that existed prior to this thesis together with the model for light guiding developed and reported in Chapter 3 of this thesis. The experiments described in this section were performed with both optical fibre and textile like fibre. The optical fibre represents an idealised system which helps to characterise the textile like fibre experimental system.

## 5.1 Partial immersion of polyester fibre

This section deals with experiments aimed at ensuring the feasibility of the experimental method and the fibres used. These involved simple deposition experiments of mainly water droplets onto the surface of polyester fibre. The experimental arrangement used for this study (see Figure 4.2) is relatively primitive since the aim was to demonstrate the principle of the sensing mechanism. A short, 13 cm long, section of 800 $\mu$m polyester fibre was used to minimise the material absorption and this was mounted between the laser diode and the detector box.

Droplets of water with known volumes were then deposited onto the fibre surface and the transmission signal during the deposition process was recorded. A microlitre syringe was used to deposit water drops ranging from 0.5 $\mu$l to 5 $\mu$l in volume onto the fibre. The water drops have to be sufficiently small to form a clam shape on top of the fibre surface. Droplets too large would hang down from the fibre and would cause considerable difficulties in determining the contact area on the fibre. Images of drops small enough to form a clam shape on the upper side of the fibre were recorded and by measuring the drop profile from the top view of the system, the covered area or wetted area of the fibre could be estimated. A plot of the results of experiments is given in Figure 5.1. The laser position relative to the fibre axis was also varied to investigate the coupling conditions.

From Figure 5.1 it is apparent that the attenuation increases with increasing wetted area of the fibre. The amount of light leaked out from the fibre is also dependent on the launching condition. The higher the coupling angle the larger the attenuation caused by the same wetted area. The next step forward was to immerse the fibre to give a larger wetted area.

After ensuring that the system could respond to the deposition of single droplets, experiments where the polyester fibre was partially immersed were performed to give a systematically increasing wetted area. The experiments were carried out for comparison to the light guiding theory presented in Chapter 3. A number of liquid level sensors also use the same mechanism to detect, e.g. water level with optical fibres [1]. Therefore, a comparison of the results with textile like fibres may also be of interest.

The aim of the experiments was to determine the relationship of immersed length of the fibre and the attenuation of transmitted light intensity. Additionally, the coupling angle into the fibre was varied to investigate the effects on the light attenuation. Figure 4.4 shows the experimental arrangement.
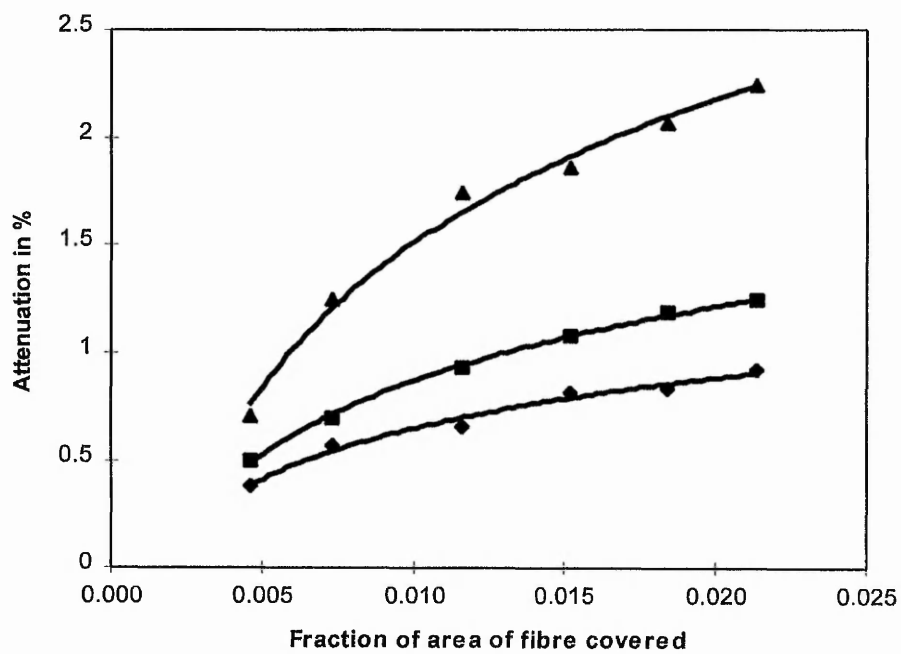
Figure 5.1. Deposition of single drops of water on 800μm polyester fibre. Laser position, ◆: laser in, ■; laser 15° off, and ▲: laser 30° off, fibre axis.

The results of the partial immersion study are shown in Figure 5.2. Immersion of polyester in water suggests that the relationship of length covered and attenuation is linear for the length range considered. However, if one also considers the coupling angle it becomes apparent that the higher the angle the higher the attenuation. The coupling angle determines the cone angle of light travelling down the fibre in a manner that the higher the coupling angle the larger the proportion of light at the total internal reflection border. In other words, the larger the coupling angle the higher the proportion of light travelling near the critical condition for TIR. Hence, small perturbations of the critical condition for TIR, e.g. replacement of air by water, cause this portion of light to be leaked out into the outer medium and reduce the total transmitted light intensity.

## 5.2 Immersion experiments with optical fibre

These experiments were conducted with optical fibre to ensure that the experimental arrangement was working as predicted by the theory and to check with already published material in the literature. Carroll [2] published results for similar experiments using a different experimental system and these supply a data set against which the results obtained in the present investigation can be compared for consistency. Another reason for performing the immersion experiments with an optical fibre was to determine whether this method was feasible and sensitive enough to use for textile or textile like fibres.
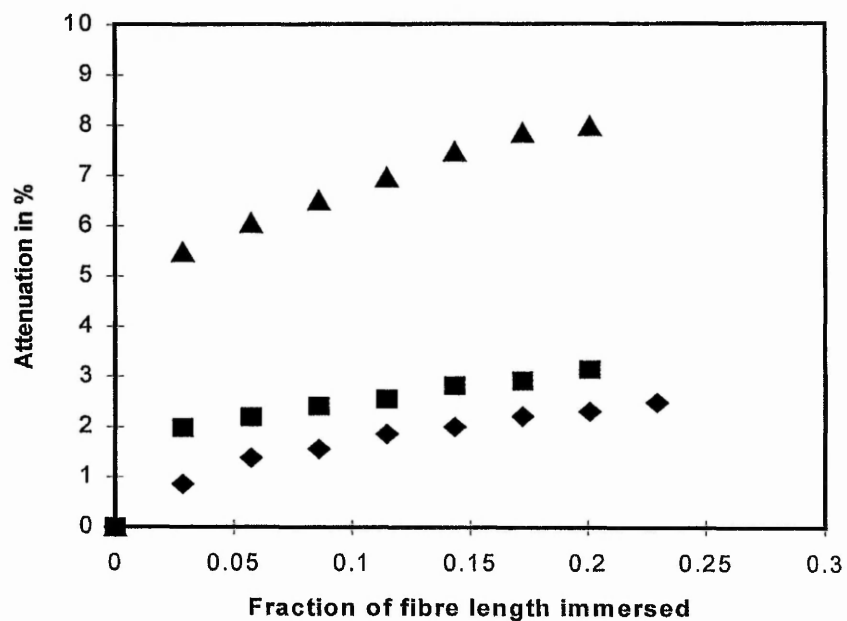
Figure 5.2. Partial immersion of 800μm polyester fibre in water. Laser position, ◆: laser in, ■; laser 15° off, and ▲: laser 30° off fibre axis.

In this set of experiments the optical fibre was immersed completely in a series of alkanes. Alkanes were used since they are readily available to very high purity and since they were used previously by Carroll [2], they offer a method for comparison. Moreover, a sequence of alkanes can also be selected with a set of refractive indices covering the one at which significant light loss from the fibre is expected to occur. The purpose of the experiments was to verify the relationship of the transmitted light and the refractive index of the outer medium (series of alkanes).

### 5.2.1 Coiling of fibres

In Chapter 2, the structure of an optical fibre was shown to involve several layers with the light-guiding core shielded by another two layers for protection. To make the fibre sensitive to the environment, either the light-guiding core has to be exposed to the surrounding medium or light transmission in the cladding layer has to be achieved and the jacket layer has to be removed. Since the optical fibre used had a cladding layer of only 5 μm it was found more convenient and less complicated to coil the fibre to obtain light transmission in the cladding layer. Removal of the cladding layer is not realisable without complications and direct launching of light into the cladding is very difficult due to its thinness. The coiling of the fibre in this case is equal to inducing bending loss in optical fibres. A theory of bending loss can be found in the optical fibre literature [3] and a schematic illustration is given in Figure 5.3. $R$ represents the arc radius of the bent fibre, $n_{core}$ and $n_{clad.}$ the core and the cladding refractive indices, respectively, and $d_{core}$ the core diameter. In Figure 5.3, an incident ray at an angle $\Theta$ is refracted at the entrance of the fibre and strikes the outer wall of the curved fibre at an angle $\varphi$ with respect to the normal. The angle $\varphi$ is then given by the expression [4]:

$$\sin\varphi = \frac{\cos\Theta_o \left[ R + \left( \dfrac{d_{core}}{2} \right) + h \right]}{R + d_{core}} \tag{5.1}$$
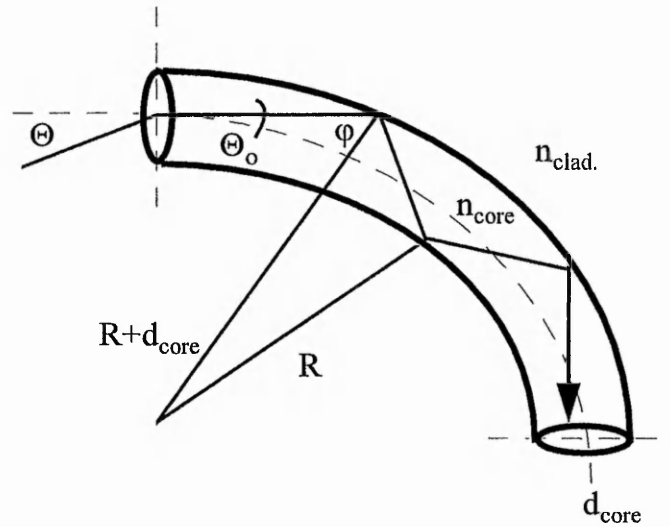
Figure 5.3. Meridional ray passage along a curved optical fibre [4].

where $h$ is the incident height of the ray with respect to the fibre axis. By using geometrical relationships and ignoring small quantities, equation (5.1) can be simplified to an expression [4],

$$\sin\varphi = \frac{R}{R + d_{core}} \tag{5.2}$$

Therefore, the light ray enters into the cladding when $\varphi$ is less than the critical angle $\varphi_{crit.}$. The equation above can be expressed in a different manner that allows the radius of the arc bend of the fibre to be estimated [2],

$$\frac{n_{clad.}}{n_{core}} = \frac{R}{R + d_{core}} \tag{5.3}$$

It is worth mentioning here that the light transmission model described in the theory chapter does not include the case of bending the fibre. According to Kapany, only a small fraction of the total rays that are incident on a fibre lie in the meridional plane [4]. Therefore, the theory developed based on meridional rays can not strictly be used here. A theory which would take care of the bending problem would have to consider the skew rays whose behaviour is highly complex within the fibre.

### 5.2.2 Experimental procedure

In experiments with coiled fibres, a 250 $\mu$m PMMA optical fibre with a 5 $\mu$m thick cladding layer was used. The fibre was wound repeatedly (around 20 coils) onto a former with a diameter of 4 mm. The coil then was transferred into an oven which was kept at a constant temperature of 100 °C. After a few minutes the coil was taken out of the oven and the fibre was carefully removed from the former. In this manner a coiled fibre with a defined coiling or bending radius was obtained. The coiled fibre was then allowed to cool down before its ends were polished to reduce roughness which might scatter light and so reduce the coupling efficiency. After polishing, the ends were looked at under a microscope. The polishing of the ends was carried on until a circular dot could be seen under the microscope when white light was shone through the other end of the fibre. Subsequently, the ends were mounted in two PTFE holders which were attached to either end of the glass cell. Two plastic caps were used to close the glass cell and make it

water tight using PTFE o-rings. The laser beam was focused onto the fibre endface and adjusted so that maximum output was obtained at the lock-in display after which it had been set to synchronise with the reference frequency of the laser diode. The output of the fibre was recorded until an equilibrium signal in air was obtained.

The experiments were performed using the equipment described in the experimental development section. The flow cell was filled with individual alkanes through an inlet port. To limit the vibration of the coiled fibre, which would cause fluctuations in the transmission intensity signal, the filling process was carried out as smoothly as possible. Once the cell was completely filled up an equilibrium was achieved before the cell was emptied. This procedure was repeated at least three times for each alkane. A typical result of the immersion experiment of coiled PMMA optical fibre is given in Figure 5.4.

### 5.2.3 Results and discussion

The transmission signal in Figure 5.4, shows three distinct parts. Part (a) represents the transmission signal when the optical fibre was equilibrated in air. One can see that the signal is very stable and an equilibrium of the experimental conditions has been met before the alkane was introduced into the glass cell. As soon as the fibre comes in contact with the alkane the transmission intensity decreases until the whole length of the fibre is fully immersed. It can be seen that an equilibrium signal of the immersed fibre is very quickly achieved since the temperature difference of the fibre and the alkane system was minimal. This temperature effect can be deduced from part (b) of the graph. It was observed that lowering the room temperature would result in an increase in transmission. After it was ensured the signal had reached its equilibrium state the alkane was drained from the glass cell via an outlet valve. Part (c) in the diagram represents the emptying process. At first the transmission signal increases instantaneously until all the cyclohexane has been removed from the cell. After that the increase in transmission has a lower slope due to droplets remaining on the fibre surface after the emptying process. The droplets eventually evaporate leaving the fibre surface exposed to air as at the start of the experiments. Finally, the transmission

signal reaches more or less the previous level, although, due to temperature fluctuations in the open lab small gradients in the transmission signal can be observed. The reduction in transmission of part (a) to part (b) of the graph was determined and the experiment reproduced for the whole series of alkanes.

The effect of the alkane sequence on light transmission in the coiled optical fibre is shown in Figure 5.5. From the results it can be seen that the amount of loss increases with increasing refractive index of the alkanes. A saturation of loss, however, occurs once the refractive index of the liquid approaches that of the fibre cladding [5]. This part of the graph represents the case that all light travelling in the cladding would be leaked out into the liquid phase – complete loss. The value of 8% saturation loss therefore indicates the total amount of light travelling in the cladding layer due to coiling of the fibre.

Carroll in his paper, published results for similar experiments and his and the results presented here show the same qualitative trends [2]. In Carroll's experiments an LED and spectrally matched detector were used instead of a laser diode and the lock-in technique. However, both sets of results show the saturation of loss when the refractive index of the alkane is close to that of the fibre cladding.
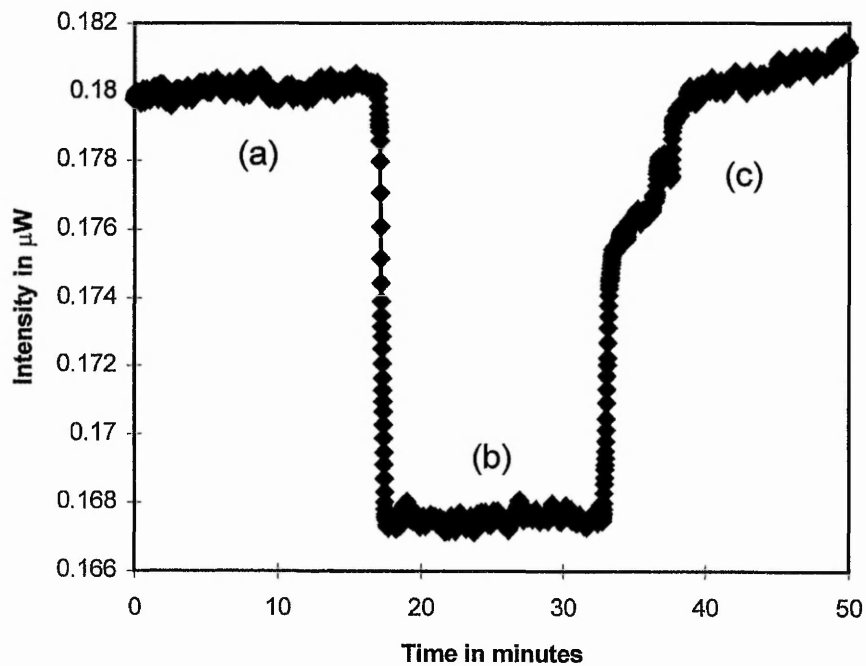
Figure 5.4. Typical transmission signal of immersion experiments. Full immersion of a coiled 250 µm PMMA optical fibre in cyclohexane, n=1.426.

Theoretically, one would expect the light attenuation to show a similar graph to Figure 5.5. Changing the environment around the fibre from air to pentane caused only minimal attenuation since the refractive index of pentane ($n_{pentane}$ = 1.358) is small compared to that of the fibre ($n_f$ =1.55-1.70) and when the total loss is only 8 %. However, if higher alkanes and so higher refractive index media are used the condition for TIR changes significantly resulting in a decrease in the cone of angles that undergo TIR. Additionally, the reflectance coefficient at the fibre wall-liquid boundary decreases as higher refractive index media are used. Thus, one would expect the rise in attenuation with increasing refractive index of the alkane. However, as soon as the refractive index of the liquid matches that of the fibre cladding all light transmitted within the fibre will be leaked out into the outer medium since the optical interface between fibre and liquid ceases to exist. Once this has been reached further increasing the refractive index of the outer medium does not have any further effect on the attenuation. Therefore, a saturation of loss is expected as soon as the refractive index of the alkane matches that of the fibre cladding.

## 5.3 Immersion experiments with straight polyester fibre

After the system had been tested with commercial optical fibre and its operating conditions established, textile like fibres were introduced. A relatively large diameter polyester fibre was chosen for the initial experiments. Since this type of fibre does not have a cladding layer, there was no need for coiling. The immersion experiments as described above were repeated with a straight 800 μm polyester fibre.
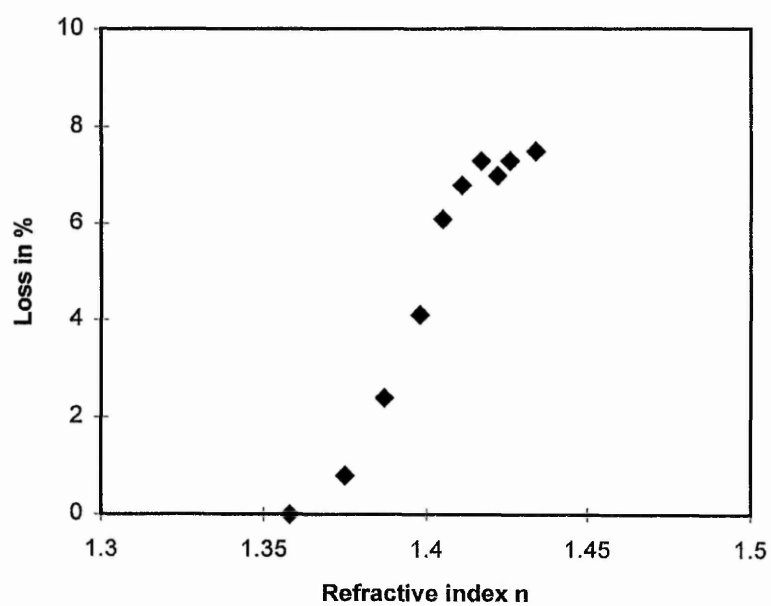
Figure 5.5. Loss in transmission of light by a coiled PMMA optical fibre as a result of immersion in a range of alkanes.

### 5.3.1 Experimental procedure

The experimental procedure of the immersion experiments with straight polyester fibre did not differ much from that with PMMA optical fibre. A piece of fibre of 35 cm in length was used for the immersion process. The fibre ends were treated with 3M non-abrasive polishing paper before they were mounted in the glass cell using olives and fibre holders. The laser focus point was then adjusted onto one end of the fibre and fine tuned for the case of maximum output from the lock-in amplifier.

Once the polyester fibre had been mounted in the cell it was left some time to reach thermal equilibrium. Experiments were then started and the liquid introduced in the same manner as before. After the immersion the liquid was removed from the glass cell via an outlet valve and the fibre was left until the transmission signal had reached a stable level; the experiment was then stopped.

### 5.3.2 Results and discussion

The immersion experiments on straight polyester fibre were performed with the same series of alkanes used in the coiled optical fibre investigation. However, as a test before the series of alkane was used, experiments were conducted with distilled water. A typical result of the experiments can be seen in Figure 5.6. The three distinct regions of the graph, as seen in the coiled optical fibre case, are apparent. These regions are i) a rapid reduction in intensity as the fibre is immersed in water, ii) a stable period of time during immersion and iii) the recovery back to the original level when the immersion fluid is removed from the glass cell.
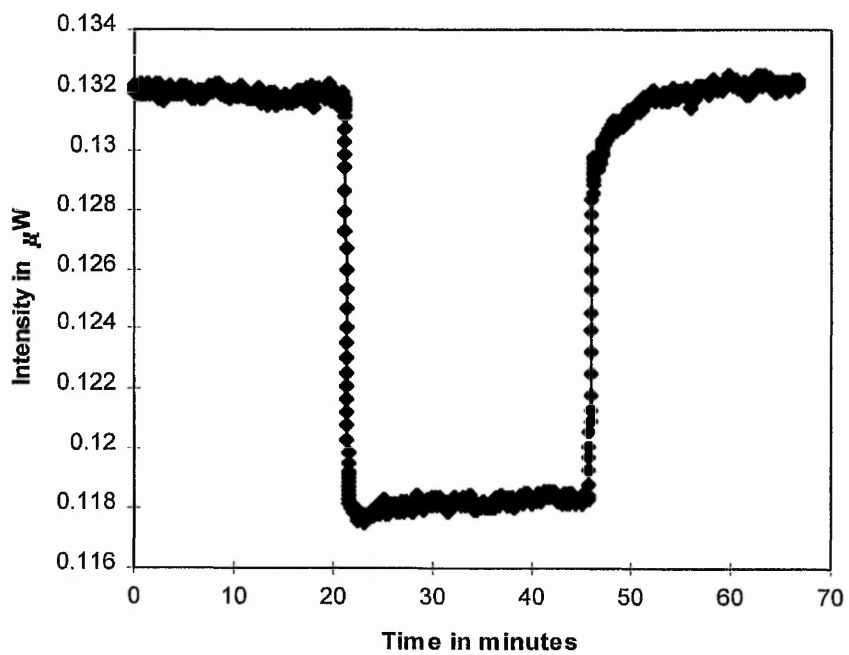
Figure 5.6. The transmission intensity of straight 800 μm polyester fibre immersed in water.

The attenuation of the transmitted light caused by immersion of a straight polyester fibre in the series of n-alkanes is shown in Figure 5.7. It is notable, that the same alkanes cause higher losses in the case of straight polyester fibre than in the coiled optical fibre case. This is due to the fact that in the case of coiled optical fibre only the 8% of the light transmitted – the proportion which travels in the cladding - could interact with the liquid medium. In the straight polyester case, however virtually all of the transmitted light is interacting with the outer medium. After normalising the loss values for the optical fibre case, Figure 5.8, one can see that the loss due to immersion in the alkanes is smaller for polyester than the PMMA optical fibre. Normalising means that the saturation loss of 8 % is set to 100% total loss to give a method to compare with the polyester fibre case.

This can be explained with the refractive index of the fibre materials. PMMA possess a refractive index which lies within the range of that of the alkanes used. Polyester, however, has a much higher refractive index of between 1.55 and 1.7, which is higher than that of all the alkanes used. Therefore, only a partial loss in transmitted intensity occurs in polyester fibre.
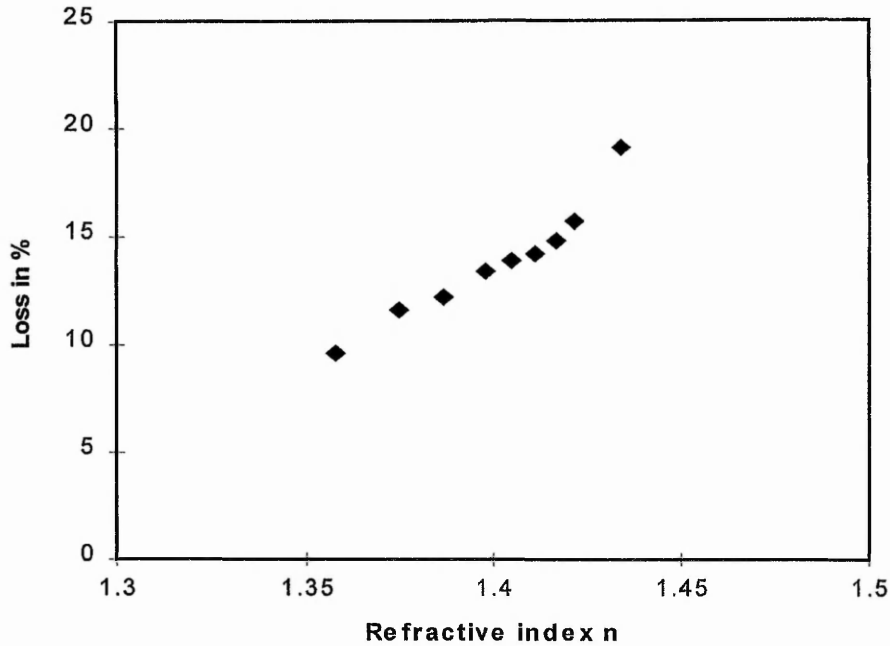
Figure 5.7. Loss in light transmission in an 800 μm straight polyester fibre due to immersion in a range of liquids of an n-alkane series. The data shown represent the average of at least 5 experimental results.
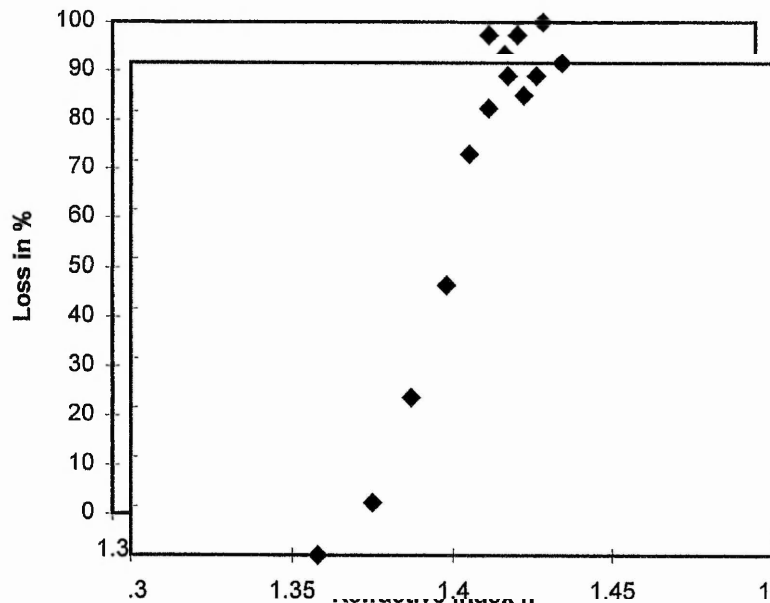


Figure 5.8. Normalised loss in transmission of light by a coiled PMMA optical fibre as a result of immersion in a range of alkanes. The total loss of 8 % is set to 100 % in this figure to give representative comparison to polyester fibre.

### 5.3.3 Comparison of experimental data with model

Calculations using Mathematica were carried out to simulate the immersion experiments of polyester fibre. However, no attempt to realistically model the immersion process of PMMA optical fibre was made as the light transmission in coiled fibres are extremely complex. Problems such as the coiling of the fibre which will give rise to skew rays will appear and a model beyond that using meridional rays would be required. Nonetheless, for completeness the comparison between the meridional ray theory and the experimental data for the PMMA case is shown in Appendix 3. In the case of large diameter polyester fibre the light guiding model using meridional rays is expected to give a much better description of the transmission intensity. This is due to the fact that the polyester fibre was not coiled but straight and it did not include a cladding layer. Figure 5.9 shows a plot of the experimental data combined with the theoretical fit.

Figure 5.9 suggests that the light guiding model is, to a first approximation, adequate in describing the experimental data. The immersion process can be understood as the air around the fibre is replaced by each liquid with the refractive index $n$ in turns. The fitting parameters are as follows, $\Theta = 25°$, $n_f = 1.55$, $k = 0.0003$; $\alpha = 100 \%$ in 1m, $L = 30$ cm, $d = 800$ $\mu$m.
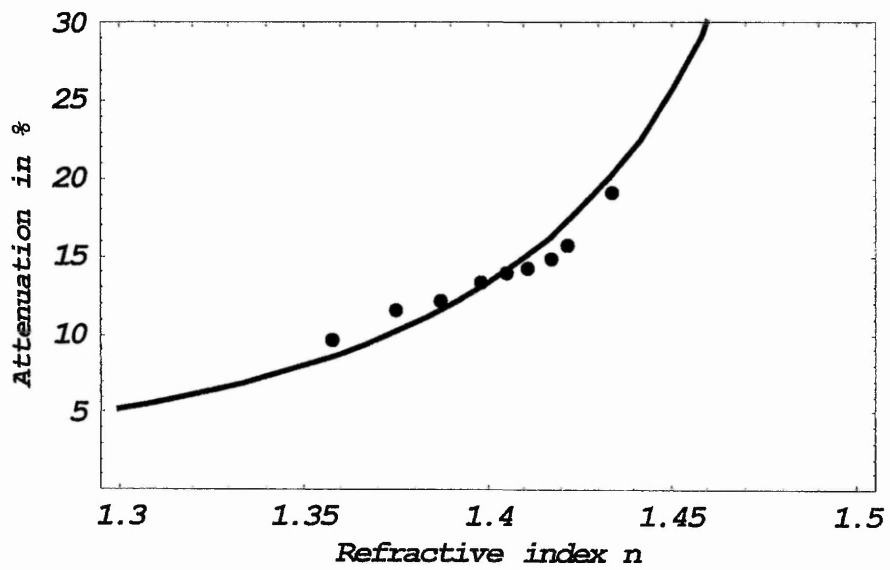
Figure 5.9. Comparison between theory and experiments. The solid curve is obtained from the light guiding model described in Chapter 3 and the points indicate the experimental results.

## 5.4 Deposition of oil droplets from an emulsion onto coiled PMMA optical fibre

It was noted in Chapter 3 that the detergency process or the efficiency of soil removal is very sensitive to the way the soil is brought into contact with the fibre, i.e. the soiling process. In this set of experiments a closer look at the soiling process was attempted. Oily soil was deposited onto the coiled optical PMMA fibre. This provides information on the adhesion of oily soil (soiling process and soil redeposition) onto a fibre surface from an aqueous environment. Deposition was achieved by immersion of a coiled fibre in an emulsion. The emulsion used consisted of a 15 mM Dodecyl-trimethyl-ammonium Bromide (DTAB) and 5 % decane. DTAB is a cationic surfactant added to stabilise the oil-phase.

### 5.4.1 Experimental procedure

The preparation of the emulsion is described in section 4.1.3. Dependent on the concentration of the emulsion an amount of decane was added into a 15 mM DTAB solution. A Silverson laboratory mixer with an emulsifier screen was used to prepare the emulsion. The drop sizes ranged from around 2 $\mu$m to 8 $\mu$m in diameter as shown in Figure 5.10.

The experimental arrangement was altered slightly for this type of measurement. A smaller flow cell constructed out of PTFE was used and this was connected to a peristaltic pump to form a closed-pump circuit. The pump speed was set to 5 ml/min to avoid any vibration which might occur at higher pump rates.
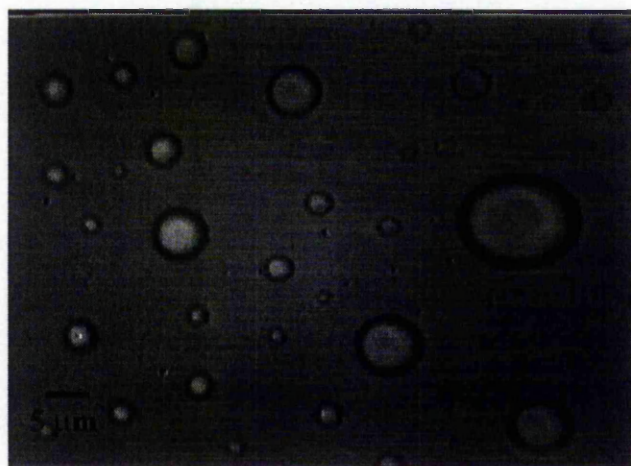
Figure 5.10. Emulsion comprising of decane oil-phase and 15 mM DTAB solution.

### 5.4.2 Results and discussion

After the fibre had been mounted within the cell and an equilibrium in transmission obtained, the cell was filled with a 15 mM DTAB solution. This was necessary because surfactant solution might interfere with the deposition process of the decane emulsion droplets. By equilibrating the fibre in the surfactant solution the effects can be minimised. The liquid was introduced via the peristaltic pump. Once the equilibrium had been achieved the emulsion was introduced into the cell. A typical result of the deposition of decane oil drops from an emulsion onto coiled PMMA optical fibre is shown in Figure 5.11. The horizontal part of the signal (the first 30 minutes) represents the equilibration of the fibre in the surfactant solution. At around 30 minutes the emulsion was introduced into the cell. At this point the graph shows a steady decrease in the transmission signal which suggests the deposition of single decane drops onto the fibre surface. At about 60 minutes a change in the slope of the signal arises suggesting that the rate of deposition is decreasing. After a further 20 to 30 minutes a saturation in the signal is reached and a small drift in the signal due to temperature changes can be observed.

A discussion of the results obtained from the emulsion experiments is very difficult since many parameters are unknown. The deposition rate is vital for an exact quantitative discussion, but this parameter is not accessible. Even if the deposition rate is known it is sensitive to the decane concentration or/and the surfactant concentration and on the properties of the fibre surface and temperature. With the present arrangement it was found to be very difficult to control these parameters.
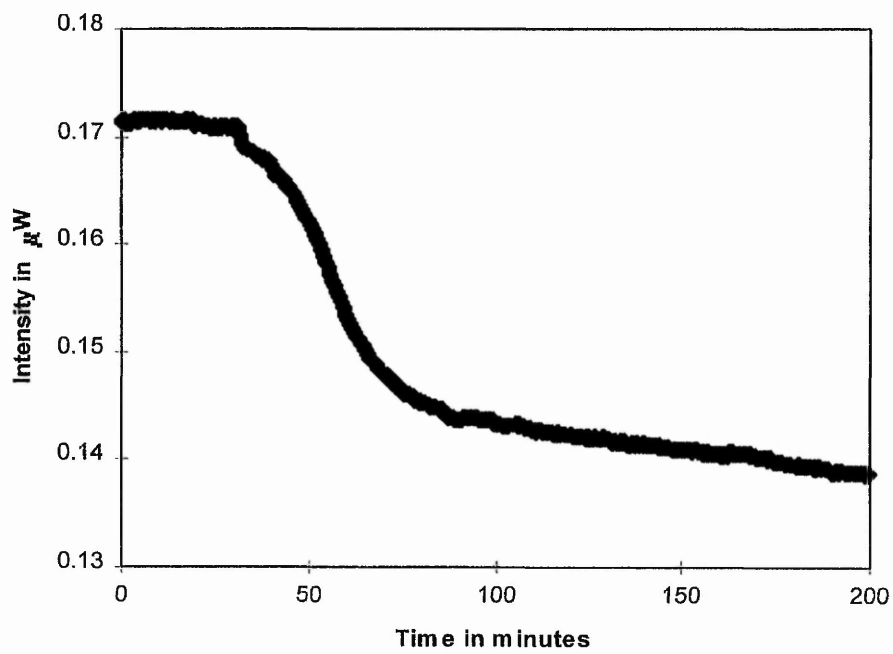
Figure 5.11. Deposition of oil droplets from an emulsion onto the coiled optical PMMA fibre.

Carroll hypothesised that the deposition process of decane drops from an emulsion onto a coiled PMMA optical fibre consists of 3 stages [2]. He explained the shape of the intensity signal via Figure 5.12. At the start of the deposition the fibre surface is bare and single drops adhere to the fibre surface. This single droplet deposition, assumed the droplets are monodisperse and can be represented by a surface coverage rate $k_1$, Figure 5.12(a). The second stage will occur when the incoming decane drops are not deposited as single drops but coalesce with ones already sitting on the fibre surface. This stage is represented by a rate $k_2$ where $k_2 < k_1$ since the surface coverage is smaller for the second stage, Figure 5.12(b). Finally, incoming drops will cause the coalescence of, for example, two droplets already on the fibre. This stage will be described by an even smaller $k_3$ and it forms the final process of deposition, Figure 5.12(c). It is possible that the last stage would represent the transitional phase of single droplets to a film on the fibre surface. Since the light transmission intensity is dependent on the surface coverage of the fibre, one would expect a graph with decreasing intensity with three distinct slopes. However, the presumption of monodispersivity is not true in this case and the three distinct slopes will be slightly distorted. Therefore, one would expect the rate of deposition to change through the course of the deposition process and the light transmission signal would show behaviour similar to Figure 5.11.

Although the explanation of the deposition mechanisms proposed by Carroll is logical and of high relevance in the latter stages of the experiments, it was not observed in the experiments. Video sequences of the deposition of emulsion drops onto 800 $\mu$m polyester fibre surfaces were undertaken and pictures from the different stages of the deposition process were obtained. Pictures of the deposition process taken in the earlier stages showed that the oil drops deposit themselves on the surface of the fibre as single droplets. Further deposition is in covering the whole surface of the fibre with single oil droplets. The oil droplets did touch each other, but coalescence was not observed. Further deposition resulted in the building up of a thick layer (around 4-5 droplets thick, dependent of the concentration) of oil drops. Coalescence will occur when the emulsion becomes unstable, but this was not observed under the microscope. Especially, towards

the end of the measurements coalescence might be likely to occur because of the short lifetime of the emulsion. Furthermore, Jachowicz et al reported that coalescence of silicone oil droplets readily occur on a fibre surface which is already modified by a layer of oil [6].

## 5.5 Deposition of oil droplets from an emulsion onto straight polyester fibre

The emulsion experiments were also carried out using a short section of 80 $\mu$m diameter polyester fibre. It was only feasible to use the smaller diameter polyester in a smaller flow cell. In longer sections of the small diameter fibre the coupled light intensity was insufficient to overcome the material absorption and no detectable transmission could be observed through the polyester fibre using the relatively low intensity laser diode based experimental system.

### 5.5.1 Experimental procedure

The experimental procedure and apparatus for this investigation can be found in section 4.1.2.1. A section of typically 10 cm of the 80 $\mu$m polyester fibre was carefully mounted in the PTFE cell and the latter was connected to the pump circuit. After this had been done the laser was focused onto the entrance of the fibre; the small fibre diameter makes this process very difficult. Once the position of the laser giving maximum output was found the set-up was left alone until the equilibrium in the transmission signal had been achieved. The procedure for introducing liquid was the same as with the coiled optical fibre system. After equilibrating the polyester fibre in a 15 mM DTAB solution the emulsion was slowly pumped into the cell. The transmission signal was then recorded.
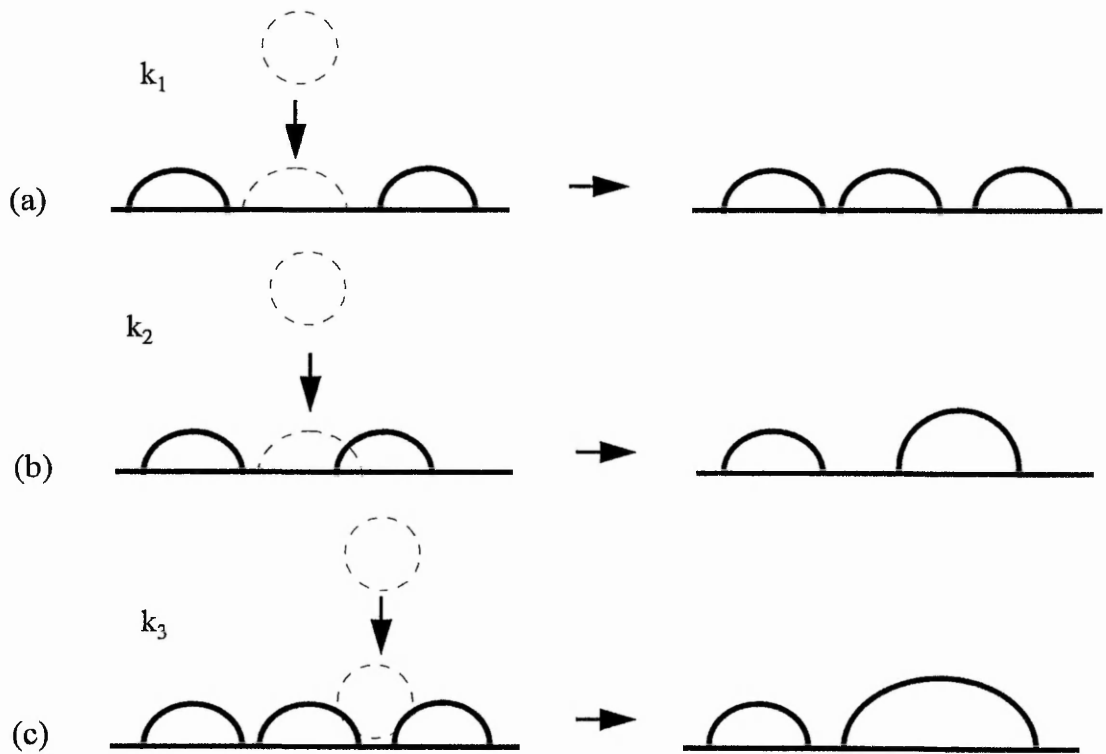
Figure 5.12. Oily droplet deposition mechanisms [2].

It must be noted that working with these small diameter fibres proved very difficult. The fibre needs to be mounted solidly in the cell which was very tedious since the fibre is easily damaged. Furthermore, the fibre also has to be under a slight tension so that it is straight and rigid and will not be affected by the flow of liquid.

### 5.5.2 Results and discussion

A typical result for the emulsion experiments with an 80 μm polyester fibre is shown in Figure 5.13. Qualitatively similar results to the case of coiled PMMA optical fibres were found. The transmission decreases with deposition time and finally reaches saturation when the whole length of the fibre is covered with decane. However, the overall loss is much higher as almost all light guided by the fibre is being reflected at the fibre-fluid interface, so that the 80 μm polyester fibre shows much higher sensitivity towards surface changes. This fact is further enhanced by the small diameter of the polyester fibre which causes more reflections of light at the fibre-fluid boundary per unit length leading to a further increase in the interactions of the transmitted light with the fluid.

Similar experiments were also performed for the 800 μm polyester fibre. The small cell was replaced by the larger glass cell and this experiment was carried out without the peristaltic pump. Light transmission in 800 μm was fairly high so that the larger cell could be used. This stagnant emulsion experiment was carried out to see how the size of the fibre and the hydrodynamic flow affect the deposition process. In Figure 5.14 a typical result for the stagnant emulsion experiment with 800 μm polyester fibre is shown.
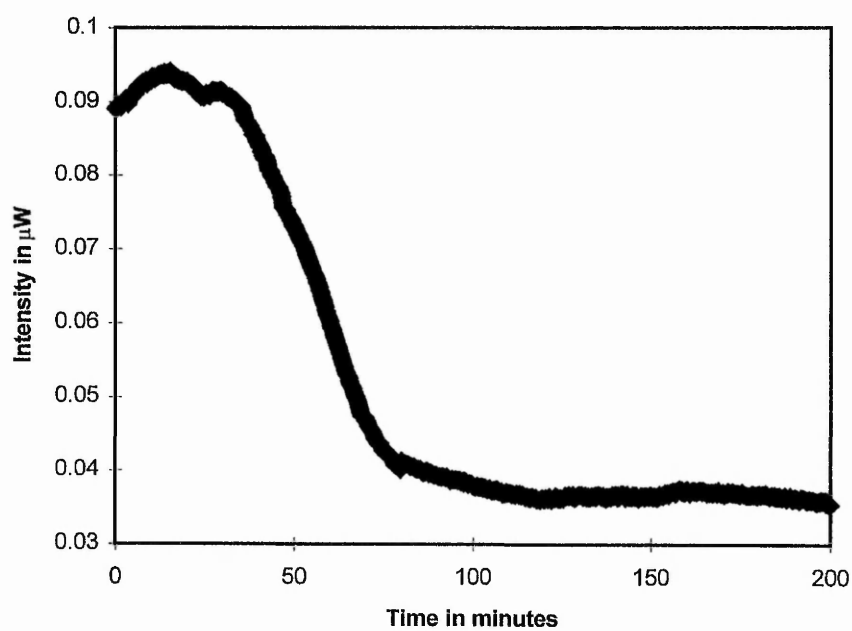
Figure 5.13. Deposition of oil droplets from emulsion onto an 80 μm diameter polyester fibre.
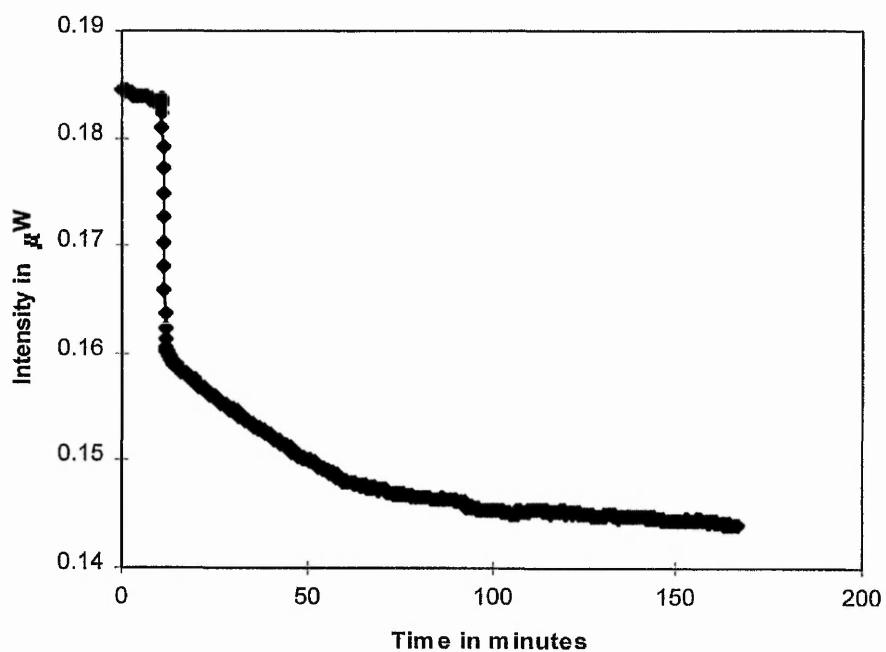
Figure 5.14. Deposition of oil droplets from emulsion onto an 800 μm diameter polyester fibre. Stagnant experiment.
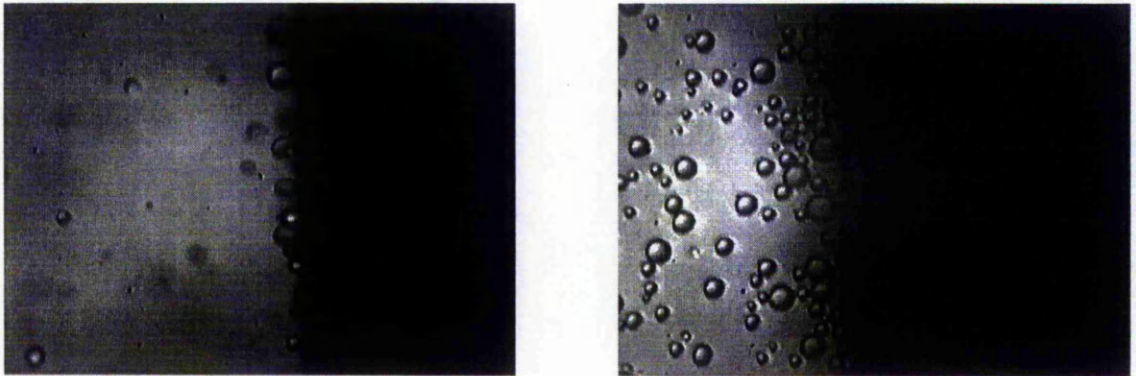
Figure 5.15. The deposition of emulsion drops onto the surface of a 800 μm polyester fibre. The black shadow to the right marks the fibre. Note that the oil drops do not coalesce even though they are touching each other.

The first part of the graph represents light transmission of the fibre in air. A slight drift can be seen which can be explained by the change in room temperature. Filling of the glass cell with the emulsion causes a rapid fall of the transmission. Due to the change in the refractive index from air to that of the emulsion the transmission decreased rapidly when the emulsion was introduced into the cell. Once the fibre is fully immersed in the liquid phase the transmission signal shows the same behaviour to the previously described cases.

Figure 5.15 shows the deposition process of emulsion drops onto an 800 $\mu$m polyester fibre. The picture on the left illustrates the earlier stages of the deposition process whereas the one on the right the latter stages. As one can see the oil drops deposit themselves onto the surface of the fibre and they do not coalesce even when touching each other. Although the picture on the right was taken about 30 minutes into the deposition, one does not know whether this is still true for later times, especially when the emulsion becomes unstable towards the end of the measurements.

**Summary**

In this chapter the feasibility of the fibre light guiding system for the detection of changes on the surfaces of fibres have been investigated. The ability of the experimental system to perform a variety of experiments to characterise the measurement principle has also been shown. Furthermore, experimental results of tests consisting of the liquid soiling of fibres, including both optical and textile like fibres, have been reported. From these a relationship between the wetted area of the fibre and the attenuation of light transmitted by the fibre could be observed. The larger the area wetted the higher the percentage of attenuation of light transmitted down the fibre. Additionally, the amount of attenuation is also highly dependent on the light coupling angle with a larger coupling angle giving higher attenuation.

The light guiding theory described in Chapter 3 has been used to explain the experimental data. Theoretical predictions for the immersion study of 800 $\mu$m polyester fibre in alkanes match quite well with the experimental results. This

suggests that the simple approach to describe the light guiding by considering only meridional rays is satisfied for large fibres and simple systems. For more complex systems, such as the coiled PMMA optical fibre immersion experiments, the theory does not match the experimental data. The discrepancy is due to the coiling of the fibre and the coupling of light from the core into the cladding induced by coiling. However, since the polyester fibre system will be the centre of this study, the light guiding model should be sufficient for these purposes.

## References

[1] G.Betta, L.Ippolito, A.Pietrosanto, A.Scaglione, *An optical fiber-based technique for continuous-level sensing*, IEEE Transaction on Intrumentation and Measurement, **44**, (1995), 686

[2] B.J.Carroll, *Droplet deposition effects on light transmission by an optical fibre*, Colloids and Surfaces, **58**, (1991), 303

[3] J.M.Senior, *Optical fiber communications: principle and practice*, Prentice Hall, New York, 1992, 2nd ed.

[4] N.S.Kapany, *Fiber optics - principles and applications*, Academic Press, New York, 1967

[5] G.McHale, B.J.Carroll, N.T.Pham, S.M.Rowan, *Measurement of droplet deposition on fibers*, Accepted: Contact Angle, Wettability and Ahesion, **2**, K.L.Mittal (Ed.) VSP, Utrecht,

[6] J.Jachowicz, M.D.Berthiaume, *Heterocoagualation of silicone emulsions on keratin fibres*, Journal of colloid and Interface science, **133**, (1989), 118

# Chapter 6: Particulate Soiling of Fibres

This chapter is focused on the soiling of fibres via particulates. The forced deposition of polystyrene latex particles was carried out via evaporation of particle suspension drops. The deposition of soil and the removal of soil can be considered as inverse processes. Knowing the adhesion during soiling it is possible to characterise the removal process and vice versa. Therefore, in this study it was chosen to approach the detergency process through soiling rather than removal.

Although experiments on the deposition of oil droplets from an emulsion onto a fibre are realistic and relevant to the detergency process, they are very difficult to characterise. A basic problem is that the oil drops are polydisperse in size and they can change their shape and merge together to form larger drops. Additionally, the contact angle of the oil drops may vary, within limits and so alter the contact area of the drop with the fibre, making controlled studies difficult. The forced deposition of polystyrene particles which are uniform in size and charge stabilised removes the problem of merging or coalescence. Furthermore, particles don't change their shapes significantly and having a refractive index comparable to that of the fibre, they represent a complete loss case. The fact that the experiments are carried out via evaporation of suspension drops ensures that the particles are deposited onto the fibre and the number of particles can be determined from the concentration of the suspension and the volume of the drop. Therefore, the deposition of monodisperse latex particles represents an idealised system which offers a more controlled study of the soiling process.

As a second tool of investigation the quartz crystal microbalance (QCM) method will be introduced to the experimental work. The QCM method is widely used to investigate the deposition of small uniform mass layers from liquids. It was believed that the method would complement the light guiding technique, which probes the mass deposited via changes in contact area and refractive index.

Finally, a more realistic application for the detergent industry will be investigated: the deposition of clay particles with the size distribution shown in Figure 4.8. To conclude the investigation, a similar study to the emulsion case has been attempted with clay particle suspensions.

## 6.1 Deposition of latex particles

The deposition of particles onto a substrate can be realised in different ways. One method considered was the immersion of the substrate in a particle suspension, similar to the emulsion experiments for the oily soil case. The surface potential of the fibre causes particles with unlike charges to the fibre surface to deposit onto the fibre due to electrostatic attraction. An alternative method considered was the forced deposition of particles via evaporation of a suspension droplet.

As noted in Chapter 5, the size distribution of the oil droplets prevented a simple interpretation of the emulsion experiments. The surface coverage from one oil drop to the next could vary significantly and deducing a deposition coefficient was therefore difficult with the non-monodisperse emulsions. To provide more controlled conditions, a monodisperse polystyrene latex particle suspension, initially with particle size of 1.9 $\mu$m in diameter was used. Particle suspension drops were first deposited onto flat polyester film in order to obtain a reference system. The results of these experiments show similar behaviour to that reported in the literature [1-3]. The key results are the formation of a ring-like single layer of particles at the drop periphery and a build up of the ring mass according to a power-law.
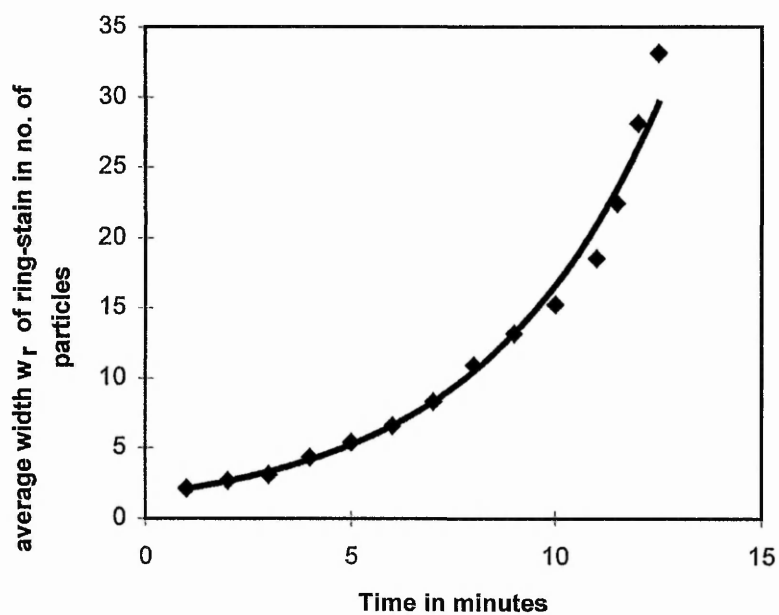
Figure 6.1. The power-law growth of the width, $w_r$ of the rim of a ring stain on a flat polyester surface. Volume of suspension drop was 0.5 μl and the solid concentration 0.25 %.

### 6.1.1 The ring stains

The power-law growth of the ring mass can be observed via the ring width growth in time shown for the 1.9 $\mu$m latex particles in Figure 6.1. To determine the average ring width, $w_r$, video pictures of the suspension drop-substrate system were captured and the width was measured in pixels. The number of pixels was then converted into a length unit using a calibration of the system.

Figure 6.1 shows that the rate of the build up of the ring-stain follows a power-growth law in time with more and more particles arriving at the rim in the closing stages of evaporation. This behaviour is in the regime where there are enough particles remaining in the bulk of the drop to be subjected to the outward flow. As the concentration of particles increases, it is more likely that multiple layers of particles will be deposited at the rim rather than a monolayer. If this occurs, the simple conversion from ring width to particle mass would no longer be true.

The ring-like deposit left on a polyester surface after all liquid has evaporated is shown in Figure 6.2. The first particles to arrive at the contact line are deposited and then reinforce the contact line pinning, Figure 6.2(a). Fresh particles delivered by the evaporatively driven outward flow, as shown in section 3.3, from the centre of the droplet continue to build up the rim and the width of the ring increases, illustrated in Figure 6.2(b). The growth in ring width continues until all particles have been deposited at the rim or all the liquid has evaporated and the outward flow has ceased. The picture of the deposit shows a very uniform arrangement of the latex particles, similar to a hexagonal pattern as shown in Figure 6.2(c). The presence of particles in the interior of the ring suggests that when the final liquid evaporated there were still some particles remaining in suspension which were then deposited in the centre of the drop. Another possibility is that these particles had already been deposited due to a surface heterogeneity, such as a scratch on the surface of the substrate, before the liquid was fully evaporated.

(a)                                              (b)
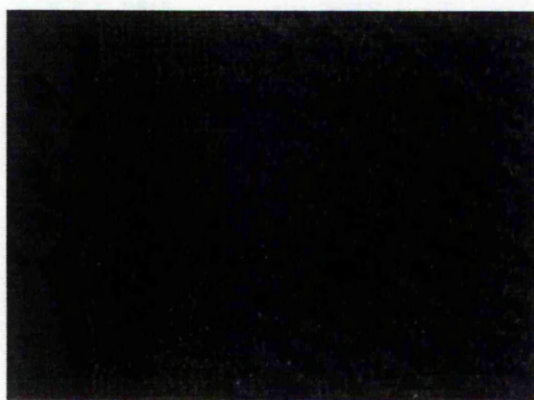


(c)

Figure 6.2. Deposit of 1.9 μm particles pattern. (a) first line of particles, (b) build up of a ring-like stain, (c) ring-stain after evaporation. The interior of the drop is to the right from the droplet boundary, which is indicated by the arrow.

After it had been ensured that the experiments on flat polyester surface gave the same results as had already been reported in the literature, the focus was changed to fibre surfaces. The same procedure was repeated with the 800 $\mu$m polyester fibre. A droplet of defined volume of suspension was deposited onto the surface of the fibre. Pictures of the deposition process were captured and the thickness of the ring was determined. A relationship between the width of the ring, corrected for the fibre curvature, and time of evaporation can be seen in Figure 6.3. It is necessary to add here that smaller drops of suspension had to be used on the fibre to give representative results. If larger drops are used they are likely to be pulled down due to gravity to the lower side of the fibre. This condition changes the deposition pattern since gravity is acting on the particles, even though the density difference between particle (1.05 g cm$^{-3}$) and water (1.0 g cm$^{-3}$) is very small.

Figure 6.3 illustrates that the width, and therefore the ring mass follows a power-law growth assuming that the ring consists of only a monolayer of particles. The monolayer assumption was verified from video pictures captured during the deposition experiments.

A typical deposition pattern of particles on the surface of polyester fibre is shown in Figure 6.4. Due to the curvature of the fibre surface it was very difficult to obtain a sharp image of the deposits across the full field of view. However, one can clearly recognise the ring stain deposits. The deposition experiments were performed and the pictures were taken for different suspensions ranging from 0.15 % to 1 % w/w particle concentrations and all show the typical ring-like deposit.
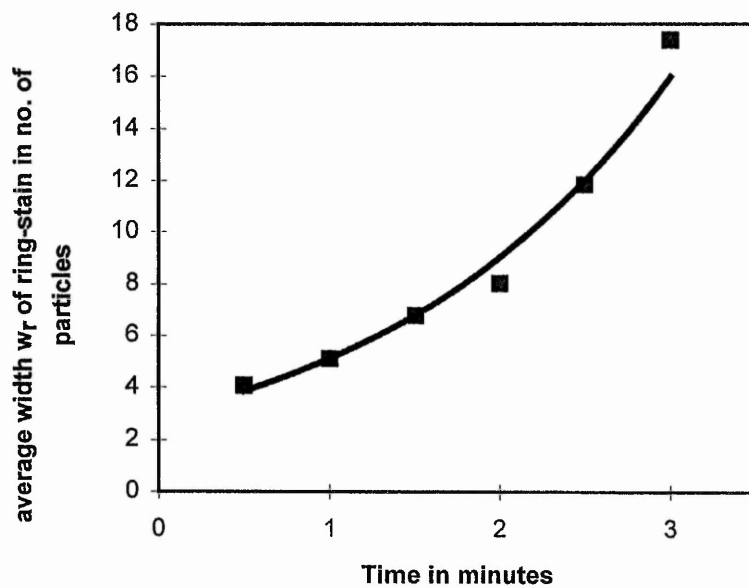
Figure 6.3. The power-law growth of the width, $w_r$ of the rim of a ring stain on a 800 μm polyester fibre surface. Volume of suspension drop was 0.1 μl and the solid concentration 0.25 %.
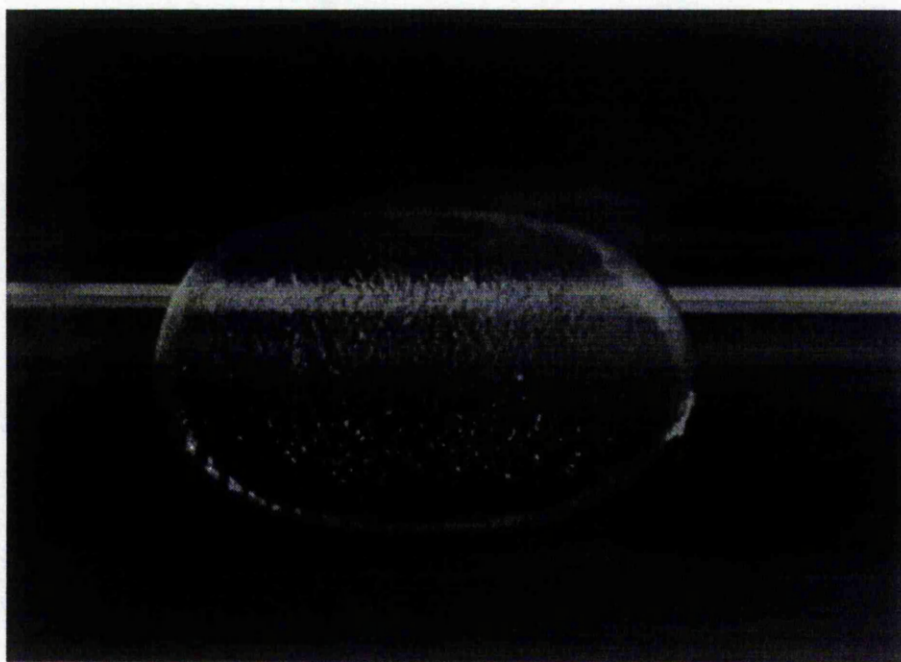
Figure 6.4. A typical ring-like deposit on the surface of an 800 μm polyester fibre.

It was shown above that the deposition of monodisperse latex particle suspension drops onto a fibre resembles that on flat surfaces. The phenomenon of contact line pinning and ring-like deposits occur on fibre surfaces as well as on flat surfaces. In the following section the effects of the deposition of particles onto a fibre surface on the intensity of light transmitted through the fibre will be reported. The intensity signal of the transmitted light will be interpreted using the known trends in the deposition process obtained from the video observations.

### 6.1.2 Light transmission technique (ATIR)

A section of around 14 cm of an 800 $\mu$m polyester fibre was used for these experiments. The ends were polished and the fibre was mounted between the laser diode and the detector box. Most of the length of the fibre was within the brass fibre mounter so that only a small length or surface of the fibre was exposed to background light. This keeps any perturbation of the signal by the open laboratory to a minimum. The laser beam was then focused onto one end of the fibre and adjusted until maximum output at the lock-in amplifier was obtained. Particle suspensions with a variety of concentrations were created by diluting the stock suspension of 1 % w/w particle concentration. Suspension drops were then deposited using a micro-syringe after an equilibrium of the transmission signal in air had been achieved. The transmission signal was recorded throughout the whole process.

### 6.1.2.1 Results and discussion

A typical transmission signal for the polyester fibre during the deposition experiments is shown in Figure 6.5. The first part of the graph represents the transmission signal of the fibre in air. At point (a) a suspension droplet, in this case a droplet of 0.3 $\mu$l volume, was deposited onto the fibre. This causes a sudden decrease of the transmission signal. The signal then stabilises over a period of several minutes (b) before a further decrease in intensity occurs, which is typically larger than that due to initial drop deposition, (c) [4]; the change indicated by (d) is due to the fibre being cleaned at the end of the experiment.

The pattern of the light intensity signal can be understood using the picture of the deposition process observed via videomicroscopy. As soon as a suspension droplet is deposited onto the fibre, the droplet spreads out on the fibre until an equilibrium state is reached. Therefore, the first reduction in intensity is due to the replacement of fibre-air interface by fibre-suspension interface over the droplet contact area. Since the refractive index of the suspension is higher than that of air one would expect a decrease in total transmitted light. So far, this picture is quite similar to that of the evaporation of a drop of pure water in Figure 4.7. However, the particles in the suspension will come into play and thus alter the picture of the evaporation. The subsequent changes in the transmission signal are dominated by the particles.

After the suspension droplet has reached its equilibrium state according to Young's equation, the contact line of the drop is pinned and the wetted area with the fibre remains constant during a considerable part of the evaporation time. This is reflected by the stable signal between (a) and (b) in Figure 6.5. According to the evidence of the deposition process from the video camera in the previous section, the particles will deposit themselves at the contact line. The rate of the deposition should be a power law and therefore one would expect an ongoing decrease in intensity. However, since there is still water remaining, it is likely that a water film will be trapped between the deposited particles and the surface of the fibre. Hence the fibre optically still sees the wetted area by water instead of particles. The second sudden decrease in intensity, indicated by (c), can be attributed to the evaporation of water film. When it has completely evaporated the fibre suddenly becomes exposed to the particles, which have a higher refractive index than the suspension, and this causes more light to leak out of the fibre; this is indicated by the sharp drop in transmitted light as shown in Figure 6.5 by (c). The refractive index of the particles is in fact very close to that of the polyester fibre, and therefore, causes far higher attenuation of the transmitted signal despite the covered area by the particles being less than the wetted area of the initial drop. Finally, the transmittance recovers to its original

level when the particles are removed from the fibre surface at time (d) by wiping with a cotton bud.

Further investigation of the characteristic response in Figure 6.5 was made and the relationship between covered area, due to the droplet and due to the particles, and light attenuation was investigated. At first the effect of the wetted area by the suspension drop on the light transmission was analysed. Drops having volumes between 0.1 and 0.5 µl were deposited onto the fibre using a particle concentration of 0.5 %. The initial fall in intensity $\Delta T_w$ and the total difference in intensity $\Delta T_p$, defined in Figure 6.5, were determined. The initial wetted area of the fibre by the suspension drop was obtained by analysing video images using a program written in C combined with the Image Tool image processing software. A short description of the program was described in the experimental development section. The results for $\Delta T_w$ and $\Delta T_p$ as a function of the wetted area of the fibre are shown in Figure 6.6.
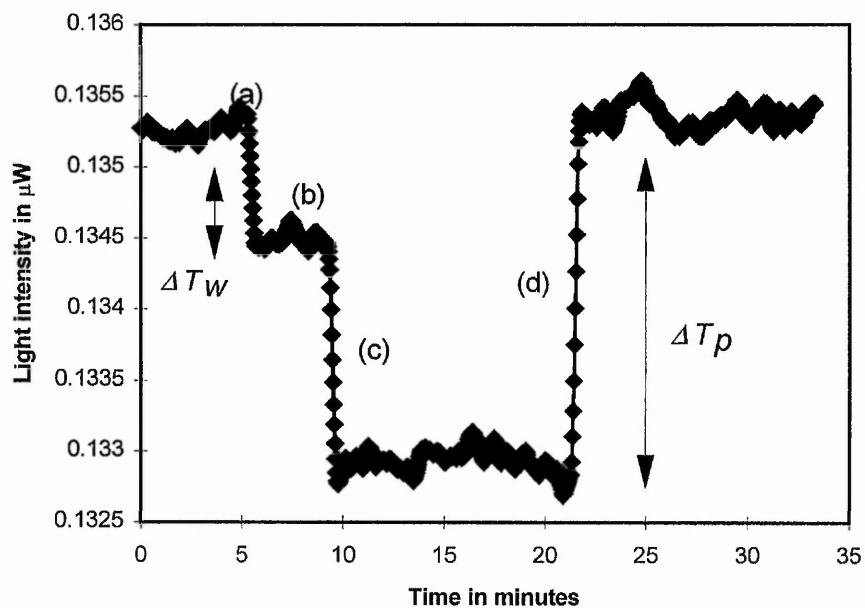
Figure 6.5. The effect of the deposition of particles on light transmission: (a) deposition of suspension droplet, (b) evaporation of droplet, (c) deposition of particles during final stages of evaporation, and (d) recovery of transmitted intensity after particles are cleaned from fibre.
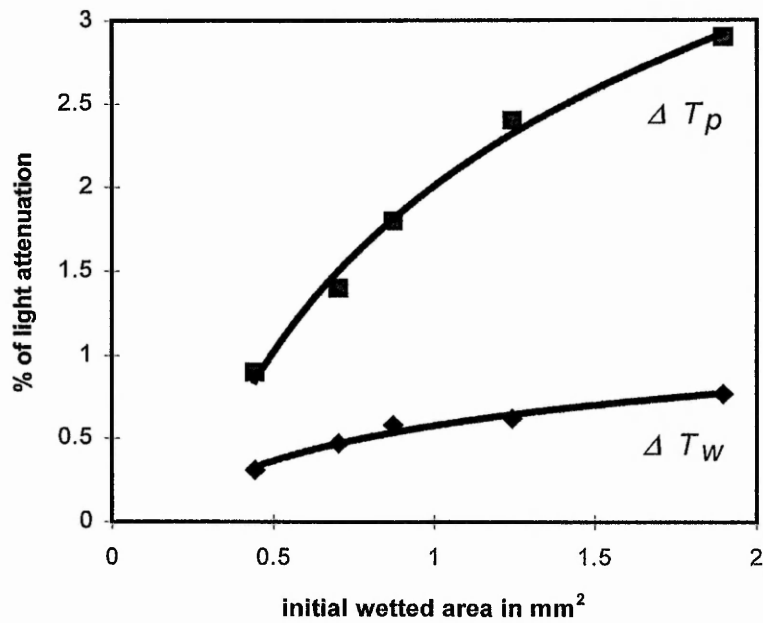
Figure 6.6. The relationship of the initial wetted area to the reduction in intensity of light transmitted in the fibre. The two curves correspond to percentage changes in $\Delta T_w$ and $\Delta T_p$ indicated in Figure 6.5.

Figure 6.6 indicates that in both cases increasing the area of the fibre covered causes a systematic increase in the percentage of light loss. Furthermore, it seems that the attenuation caused by the particles is far greater than that due to the suspension despite the fact that the particle covered area is much smaller than the wetted area. This again illustrates the effectiveness of the latex particles in causing light to leak out of the fibre. The model suggested in the theory chapter, indicates that light travelling through the fibre suffers attenuation due to intrinsic absorption of the fibre material, incomplete reflection at the fibre walls and complete loss from the fibre due to the fibre-exterior refractive indices no longer satisfying the condition for total internal reflection. Deposition of a suspension drop on the fibre causes two types of changes in the light transmission. Firstly, the range of angles undergoing total internal reflection is reduced and secondly the reflection coefficient at the fibre wall decreases. Therefore, the area wetted by the suspension will still act as a light guide, though one that is less effective. In contrast, areas of the fibre in contact with particles will no longer act as a light guide, but will become windows through which any rays arriving at that location will be leaked out of the fibre completely.

By considering the video images of the particle deposition pattern, one can see that most of the particles are concentrated in the ring-stain. Therefore, the initial wetted area of the suspension drop and the area of the fibre in contact with the particles after all fluid has evaporated are not equal. To obtain the actual area covered by the particles, images showing the ring-stain were captured and its area was determined using the C program and image processing software. The previous experiments were repeated and the data for the volume of the suspension droplet, the width $w_r$ of the ring stain, and the attenuation in light intensity, $\Delta T_p$, were recorded. The results are summarised in Figure 6.7.
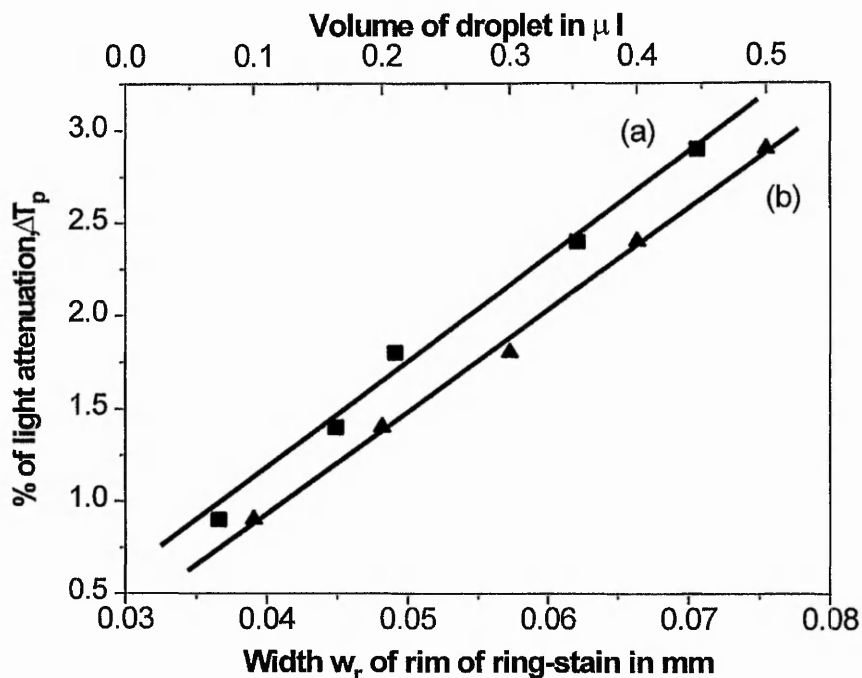
Figure 6.7. The relationship between both the width, $w_r$, of the rim of the ring-stain (curve (a), referred to the lower x-axis) and the volume of droplet (curve (b), referred to the upper x-axis) and final loss in light intensity, $\Delta T_p$. For the concentration and drop size ranges studied, the fractional change in light intensity is proportional to the number of deposited particles. Particle concentration was 0.5 %.
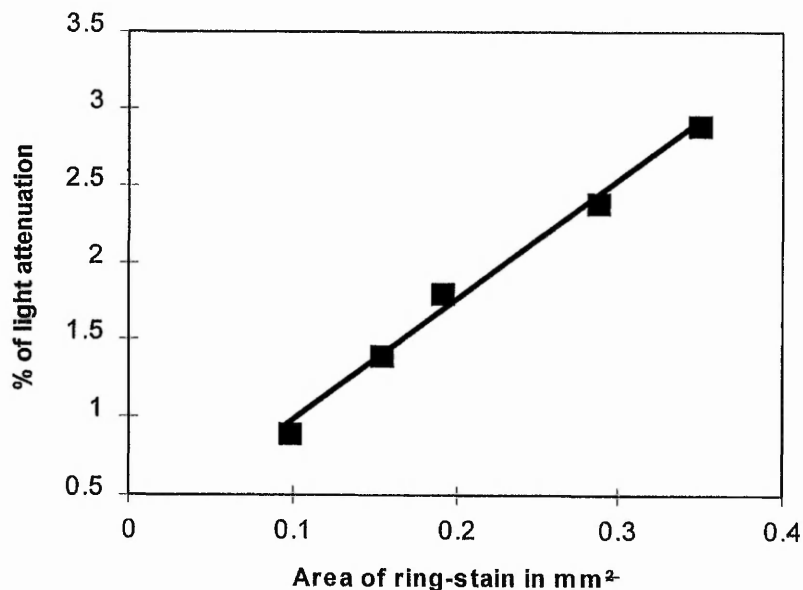


Figure 6.8. The relationship between the area of the ring-stain and the final light attenuation $\Delta T_p$.

Figure 6.7 shows a linear relationship between the width, $w_r$, of the ring-stain and the reduction in light transmission. Images of the ring-stain suggest that more than 80 % of the estimated area covered by particles is within the rim, so that approximately the ring area can be considered as the total covered area by the particles. The linear relationship of curve (a) suggests that the loss in transmitted light intensity is proportional to the area covered by particle deposits (Figure 6.8). However, since it can not be guaranteed that the thickness of particles deposited in the rim is uniform, it is not strictly correct to convert this to a coefficient relating the light attenuation to the number of particles deposited. However, the linearity of curve (b) in Figure 6.7 indicates a linear relationship between light attenuation and the volume of the initial suspension drop, which is in fact proportional to the number of particles deposited.

Comparing Figure 6.6 - 6.8, one can see the effectiveness of the deposited particles in reducing the light transmission. The loss in transmission due to the latex particle deposition is far greater per unit area than that due to the area wet by the suspension containing the particles.

Photographs of the latex particles on a glass substrate were made using an optical transmission microscope revealed that they are very close to an ideal spherical shape. This would suggest that the area of the ring-stain is not the true contact area between the particles within the ring-stain and the fibre. Consider Figure 6.9, which illustrates the expected relationship between a spherical particle on a flat substrate and the true contact area. The curvature of the surface of the 800 μm polyester fibre is far lower than that of a 1.9 μm spherical particle and, therefore, the surface of the fibre can be considered close to a flat surface.
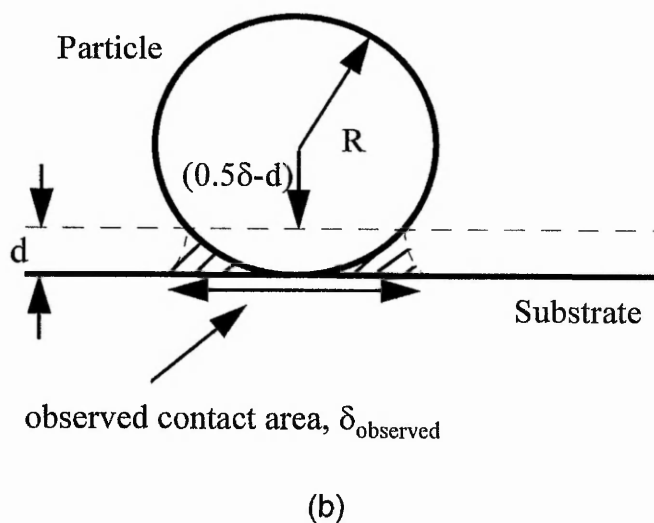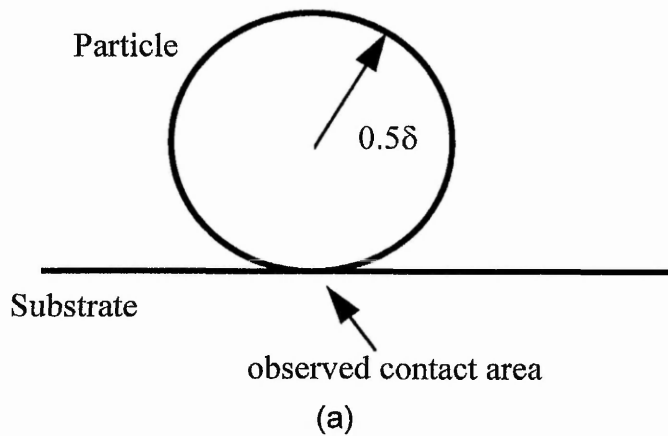
Figure 6.9. Contact area between a spherical particle and a flat surface (a). Schematic view for the determination of the contact area. d is the penetration depth of the evanescent wave field out the fibre.

The 1.9 $\mu$m polystyrene latex particles were too small to visualise the contact area accurately under the normal optical microscope. It was decided that a particle suspension of the same type, but with larger particle diameter should be used. Images obtained from the microscope are shown in Appendix 4, for a range of particle sizes, 3.15, 5, and 10 $\mu$m. It was not feasible to use a polyester fibre or thin film as the substrate, as no picture of the contact area could be obtained by the microscope due to the optical properties of polyester. Therefore, the particles were dried onto a microscope glass slide. A transmitted light arrangement was used and the photos of the contact area of the particles were taken, where the contact area appears as white dots. By having the three sizes it is possible to estimate the behaviour of the 1.9 $\mu$m particles under investigation. The observed contact area of the particles shown in Appendix 4 with the glass slide is given in Table 6.1, where $\delta$ is the particle diameter, $\delta_{observed}$ is the observed contact diameter with the substrate (not to be confused with the penetration depth in the QMC technique), and $\zeta$ is the ratio of the cross-sectional area of a particle and the observed contact area. It is believed that the contact area of latex particles on flat polyester substrate would be larger than on glass, due to the material properties. However, the fact that the particles were deposited onto a cylindrical surface may reduce the discrepancy. Therefore, to a first approximation the contact area may be valid for these simplified purposes.

| $\delta$ in $\mu$m | $\delta_{observed}$ in $\mu$m | $\zeta$ |
|---|---|---|
| 10 | 2.8 | 12.76 |
| 5 | 1.6 | 9.77 |
| 3.15 | 1.0 | 9.92 |
| 1.9 | ~ ? | ~10 |

Table 6.1. The relationship between particle diameter and observed contact diameter and the ratio of particle cross-sectional area and observed contact area.
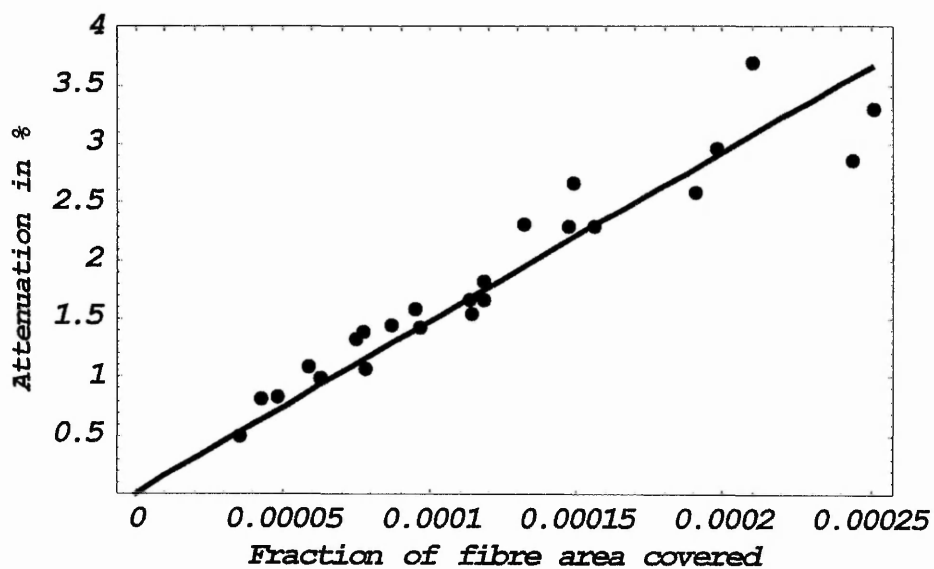
Figure 6.10 Comparison of experimental and theoretical data of the light attenuation vs. the covered area of the fibre by latex particles. Dots mark the experimental data with an area scaling factor of 10 and the solid line represents the theory.

Assuming the value of $\zeta = 10$ for 1.9 $\mu$m, the contact area of the particles with the polyester fibre can be determined. Combining the experimental data with that of the model from the Mathematica program, the diagram illustrated in Figure 6.10 can be obtained. In Figure 6.10, the dots represent the experimental data while the solid line the theoretical data for fitting parameters of, $\Theta = 30\ °$, $n_f = 1.55$, k = 0.0004, $\alpha = 100\%$ per m, $L = 14$ cm, $d = 800$ $\mu$m. Although, the light guiding model is strictly only valid for meridional rays it is quantitatively in good agreement with the experimental results. The reason for the larger scatter in the experimental data as the area coverage increases, is that area determination becomes less precise as the curvature of the fibre becomes more important. This is reflected in the quality of the captured picture of the fibre-particle system and in the subsequent calculation to estimate the area of coverage.

The evaporation experiments were extended to larger particle sizes of 3.15, 5 and 10 $\mu$m. Results for 3.15 $\mu$m particles are difficult to interpret, because they differ slightly in their material properties, though they are of uniform size. The 3.15 $\mu$m particles are composed of polymethacrylate additionally to polystyrene. Furthermore, they do not contain encapsulated dyes unlike the other particle sizes studied in this investigation. A typical graph obtained from the evaporation experiment of a 3.15 $\mu$m particle suspension drop on polyester fibre is shown in Appendix 5. The 5 $\mu$m and 10 $\mu$m particles are identical to the 1.9 $\mu$m particle except for their sizes. However, the transmission data for the 5 and 10 $\mu$m latex particle suspension showed hardly any attenuation when used in the evaporation experiments. To illustrate the findings the effect of the evaporation of a 10 $\mu$m latex particles suspension drop on the light transmission in polyester is shown in Appendix 6. This was at first very surprising. However, the behaviour can be explained by using Figure 6.9(b). One can estimate the contact area of a particles by considering a penetration depth of the EW field outside the fibre. In this case, however, it is more convenient to use the data in Table 6.1. Assuming that the mass concentration of the particles is the same for all particle sizes in a suspension of given volume, one can relate the number of particles, $n_i$ , to their

radii, $R_i$, for any drop

$$V = n_i \frac{4}{3} \pi R_i^3 \tag{6.1}$$

The constancy of volume and mass concentration then gives the ratio of numbers of particles in two drops as,

$$\frac{n_1}{n_2} = \left( \frac{R_2}{R_1} \right)^3 \tag{6.2}$$

Therefore, the total contact area for particles with a radius of $R_1$ is given by

$$A_1 = n_1 R_1^2 \pi \zeta^{-2} \tag{6.3}$$

and for particles with a radius of $R_2$, assuming $\zeta$ is constant for particle size ranging from 1.9 μm to 10 μm,

$$A_2 = n_1 \left( \frac{R_1}{R_2} \right)^3 R_2^2 \pi \zeta^{-2} \tag{6.4}$$

Combining equations (6.3) and (6.4) gives

$$\frac{A_2}{A_1} = \frac{R_1}{R_2} \tag{6.5}$$

Defining the attenuation caused by 1.9 μm as 1, the attenuation factor, assuming it is proportional to covered area caused by the larger particles can be estimated as shown in Table 6.2.

| Particle size δ in μm | Attenuation factor (normed) |
|---|---|
| 1.9 | 1 |
| 3.15 | 0.60 |
| 5 | 0.2 |
| 10 | 0.1 |

Table 6.2. The relationship between particle size and the normed attenuation factor of light transmission. Solid mass of all suspensions is equal.

From the table it is clear why there was hardly any attenuation of light transmission when a droplet of 10 μm latex particle suspension was used in the evaporation experiments. The factor of 0.1 is sufficiently small that noise is

significant and any changes could not be reliably identified.

Although the evaporation experiments gave reproducible results which could be interpreted as shown in this thesis, they are limited to the ring-stain deposits. Uniform deposition of particles on the fibre surface could not be obtained with this method. Furthermore, it can not always be guaranteed that the rim will consist of a uniform monolayer of particles. A method where deposition of particles occurs in a uniform thickness layer would be of benefit for future investigations. El Bediwi et al reported that a uniform particle layer could be achieved by using a dipping method [5]. This would enable the relationship between the thickness of particle deposition and light attenuation to be broadened and the work presented in this thesis to be extended.

In Chapter 4, the fibre transmission signal (Figure 4.7) and the quartz crystal response (Figure 4.15) to the evaporation of a water droplet were given. The signals showed similar trends with large initial response on drop deposition, followed by a constant period and a final return to the initial signal values. The QCM method complements the transmission technique by giving a known distance of interaction in liquid, which is the acoustic penetration depth which is dependent on the frequency used and the viscosity and density of the liquid. These quantities are normally accessible and therefore, the penetration depth for each individual system can be calculated. With the light transmission technique the interaction distance is dependent on the wavelength of light used, its angular distribution within the fibre, the fibre material properties and the liquid. However, the angular distribution is difficult to determine. Finally, with the QCM one can obtain a direct measure of the mass deposited and that should enable one to check the sensitivity of the light transmission technique. Therefore, the investigation of the latex particle described above was repeated using the QCM method.

### 6.1.3 Quartz crystal microbalance

After the QCM arrangement had been tested on a one phase system, water, and the system gave similar results to those reported in the literature [6-9], the study has been extended to particle suspension drops. The investigation of the latex suspension includes the volume of the evaporated drops and the particle size.

### 6.1.3.1 Results and discussion

A typical pattern of the crystal characteristics during the evaporation of a drop of 0.5 $\mu$l of 1.9 $\mu$m latex particle suspension is given in Figure 6.11. The frequency, 6.11(a) of the crystal shows a similar pattern to the signal obtained from the optical transmission experiments. The frequency decreases instantaneously when the drop is deposited onto the crystal. It then stabilises and decreases only very slowly in time, before it drops suddenly to a much lower level. The second decrease is normally much larger than the first and is caused by the deposition of particles. In the final stages of the diagram one can see that the frequency of the crystal reaches an equilibrium which is constant with time. The crystal conductance, Figure 6.11(b) follows a different pattern. It decreases suddenly when the suspension drop is deposited, followed by a slower decrease that then turns into a drastic fall. This is followed by an increase and a recovering to its previous level prior to the deposition of the suspension drop.

The deposition of the suspension drop causes the frequency and the conductance of the crystal to decrease since an additional response arises due to the viscosity-density product of the liquid in the wetted area in contact with the electrode (part (I) of both graphs). The damping of the shear wave by the liquid causes the sudden decrease in crystal conductance. The horizontal part of the graphs, part (II), marks the evaporation process of the liquid. At this stage the particles approach close to the gold electrode which leads to an increase in the viscosity-density product within the penetration depth and therefore, causes higher damping of the crystal energy. (It should be noted that the density of latex particles (1.05 g cm$^{-3}$) and water (1.0 g cm$^{-3}$) are very close, so that to a first approximation only the viscosity within the penetration depth of the shear wave

changes due to particle deposition. This is valid for all experiments with latex particles. It is believed that at this stage the particles are not necessary rigidly coupled with the electrode since water is still present which will act as a layer between the particles and the gold surface, so-called water bridges. In the final stages of the drying process, these water bridges will be removed by evaporation. The surface tension of the evaporating water starts to pull the particles closer to the surface of the gold electrode which will cause higher damping of the crystal energy, 6.11(b) (III). Furthermore, with the removal of the water bridges between the particles and the crystal, the solid particles are acting more and more as a rigid mass and a sharp decrease in frequency is expected, which can be seen in 6.11(a) (III). When all the water has disappeared the particle system is acting solely as rigid mass layer and therefore, no dissipation in crystal energy can be observed (IV) compared with the value prior to the deposition, however, a measurable frequency shift which is proportional to the deposited mass arises (IV).
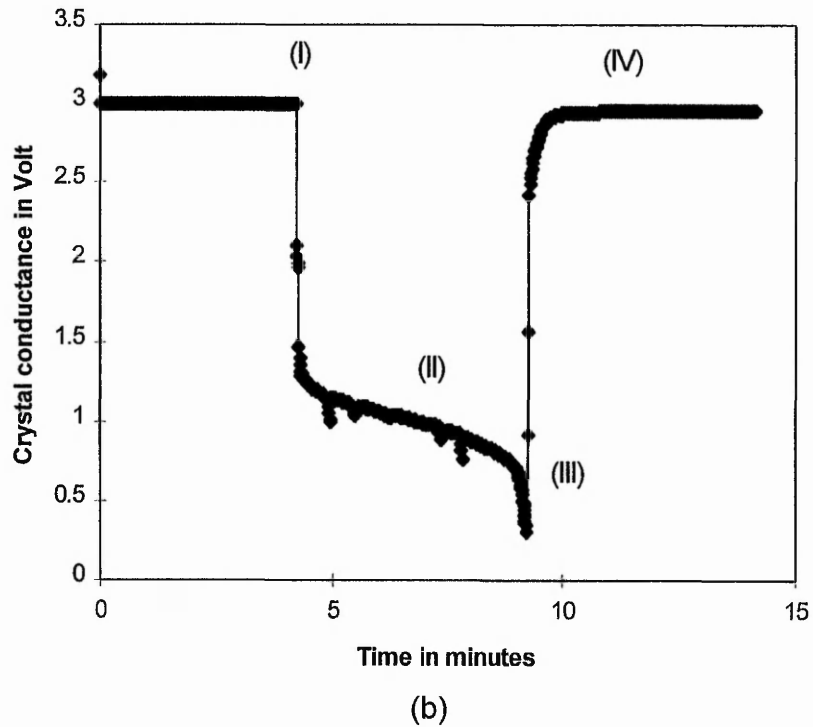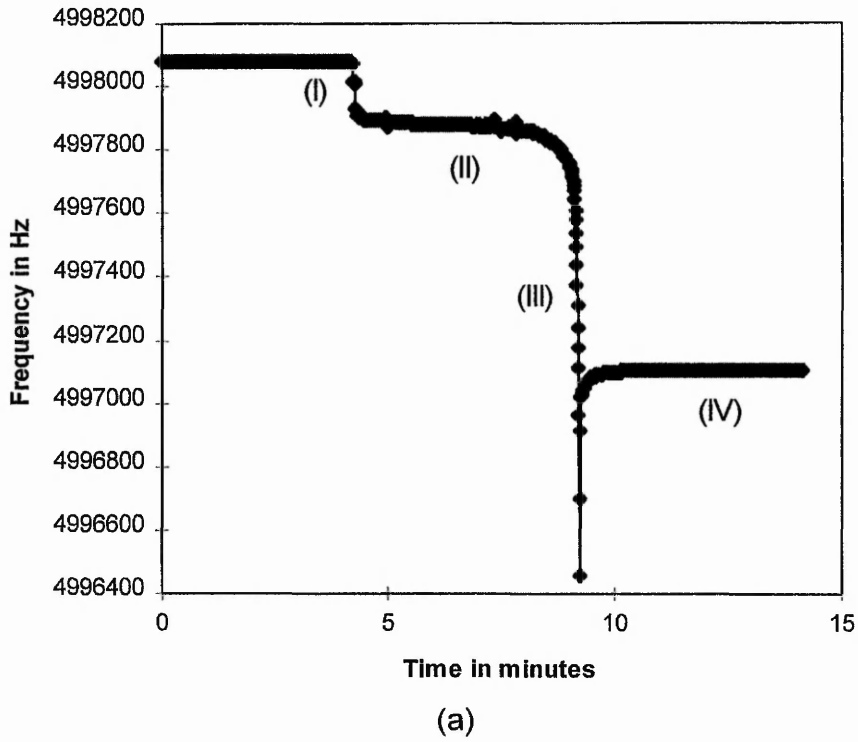
(a)



(b)

Figure 6.11. The evaporation of a droplet of 0.5 μl of 1.9 μm latex particle suspension on rough crystal. (a) frequency signal, and (b) crystal conductance signal.

Figure 6.12 shows equivalent data for the larger particles (3.15, 5, and 10 $\mu$m, all 1 % solid contents). Figure 6.12(a) illustrates that the frequency signal decreases instantaneously when the drop is deposited onto the crystal surface. The decrease in signal is of similar size for all three sizes of particle diameter. This suggests that the number and the size of the particles in the suspension do not significantly vary the contact angle of the drop on the crystal surface, which was confirmed by videomicroscopy, thus the contact area is quite similar for all three suspension drops. Furthermore, the signal shows a second sudden decrease in frequency when the particles plate out onto the crystal surface. The final change in the frequency signal is size dependent with the largest size of particle causing the largest fall in frequency and the smallest size of particle the smallest fall. As shown above, the 1.9 $\mu$m particles present on the crystal surface after complete evaporation obey the rigid mass view, where the frequency shift is directly proportional to the mass deposited, whilst no dissipation of the crystal energy is recorded. However, from Figure 6.12 (b) one can see that for 5 $\mu$m and 10 $\mu$m particles considerable dissipation arises. The 3.15 $\mu$m size gives some dissipation, however these particles are closer to a rigid mass view compared with the larger ones.

From the conductance data shown in Figure 6.12(b), one can see that the deposition of the suspension drop causes a sudden fall in the signal for all three sizes of particles to a comparable level. This decrease is caused by the change in viscosity-density product from air to water. After the sudden decrease the signals fall very slowly to a smaller value. A possible explanation therefore is that the particles are sinking down towards the crystal surface, thus increasing slowly the viscosity-density product and therefore, causing a dissipation of the crystal energy. Finally, the particles are dried onto the crystal surface and it is this stage that marks whether one has a rigid mass view or not. For the 3.15 $\mu$m size the crystal energy increases to a value near its original prior to the deposition of the suspension drop indicating an almost rigid mass view. However, a measurable dissipation of the crystal energy still exists. For the larger particles (5 and 10 $\mu$m)

there is a considerable dissipation of the crystal energy for the dried particles case, therefore, they cannot be interpreted within a rigid mass view.

The larger particles may be only loosely bound to the gold surface and, therefore, possess some viscoelasticity, which would be expected to cause higher damping of the shear wave energy. The degree of contact between the gold electrode surface and the particles may determine the viscoelastic behaviour of the particles. Figure 4.12 shows that the unpolished gold surface is scattered with craters whose widths are around 2 $\mu$m. Larger particles therefore are only loosely bound to the surface, whereas the 1.9 $\mu$m particles can fill in the craters and will be much more strongly bound to the surface and hence conform more to a rigid mass interpretation. Consequently, the downward shift in frequency for particles larger than 1.9 $\mu$m cannot so easily be related to the mass deposited onto the surface of the crystal.

The investigation of the deposition of monodisperse size latex particles onto the quartz crystal via evaporation gives reproducible results which can be related to the video observations of the evaporation process. To investigate the system further a more industrially relevant system was studied. Clay particle suspensions differ from the idealised latex system in that the clay particles are not of uniform size. Rather, they have a size distribution which is shown in Figure 4.8. Additionally, the shape of the clay particle is not spherical but plate-like and this was expected to complicate the interpretation of the signals. However, the clay system has a direct relevance in application to the detergency, which the uniform size latex system does not. The investigation into the clay particles was carried out first with the light transmission technique.
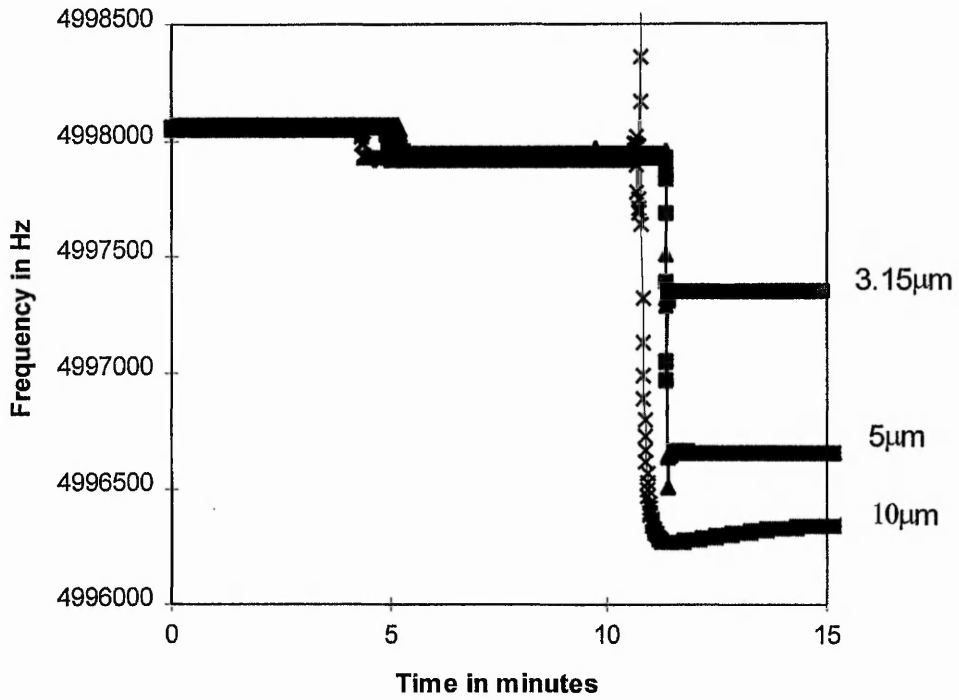
(a)
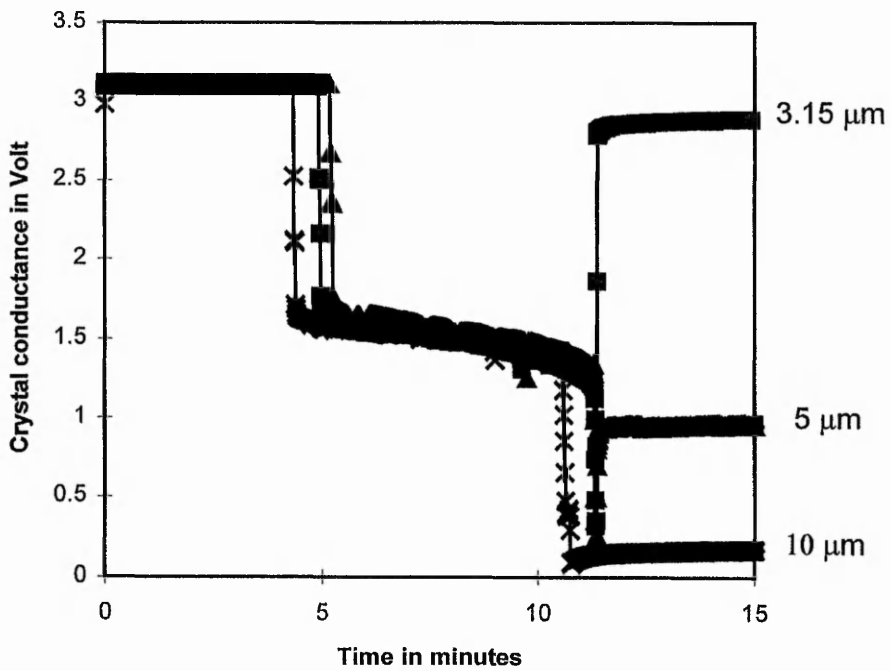


(b)

Figure 6.12. The evaporation of a droplet of 0.5 μl of 3.15, 5, and 10 μm latex particle suspension on rough crystal, particle concentration 1% solids. (a) frequency signal, and (b) crystal conductance signal.

## 6.2 Deposition of clay particles

After the investigation with the model system of monodisperse spherical latex particles, which has shown that the light-guiding method can monitor the deposition behaviour of small particles, it was decided to study a possible application of the method to a system of interest to the detergent industry. The clay particle system can be used in detergency to overcome the redeposition problem that occurs during washing by depositing a layer of clay particles onto the fibres during the washing cycle. This clay layer would prevent already removed soil being redeposited onto the fibre surface. During the last rinsing cycle the protecting clay layer would then be removed from the fibres to give a clean surface.

### 6.2.1 Light transmission technique

### 6.2.1.1 Experimental procedure

The procedure for the clay deposition experiments was similar to the one described for the latex system. A section of 14 cm of 800 μm polyester fibre was mounted between the laser diode and the detector box, after its ends were polished to ensure that the surfaces were smooth for good coupling of light into the fibre. The laser beam was then focused onto one end of the fibre and the output maximised at the lock-in amplifier.

The clay particle suspensions were obtained by dispersing dried montmorillonite particles in distilled water. 0.2 % NaCl was added to enhance the break up of the particles, thus stabilising the suspension. It was found that the prepared suspensions were stable, typically for 24 - 48 hours.
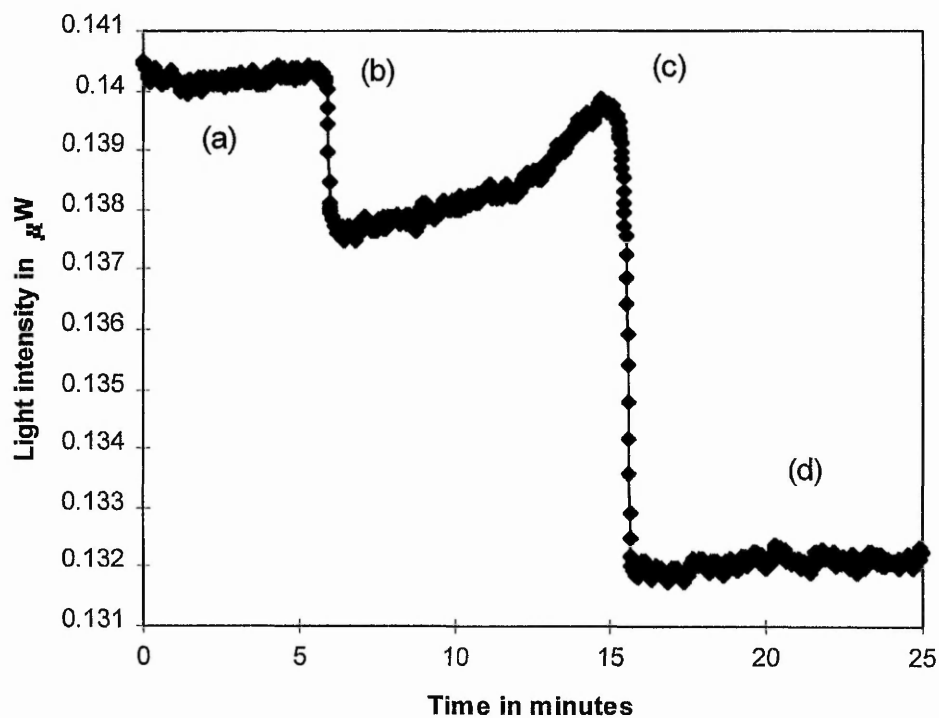
Figure 6.13. The effect of the deposition of droplet of clay suspension onto the 800 μm Polyester fibre surface on the light transmission intensity. The drop volume was 0.5 μl, solid concentration 2 g l$^{-1}$ and 0.2 % NaCl.

### 6.2.1.2 Results and discussion

The study of the clay particle suspension was based on the experiments of the latex system with the expectation that comparisons could be drawn between the two different systems. Therefore, the same experimental procedure was followed. The study of the build up of the ring stain was performed. However, the size of the montmorillonite particles was too small for them to be individually visualised under the microscope and reliable quantitative data on the number of clay particles building up in the rim could not be taken. Although video observation of the evaporation of clay suspension indicates that similar mechanisms to those working in the latex case also apply in this system, the ring-stain was not as clearly visible as for the latex case. Whether this is due to the light scattering of the clay particles or its much higher density compared with water, which could lead to a more rapid settling down of clay particles onto the substrate, could not be resolved. To simplify the determination of the area covered by the particles, the concentration was raised to achieve complete coverage of the wetted area by particle deposition from the suspension drop. Therefore, for further discussion the coverage area by the clay particles is assumed to be identical to the wetted area of the clay suspension drop.

Clay suspension drops were deposited onto the surface of the fibre using a micro-syringe. One would expect the transmission signal to have a similar pattern to the latex particles case. In fact, a typical transmission signal for the deposition of a clay suspension drop onto a 800 $\mu$m polyester fibre is shown in Figure 6.13.

During the experiments it was found that the deposited clay particles are very difficult to remove from the fibre surface. A cotton bud soaked with acetone as used in the latex particle case, did not remove the clay particles completely from the surface. Therefore, the removal of the clay particles is not shown in the transmission signal in Figure 6.13, unlike Figure 6.5, since this required more rigorous wiping of the cotton bud which affected the transmission in the fibre itself. Part (a) in 6.13 corresponds with the transmission in air. At point (b) a

droplet of clay suspension has been deposited onto the fibre surface. This causes the signal to decrease instantaneously to a lower level. After a period of a few minutes, which depends on the droplet size, the signal slowly increases, then a second decrease at (c) takes place. After the second drop in signal the transmission stabilises and remains constant with time (d).

The graph of the transmission can be characterised using the known behaviour from the latex case above. Part (a) in Figure 6.13 marks the transmission of the fibre in air, while part (b) the deposition of the suspension drop. Part (c) represents the deposition of the particles onto the surface of the fibre and (d) illustrates the stable signal of dried clay particles on the polyester fibre surface. However, the observed rise in transmission between (b) and (c) is unlike any signal in the latex case. This was surprising since one would expect a constant transmission signal according to the videomicroscopy observation of contact line pinning of clay suspension drops. A possible interpretation of the characteristic rise, which only happened for clay particle suspensions and which became more significant for smaller droplet size, can be achieved by considering a penetration depth of light into the liquid droplet. The penetration depth of two different states of polarisation $d_\perp$ (perpendicular) and $d_\parallel$ parallel to the fibre axis) are given by [11]

$$d_\perp = \frac{2n_{21}\cos\varphi}{1 - n_{21}^2} d_p,$$

(6.6)

and

$$d_\parallel = \frac{2n_{21}\cos\varphi(2\sin^2\varphi - n_{21}^2)}{(1 - n_{21}^2)(\sin^2\varphi - n_{21}^2\cos^2\varphi)} d_p,$$

(6.7)

where $d_p$ is defined by

$$d_p = \frac{\lambda_1}{2\pi\sqrt{\sin^2\varphi - n_{21}^2}}$$

(6.8)

$\lambda_1 = \lambda/n_f$, $\lambda$ is the wavelength of light in vacuum and $n_{21} = n_0/n_f$ where $n_0$, $n_f$ and $\varphi$ are the refractive index of the outer medium, the refractive index of the fibre and the incident angle of light at the fibre wall, respectively, see Chapter 3. For

unpolarised light, the effective penetration depth is given by

$$d = \frac{1}{2}(d_\perp + d_\parallel) \tag{6.9}$$

A plot of the effective penetration depth of light transmitted in a polyester fibre into a water droplet sitting on its surface is given in Figure 6.14. Note that for incident angles $\varphi$ smaller than the critical angle for TIR $\varphi_{crit}$ the penetration depth is not defined since EW field does not exist in this region.

As Figure 6.14 illustrates, the penetration depth of the EW field reaches up to 2 $\mu$m in water near the critical angle for TIR, $\varphi_{crit}$ .Therefore the light transmission method reaches farther into the liquid than the QCM method and hence it can sense changes in the droplet which the QCM cannot. Additionally, the particle size of clay (see Figure 4.8) is also smaller then the penetration depth of the EW field. Therefore, the characteristic rise in the transmission signal, Figure 6.13 between (b) and (c) might be due to the change in contact angle which reduces the effective area covered, within the penetration depth, during evaporation.

The evaporation of 1.9 $\mu$m particle suspension, Figure 6.5, did not show the characteristic rise, since the particles are too large - comparable with the penetration depth - so that any change of the contact line would be masked by the particles. Hence, the signal was constant during the evaporation process. A verification of the interpretation can be offered by the QCM technique. Due to the penetration depth of the shear wave in water, which is around 0.25 $\mu$m, the frequency response of the crystal would show a constant signal during the evaporation. Since the clay particles are larger than the penetration depth, the retraction of the contact line would be masked by the former, see Figure 6.18.
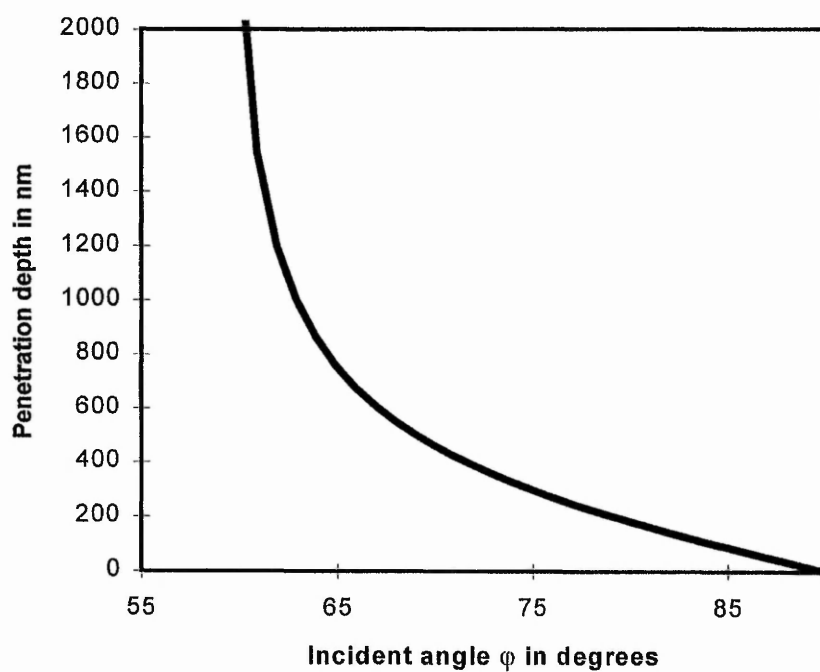
Figure 6.14. Penetration depth of the evanescent light field into the liquid drop (water $n_O$=1.33) sitting on a polyester fibre surface.
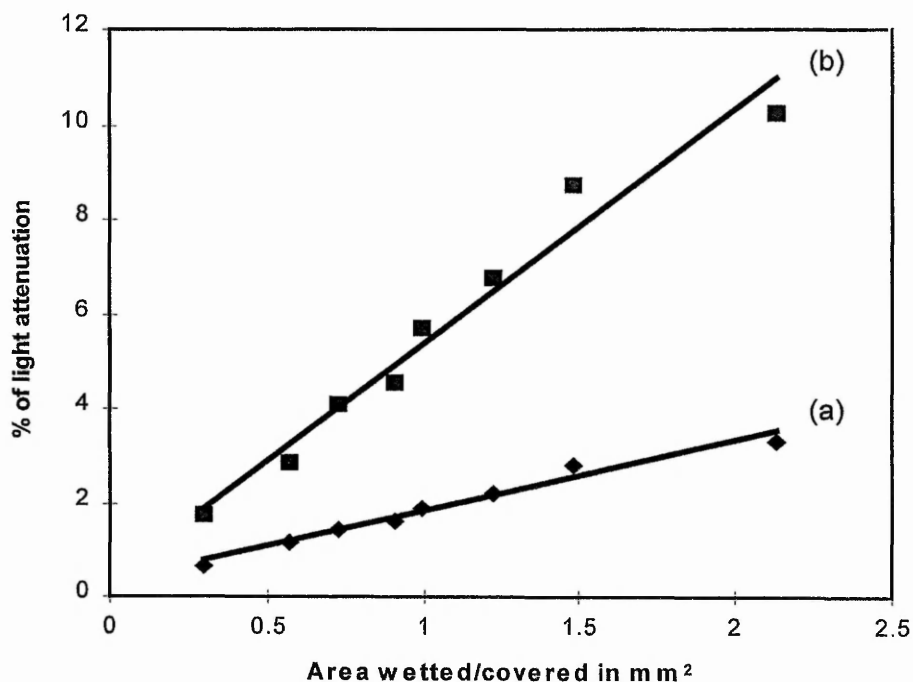
Figure 6.15. The effects of depositing a clay suspension drop onto a 800 μm polyester fibre on the light transmission intensity. Curve (a) represents the attenuation due to the wetted area by the suspension drop; curve (b) due to the covered area by clay particles. The clay concentration was 5 g l$^{-1}$ and the NaCl concentration was 0.2 % w/w.

The evaporation experiments were repeated with a range of drop volumes and concentrations. Droplets with volume ranging from 0.1 $\mu$l to 1.5 $\mu$l were studied. The reason why larger volume could be used was that the equilibrium contact angle of clay suspension drops on polyester fibre was around (77$\pm$2)°, and hence the critical drop volume to ensure a clam-shell type drop is greater than in the polystyrene case. Contact angles of latex suspension drop with polyester were around (63$\pm$2)°. The solid concentration of the clay suspension varied from 1 g l$^{-1}$ to 7.5 g l$^{-1}$. Typical results obtained from the experiments which show the relationship between the area wetted or covered by particles and the light attenuation are given in Figure 6.15. As already mentioned, the concentration of 5 g l$^{-1}$ was sufficiently high in order to give complete coverage of the wetted area by particles.

Figure 6.15 suggests a linear relationship between the wetted area, curve (a) and the attenuation of light transmitted by the fibre. It is also reasonable to claim that the area covered by particles, curve (b), shows a linear relationship with the attenuation of light, although a larger spread of the data can be seen. This might be due to the fact that although the whole wetted area seems to be uniformly covered with clay particles, microscopically this may not be exactly the case. The fact that the clay particles are not perfect spheres, but plate-like so that the orientation of the particles on the fibre surface may play a critical role in determining the effective covered area. Additionally, the refractive index of clay is between 1.55 - 1.57, dependent on the orientation of the particles [10]. Therefore, not only the surface coverage but also the effectiveness of the leakage of light out of the fibre depends upon the orientation of the particles on the surface of the fibre. The complexity of the clay system may account for the spread of the transmission data of curve (b) in Figure 6.15.
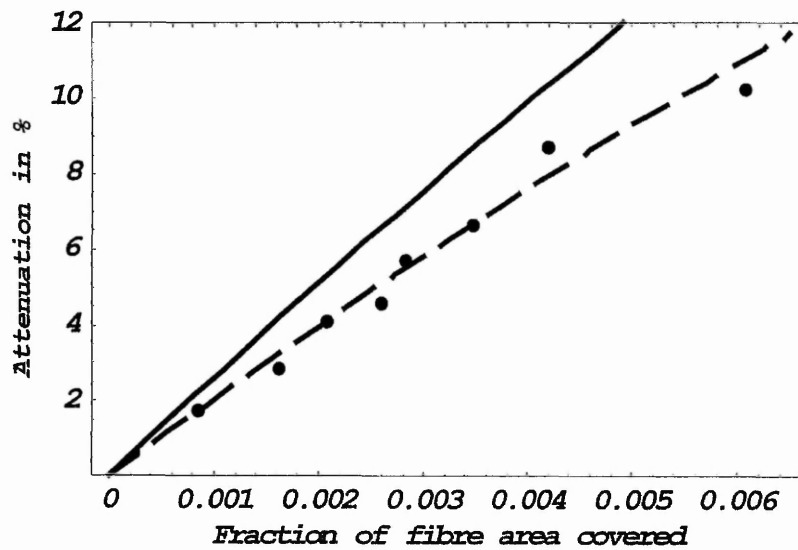
Figure 6.16 Comparison of experimental and theoretical data of the light attenuation vs. the covered area of the fibre by clay particles. Dots mark the experimental data, the solid line ($n_{clay}$ =1.57) represents the theory. A fit can be forced by changing $n_{clay}$ =1.545 (dashed line), which is close to the literature value of 1.55-1.57.

Figure 6.16 shows that the theory and the experimental results are in poor agreement, for fitting parameters of: $\Theta$ =10 °, $n_f$ = 1.55, $k$ = 0.0004, $\alpha$ = 100 % per m, $L$ = 14 cm, and $d$ = 800 $\mu$m. The reasons just mentioned to explain the spread of the experimental data in Figure 6.15 also contribute to the lack of agreement between theory and experiment. An improved determination of the covered area would be needed to interpret further the data and perform an effective comparison to the theory.

After the light transmission signal caused by the deposition of clay particle suspension had been characterised, the focus was drawn back to the QCM technique. It was interesting to see whether the characteristic rise in signal as seen in Figure 6.13, just before (c) would also occur in the frequency response of the quartz crystal. Therefore, the clay experiments were repeated with the QCM technique.

### 6.2.2 Quartz crystal microbalance

### 6.2.2.1 Evaporation of clay particle suspensions on rough crystal

The evaporation of clay particle suspension drops was performed first on the rough crystal. A similar experimental procedure to that of the light transmission method was used.

Typical results of the evaporation experiment are shown in Figure 6.17. The frequency characteristic, Figure 6.17(a), of the crystal is quite similar to that of the evaporation of 1.9 $\mu$m latex particle suspension. After an initial reduction which is caused by the deposition of the suspension droplet, the signal displays a slow fall in the frequency, which then suddenly turns into an abrupt decrease. The characteristic rise which was recorded by the light transmission method does not appear in the frequency signal. After a recovery the signal stabilises at a much lower level than that at the start of the measurement. The conductance of the quartz crystal, Figure 6.17(b), is also quite similar to that of the evaporation of 1.9 $\mu$m latex particles. As soon as the drop is deposited on the crystal the conductance decreases abruptly. It then declines at a much slower

rate. This is followed by a rise back to a level comparable with that prior to the deposition of the suspension drop, indicating that the final response can be interpreted as rigid mass.

The deposition of the suspension droplet causes both the frequency and the conductance of the crystal to decrease because of the wetting of the contact area of the crystal. The clay particles then begin to settle out towards the crystal surface, which causes the slow decrease in both signals due to increasing the viscosity-density product within the penetration depth of the crystal. (Note that for the clay system the increase in density can not be neglected unlike to the latex system; density of clay is 2.5 g $cm^{-3}$). A layer of water acts as a shield between the particles and the electrode surface so that the particles do not have such a significant effect on the crystal at this stage, due to the short penetration depth of the shear wave in water, which is around 0.25 $\mu$m for a 5 MHz crystal resonance frequency. In the final stages of the evaporation, the thickness of water layer becomes thinner and finally falls below the penetration depth. The crystal starts to experience the mass loading effect by the particles, which is reflected by the sharp decrease in the frequency of the crystal, as seen in Figure 6.17(a). The sharp fall of the conductance might be due to reducing of the thickness of the water layer combined with the approach of the particles towards the surface of the gold electrode, causing a sudden increase in the viscosity-density product and hence to dissipate large amount of energy. When all the water has evaporated the particles will be bound to the gold surface and are not able to dissipate any energy from the crystal, so that the conductance will recover back to its original level.

A likely explanation for the overshoot in the frequency graph is that in the final stages of the evaporation, the surface tension of the water will pull the particles closer to the surface of the gold electrode thus enhancing the effect of mass loading. When the water has evaporated the downwards pull is ceased and the particles will recover to an equilibrium distance from the surface of the electrode. Note, that the evaporation of the water layer takes longer for the clay particles

than the latex. This might even be prolonged by the fact that the plate-like clay particles might be undergoing some preferable re-orientation towards one another at this stage. It has also to be mentioned that a corresponding increase in frequency similar to that of the transmission just before the particles were deposited does not arise. This might be due to the short penetration depth of the shear wave in water, meaning that any changes further than 0.25 $\mu$m can not be registered by the crystal.

Comparing the QCM data with the theory given in Chapter 3, the dried clay particles can be represented by a rigid mass case. However, before the relationship between the deposited mass and the frequency shift is drawn, it would be interesting to investigate whether there are any differences between the response from an unpolished and that of a polished quartz crystal. Additionally, some results for the evaporation of latex particle suspension on a polished crystal will be presented in the next section.
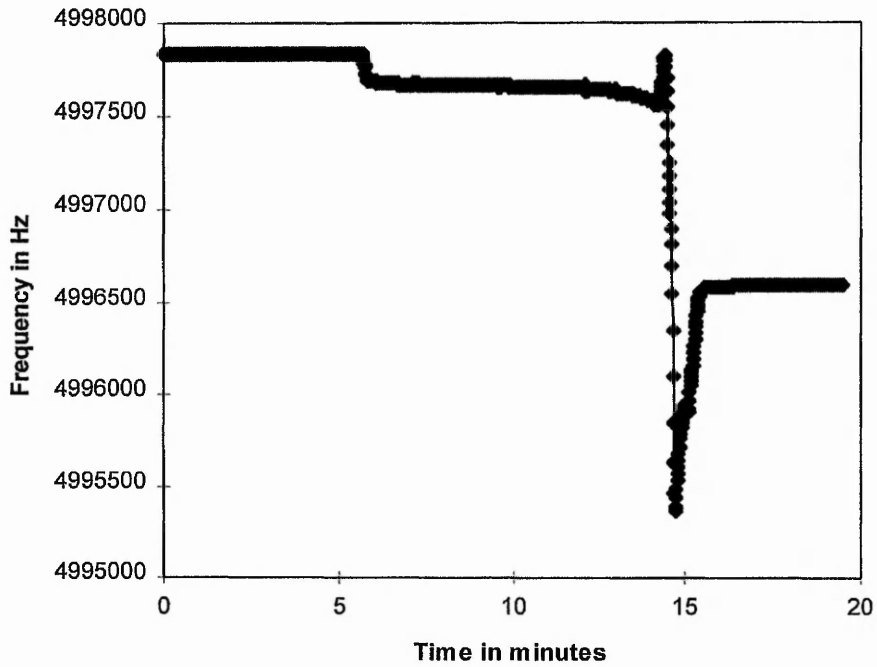
(a)
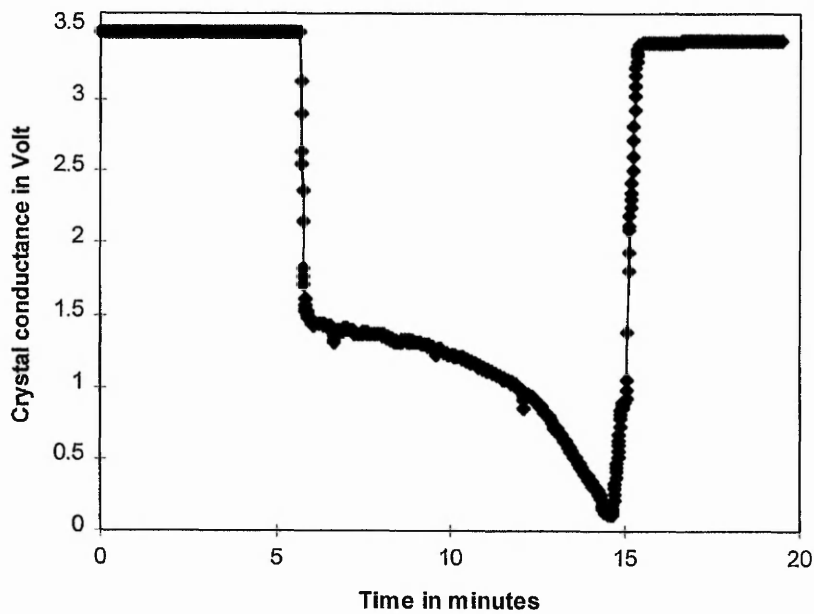


(b)

Figure 6.17. The evaporation of a droplet of 0.5 μl of clay particle suspension on a rough crystal. (a) frequency signal, and (b) crystal conductance signal. Suspension consists of 7.5 g l$^{-1}$ solid, and 0.2 % NaCl.

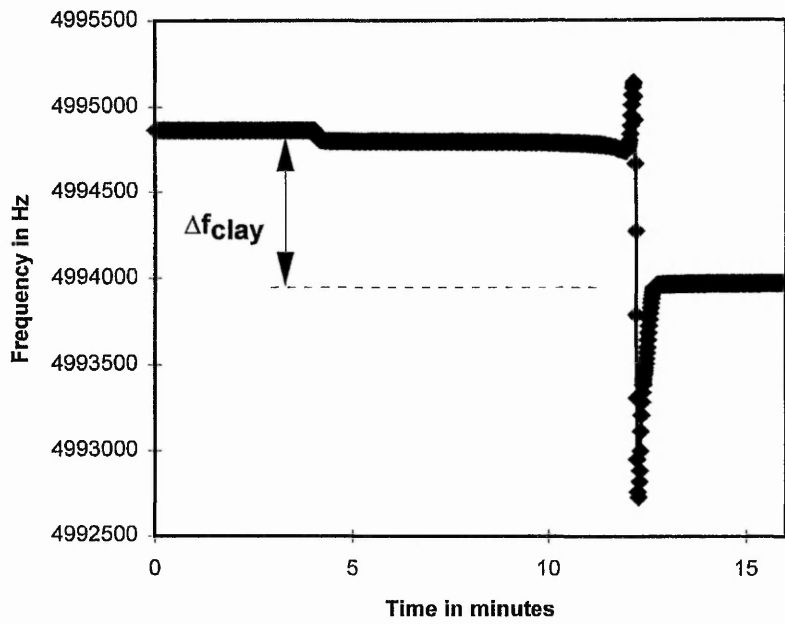## 6.2.2.2 Evaporation of clay particle suspensions on polished crystal

The evaporation of the larger latex particle suspension on polished gold crystals gave no new insights into their behaviour. Crystal responses for these particles were very similar to the ones obtained from the rough crystal. Whilst the interpretation of these results is not yet fully understood, the data nonetheless suggest that larger particle sizes may represent a mass deposition which possesses some viscoelasticity. A possible cause for the viscoelasticity might be the inter-particle locking due to long range interactions as well as the degree of bonding of the particle onto the gold electrode surface.

Results for the 1.9 $\mu$m latex particles and the clay confirmed that the rigid mass interpretation, as shown in Figure 6.18, was appropriate for these cases. The frequency data, 6.17(a), illustrates a sudden fall when the clay suspension drop was deposited onto the crystal surface. This is followed by a constant signal during which the evaporation of the water occurs. Note that the stable signal during the evaporation process confirms the interpretation for the rise, which occurred between (b) and (c) in Figure 6.13. The contact line of the drop is pinned at this stage and a constant contact area is the result, which is reflected by the relatively constant frequency of the crystal. In the final stages of the evaporation, the signal displays a second decrease in frequency due to the drying out of the particles onto the polished gold surface. This is followed by a rise and finally a stabilisation of the frequency. This represents the completely dried particles on the gold surface. It is notable that the drying process does not take as long as in the rough crystal case, since the absence of roughness means less water is trapped between the particles and the gold electrode surface.

Figure 6.18(b) shows the conductance characteristics of the quartz crystal. A large decrease can be seen when the suspension drop is deposited onto the crystal. During the evaporation of the drop the dissipation increases very slowly suggesting the settling out of clay particles, which increases the viscosity-density product within the penetration depth of the shear wave. In the final stage of evaporation the dissipation increases further until it reaches the point where all

the water has evaporated. The conductance data show a very smooth curve during the evaporation stage. This is probably due to the smoothness of the gold electrode surface. When all the particles are dried the crystal conductance recovers to a level very close to that prior to the deposition of the drop, resulting in virtually no dissipation of the shear wave energy.

Since the behaviour of the evaporation of clay suspension drops on rough and polished crystal can be interpreted within the rigid mass view, a relationship between the mass deposited and the frequency shift, $\Delta f_{clay}$, can be drawn. The diagram in Figure 6.19 indicates a linear relationship between the volume of the deposited suspension drop, which is proportional to the solid mass, and the frequency shift of the crystal. An experimental mass loading parameter cannot be obtained from the Sauerbrey equation, since it is only valid when the whole surface of the crystal electrode is uniformly covered, which is not the case in this investigation. However, using the concentration of the suspension one can estimate that micrograms of mass deposition were detected in the experiments. In fact the QCM can be used to detect much smaller quantities of mass loading, in the region of nanograms.

(a)
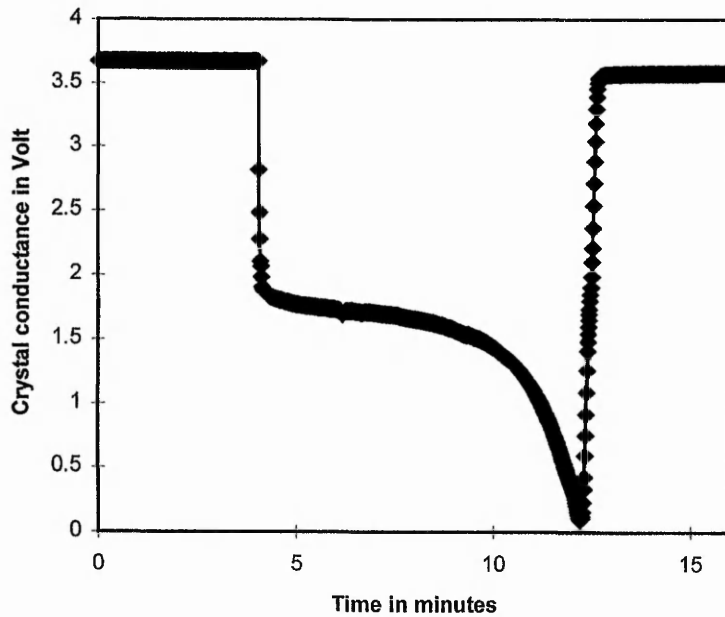


(b)

Figure 6.18. The evaporation of a droplet of 0.5 μl of clay particle suspension on polished crystal. (a) frequency signal, and (b) crystal conductance signal. Suspension consists of 5 g l$^{-1}$ solid, and 0.2 % NaCl.
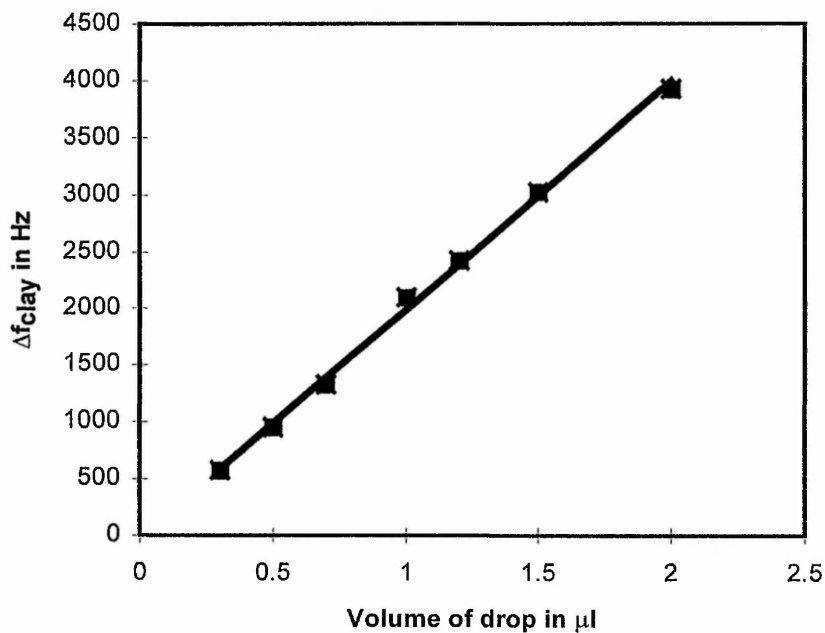
Figure 6.19. The relationship between the volume of the deposited clay suspension drop and the total frequency shift, $\Delta f_{clay}$ (absolute value). Clay suspension contains 5 g l$^{-1}$ solids and 0.2 % NaCl. Polished crystal.

To round up the experimental work a study similar to that of the oil drop deposition from an emulsion, described in Chapter 5, was conducted. This investigation has the aim to study the effects of the concentration of electrolyte on the deposition of clay particles, and to see whether the rate of the deposition of clay particles from an aqueous solution could be regulated by the electrolyte concentration in the latter. This work is of particular relevance to the laundry industry.

### 6.2.3 Deposition of clay particles from aqueous solution

The evaporation experiments above showed that the deposition of clay particles follows the general pattern of that found for small monodisperse latex particles. The clay system is not monodisperse, which is reflected in the spread of the data presented. In the laundry process, the clay particles present in the wash cycle are in a mixture with water, surfactants, and other additives. Therefore, the investigation in this thesis of the deposition of clay particles from an aqueous phase represents a realistic system. The aim of this experiment is to observe whether the rate of clay deposition can be regulated by changing the electrolyte concentration in the aqueous phase. Electrolyte was added to the system to lower the energy barrier $V_B$ in Figure 3.7(d) and to achieve flocculation of the clays. Additionally, due to the presence of electrolyte, the charge effect in the repulsive double layer will be suppressed so that purely van der Waals attraction exists, which would cause a higher deposition rate. It was expected that as soon as the critical flocculation concentration (CFC) is reached the clay particles would flocculate together and be deposited as an agglomeration of particles, which have a larger area than single particles. Therefore, one would expect that the agglomerations would cause far higher attenuation of the light intensity transmitted by the fibre.

### 6.2.3.1 Experimental procedure

The experimental set-up used for the deposition of clay particles is similar to the one used for the emulsion experiments. A glass cell, see Appendix 1, was used to mount the 800 $\mu$m polyester fibre. The glass cell consisted of inlet and outlet

ports, and it was of 15 cm in length and 2.5 cm in diameter. The cell was connected to a peristaltic pump to form a closed pump circuit. Hence the suspension can be introduced into the cell at a controlled rate and any vibrational perturbation of the fibre should be minimised. The electrolyte solution was added into the clay suspension reservoir, which was kept stirred throughout the course of the experiments to ensure a minimum electrolyte concentration gradient in the suspension. The transmission intensity along the fibre and the electrolyte concentration were recorded throughout the experiment.

### 6.2.3.2 Results and discussion

The electrolyte used in the experiments was $La(NO_3)_3$. The first experiments were carried out using NaCl as the electrolyte due to its ready availability. However, the results of the experiments did not show any effects on the light transmission at all when NaCl was added to the suspension, even at its CFC. One reason could well be that the CFC of NaCl is quite high (around 1 mol $l^{-1}$) and this might be sufficiently high enough to affect the whole nature of the deposition process of the clay particles. It was observed that the deposit left on the fibre after the evaporation of a suspension drop, consists of considerable amount of NaCl crystal, which certainly would affect the light transmission itself. A different electrolyte with a much lower CFC was attempted. The CFC of $La(NO_3)_3$ is around 1/1000th smaller than that of NaCl, according to Schulze-Hardy rule [12].

The first study of the deposition was a stagnant experiment, where the clay suspension was pumped into the glass cell in which the fibre was mounted. As soon as the glass cell was completely filled the pump was turned off. $La(NO_3)_3$ stock solution was then added into the cell through a port via a syringe. The clay suspension had a solid concentration of 5 g $l^{-1}$ and 0.2 % of NaCl to stabilise the suspension system. A typical result of the stagnant experiment is given in Figure 6.20.
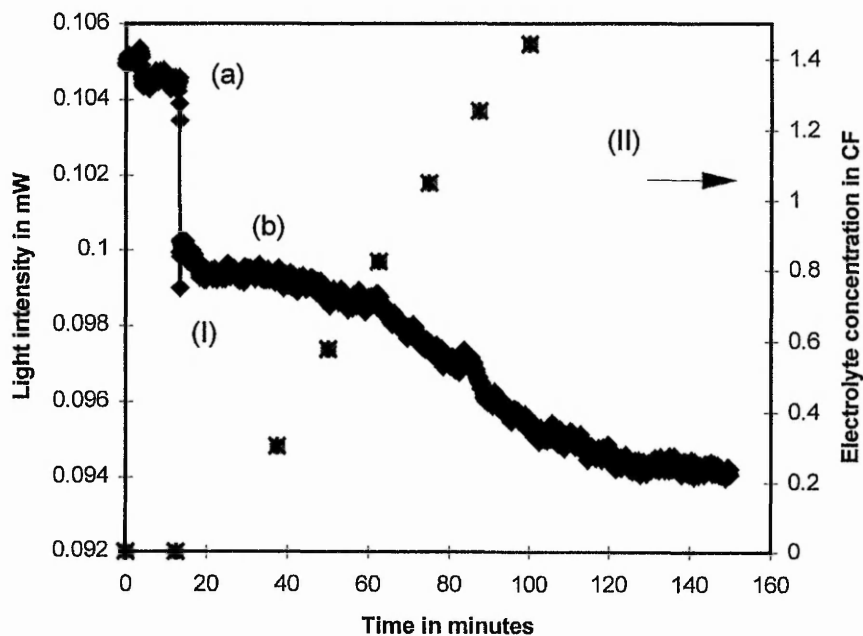
Figure 6.20. The effects of the deposition of clay particles onto 800 μm polyester fibre under aqueous conditions on the light transmission; stagnant experiment. (♦——♦ ) Transmission intensity curve (I) left y-axis, (■) electrolyte concentration values (II) right y-axis. The solid concentration was 5 g l$^{-1}$ and 0.2 % NaCl, electrolyte was La(NO$_3$)$_3$. (a) Attenuation caused by immersion of fibre in emulsion, (b) attenuation caused by deposition of clay particles.

The first part of the graph in Figure 6.20 shows the equilibrium state of the transmission of the fibre in air. As soon as the fibre is fully immersed in the clay suspension the intensity decreases and stabilises itself for a period of some minutes. At around 40 minutes the electrolyte solution is added to the suspension inside the glass cell. The addition of 6.25 mg of $La(NO_3)_3$ continues every 20 minutes until the $La(NO_3)_3$ concentration reaches 1.5 of its CFC. When $La(NO_3)_3$ was first added to the system, no effects could be seen on the light transmission. However, further increase in electrolyte concentration results in a decrease of the transmission intensity of the fibre. Finally, when the addition of $La(NO_3)_3$ is ceased the transmission signal reaches a stable level.

Although it is not very significant, there is a relationship between the electrolyte concentration and the intensity of the transmitted light, as one can deduce from Figure 6.20. The transmission signal is very stable for low $La(NO_3)_3$ concentrations ( <0.5 CFC). At this stage the electrolyte concentration is too low to cause the clay particles to flocculate. However, due to the stagnant nature of the experiments, there may be some concentration gradients in the suspension which cause some particles to flocculate locally. This is shown in the slight decrease of the transmission signal. Further increase in the $La(NO_3)_3$ concentration around the CFC leads the transmission intensity to fall quite considerably. Before the experiments were conducted, it was expected that when the electrolyte concentration reaches its CFC there would be a sudden decrease in light transmission with the flocculation at the CFC. However, the problem with a stagnant experiment is that a zero concentration gradient of the electrolyte can never be ensured and therefore, the flocculation might be happening locally before the CFC is reached. The deposition of the flocculated particles would then decrease the light transmission when deposited onto the fibre. Once the CFC is reached more and more particles are starting to flocculate and some deposit themselves onto the fibre, which causes further reduction in the transmission intensity. Therefore, the light transmission signal in Figure 6.20 which shows a continuous reduction of light transmission can be understood.

Additionally, one has also to consider that the flocculated agglomerations are far heavier than single particles. Therefore, they tend to sediment down to the bottom of the flow cell due to gravitational effects instead of clinging to the fibre, which would account for the relatively small effects on the transmission intensity, shown in Figure 6.20.

The next set of experiments were conducted in a closed pump circuit rather than as a stagnant experiment. The electrolyte concentration of the suspension reservoir is recorded before the suspension is pumped into the glass cell. Naturally, there will be a time offset when the suspension reaches the glass cell (through the tubing). However, this is a method which gives a better control of the overall electrolyte concentration, since the reservoir is stirred throughout the course of the experiment. A typical result of the experiment is plotted in Figure 6.21.

The first part of the intensity signal represents the light transmission of the fibre in air. As soon as the suspension is pumped into the cell and the fibre is immersed the transmission drops. After that decrease, the transmission stabilises although some fluctuations occur in the signal. This may be due to the flow of suspension around the fibre and any fluctuations in the particle concentration. As soon as the electrolyte is added into the reservoir the transmission signal decreases, assuming a time delay (~30 secs) during which the suspension travels from the reservoir into the glass cell. Further addition of the electrolyte causes the intensity signal to decrease even more, until it stabilises at the end of the experiment, when the addition of $La(NO_3)_3$ has stopped.
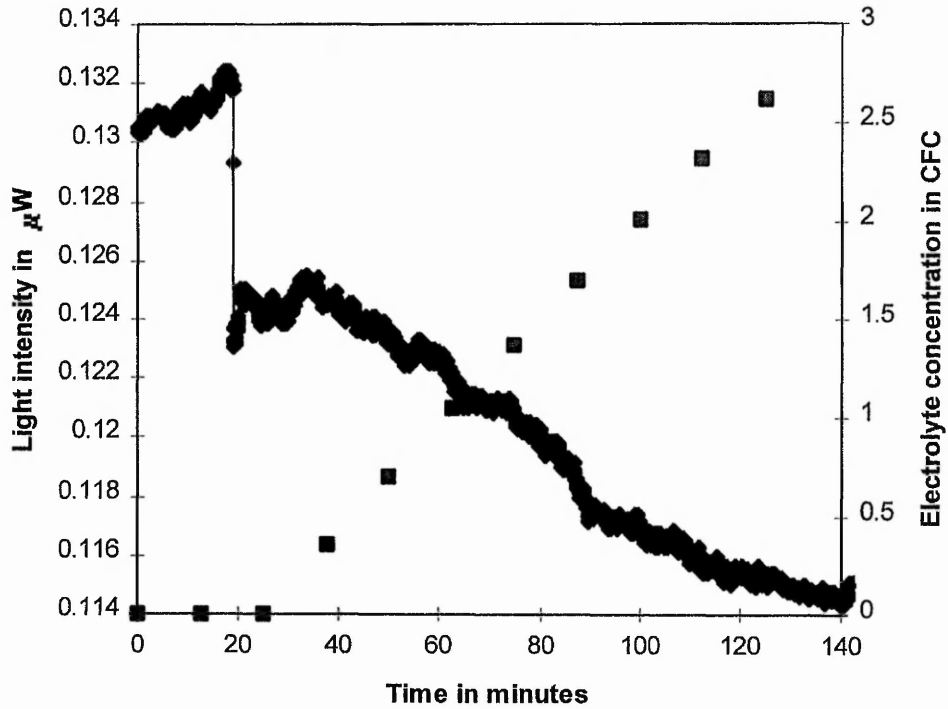
Figure 6.21. The effects of the deposition of clay particles onto 800 μm polyester fibre under aqueous conditions on the light transmission. Closed pump circuit experiment. Clay concentration was 5 g/l solids and 0.2 % NaCl. Electrolyte used was La(NO$_3$)$_3$.

Figure 6.21 suggests that with increasing $La(NO_3)_3$ concentration the transmission intensity decreases. The diagram is very similar to that of the stagnant case and it shows that the greatest rate of reduction in light transmission occurs around the CFC concentration of the electrolyte. Furthermore, it shows that the deposition rate of the clay particles onto the polyester fibre can be enhanced by increasing the electrolyte concentration in the suspension. However, the nature of the experiments limits the deposition, since the surface area of the fibre is quite small, hence, the tendency towards deposition of the agglomerated clay particles onto the fibre is also small. This fact will be further enhance by gravitational effects, which means that agglomerated particles are very likely to sediment to the bottom of the cell. Additionally, the concentration gradient of the electrolyte in the glass cell has a significant effect on the flocculation and it was found quite difficult to eliminate this problem. The CFC is also dependent on temperature and pH value of the suspension and since the experiments were conducted in the open lab environment it was difficult to keep the temperature constant. However, the results of the experiments show that it should be possible to regulate the deposition of clay onto a polyester fibre via the electrolyte concentration in the suspension. It should be noted that the signal would stabilise between the steps of addition of the electrolyte if left long enough to reach equilibrium.

## Summary

In this chapter it has been shown that the light transmission method is not only capable of detecting large fibre area coverage by liquid but also local coverage by small amounts of particles, thus demonstrating its high sensitivity. The evaporation experiments with first polystyrene latex particle suspension, as an idealised system, and then with clay particle suspension, indicate a linear relationship between the wetted or covered area by the suspension drop and the particles respectively, and the light attenuation. Furthermore, the deposition of clay particles onto the polyester fibre from an aqueous phase can be controlled by the concentration of electrolytes in the suspension.

The light guiding theory in fibres described in Chapter 3 has been compared with the experimental results. Agreement of the theory and experimental data was very good for the model system of monodisperse spherical latex particle. For the clay particle system, where many parameters are unknown, no quantitative matching of the theory and experiments has been found. Not only was the size distribution of the clay particles a problem but also their orientation after the deposition process was unknown, which would affect the light transmission intensity. However, the evaporation of clay particle suspension suggested that the penetration depth, which is a fundamental parameter for the sensing mechanism of ATIR, of the EW field in water is larger than that of the QCM.

The QCM technique has been included in the investigation and it provided complementary results to those obtained by the light transmission method. It helped to characterise the process involved when a droplet of suspension is evaporating on a surface. The mass loading, which can be deduced from, and is proportional to the volume of the suspension drop, has a strong linear relationship with the frequency shift of the crystal for the 1.9 μm latex particles and the clays. Practically, no dissipation of the crystal energy has been observed in these two cases, indicating a rigid mass interpretation of deposition. The results for larger latex particles, 3.15, 5, and 10 μm showed both a downwards frequency shift and a dissipation of the crystal energy and thus the results can not be interpreted using a rigid mass view.

The video microscopy plays an essential part in trying to understand the signals obtained in both ATIR and QCM techniques. In this way the processes occurring during the evaporation of a suspension droplet have been visualised. These observations were then related to the signal response of the light transmission and the QCM data. The single fibre light transmission method shows promising characteristics and it can be used to sense surface changes, for example the soil deposition and removal in the detergent industry.

# References

[1] R.D.Deegan, O.Bakajin, T.F.Dupont, G.Huber, S.R.Nagel, T.A.Witten, *Capillary flow as the cause of ring stains from dried liquid drops*, Nature, **389**, (1997), 827

[2] R.D.Deegan, *Pattern formation in drying drops*, Physical Review E, **61**, (2000), 475

[3] R.D.Deegan, O.Bakajin, T.F.Dupont, G.Huber, S.R.Nagel, T.A.Witten, *Contact line deposits in an evaporating drop*, Physical Review E, **62**, (2000), 756

[4] N.T.Pham, G.McHale, M.I.Newton, B.J.Carroll, S.M.Rowan, *Investigation of deposition of monodisperse particles onto fibers*, submitted to Langmuir (2001)

[5] A.B.El Bediwi, W.J.Kulnis, Y.Luo, D.Woodland, W.N.Unertl, Mat. Res. Soc. Sump. Proc., **372**, (1995), 277

[6] R.G.Picknett, R.Bexon, *The evaporation of sessile or pendant drops in still air*, Journal of Colloid and Interface Science, **61**, (1977), 336

[7] K.S.Birdi, D.T.Vu, A.Winter, *A study of the evaporation rates of small water drops placed on a solid surface*, J. Phys. Chem., **93**, (1989), 3702

[8] C.Bourges-Monnier, M.E.R.Shanahan, *Influence of evaporation on contact angle*, Langmuir, **11**, (1995), 2820

[9] L.McKenna, M.I.Newton, G.McHale, R.Lucklum, J.Schroeder, *Compressional acoustic wave generation in microdroplets of water in contact with quartz crystal resonators*, Journal of Applied Physics, **89**, (2001), 676

[10] D.Lide (Ed.), *CRC handbook of chemistry and physcis: a ready-reference book of chemical and physical data*, CRC Press, London, 1995, 76th. Ed.

[11] I.Paiss, D.Bunimovich, A.Katzir, *Evanescent-wave infrared spectroscopy of solid materials usind deformable silver-halide optical fibers*, Applied Optics, **32**, (1993), 5867

[12] J.Israelachvili, *Intermolecular and Surface Forces*, Academic Press, London, 1992, 2nd. Ed.

# Chapter 7: Conclusion and Further Work

This project studied the effects of the soiling process on the light transmission intensity through textile type fibres. Fibres were used as light guides to characterise the kinetics of the deposition of liquid drops and particles via the attenuation of the intensity of light transmitted by the fibre. In the following pages an overview of the project will be given and a summary of the important results will be presented. Finally, some ideas for further development and possible applications of the light guiding method used in this study will be discussed.

## 7.1 Conclusion

The main aim of this project was to investigate light guiding in textile fibre according to the mechanism of total internal reflection. The motivation for this application of "textile like fibre sensor" was to investigate interactions on the fibre surface of relevance to the detergency process. In this thesis, studies including the interactions of the fibre surface with liquid and solid soil so as to mimic the soiling process of fibres with two different types of soil, were reported.

It was established that it is feasible to use textile-like fibres for light guiding purposes. Even though a much higher attenuation of light intensity occurs due to the material properties of the fibres, some textile fibres can be used as a light guide. Transmission of light in a textile fibre, Tencel, down to 57 $\mu$m in diameter has been achieved, although in this thesis, most of the experiments were carried out with a large polyester fibre (800 $\mu$m in diameter). Light transmission in a 80 $\mu$m polyester fibre has also been demonstrated. Polyester and Tencel were chosen to represent the two types of textile fibres widely used in today's textile industry. Polyester is the most widely used man made or synthetic fibre, whereas cotton is the equivalent for the natural fibres. However, due to its morphology cotton cannot be used for light guiding purposes. Tencel, although a synthetic fibre, is in its properties very similar to cotton and hence was used as a model for cotton.

An experimental arrangement has been designed capable of carrying out quantitative studies of the effects of the soiling of the fibre on its light transmission efficiency. The set-up has been tested and characterised with plastic optical fibre, which allowed a comparison with textile fibres. The experimental arrangement included a lock-in amplifier in the detector circuit enabling the measurement of small signals embedded in high noise.

Immersion experiments with coiled plastic optical fibre showed that the attenuation of the light intensity reaches a theoretically expected saturation, normally 100 % loss, when the surrounding medium has a refractive index greater than or equal to that of the fibre. A light guiding model based on meridional rays for multimode fibres, designed to explain quantitatively the experimental results, showed the same behaviour, although, due to coiled fibre system a quantitative agreement could not be obtained. Immersion experiments with straight polyester fibre gave similar experimental results. However, the saturation of light loss could not be observed since the refractive indices of the immersion liquids (higher than that of PMMA) were now too low. Nevertheless, the expected trend in the light attenuation with increasing refractive index has been obtained and a good agreement between the experimental data and the theoretical predictions was found.

In order to investigate the kinetics of the oily soiling process, deposition of oil drops from an emulsion in which the fibre was immersed has been studied. The experimental data for the optical fibre and small diameter polyester fibre were quite similar and they suggested that the deposition process shows an exponential decay relationship between the light attenuation and the time of deposition. In other words, the rate of deposition of oil drops onto the fibre surface decreases with time. Similar behaviour has been reported in the literature for coiled plastic optical fibre.

The kinetics of particulate soiling has been investigated via the evaporation of particle suspension drops from the fibre surface. Monodisperse polystyrene latex

particles were used as a model system. A videomicroscopy apparatus has been used to visualise the deposition process and the results of these observations were used to interpret the data obtained from the light transmission method. The contact line pinning of liquid and suspension drops were observed in both cases. Furthermore, a linear relationship between the fibre area covered by the latex particles and the light attenuation was found. Due to the high refractive index of the particles, higher than that of the fibre, small area coverage will result in high attenuation of the transmitted light. A clay particle suspension, which is a more complicated but more realistic system, showed similar results. However, due to their particle size distribution and particle shape the relationship between area covered and the light attenuation was not as strong as with the latex particles. The theoretical predictions agreed very well for the latex model system, whilst a discrepancy existed between the theory and experiment for the clay particles. However, one has to keep in mind that the clay system is far more complicated than the latex.

A further investigation into the kinetics of the solid soiling process has been undertaken to complement the emulsion system. The deposition of clay particles from an aqueous phase in which the fibre is immersed has been studied. It was found that the deposition rate of the clay particles could be manipulated by the electrolyte concentration in the aqueous phase. The two systems, emulsion and latex particle suspension, were different in their particle sizes and this prevented a complete comparison of the deposition process between liquid and particulate soil.

Finally, the quartz crystal microbalance method has been included in this investigation to give a second view of the kinetics of the deposition of particles from liquid onto surfaces. The QCM method gave similar results and provided an independent verification of the results obtained by the light transmission method. Although further work on the quantitative interpretation of the QCM data is required, qualitatively the deposition of particles from liquid can be considered as a deposition of a rigid mass layer onto the crystal surface, for small particle

sizes. Additionally, it was found that the penetration depth of the evanescent wave in the light transmission method is larger than that of the QCM.

## 7.2 Further work

This thesis has demonstrated that the attenuated total internal reflection method can be used for sensing interfacial processes occurring on textile like fibres. Interfacial interactions of both liquid and solid soil with the fibre surface have been investigated with this method. Results showed that the intensity of the transmitted light could be directly related to the soiling process of the fibre surface. The light transmission signal has been characterised using videomicroscopy observations of fibre-soil systems.

Fibres used in textile industries are normally around 10 μm or smaller in size. The existing experimental arrangement is capable of producing light guiding in fibres down to 57 μm. However, it is believed that a more powerful laser diode or laser would enable the light guiding method to be used in much smaller textile fibres. This would give a realistic system for the detergent industry to use for investigations on the soil deposition and removal processes occurring during washing.

The emulsion experiments described in Chapter 6 showed that the deposition of oil droplets onto the fibre surface from an aqueous phase could be detected with the transmission method. Due to the droplet size distribution, surface coverage and thus the rate of deposition could not be determined. However, if an emulsion with a very narrow droplet size distribution is used, one could work out the rate of deposition and thus the relationship between light attenuation and surface coverage for oily soil may be obtainable.

Surface coverage was difficult to determine for the particle experiments. Due to the high refractive index of the particles, and thus the high light attenuation, minimal variation of the surface coverage will result in a large change in the light intensity. Therefore, a more exact method to determine the surface area covered

by the particles would be of advantage for the investigation. In addition, a way to obtain uniform particle coverage of the fibre would also simplify the determination of the covered area. Through this, a larger coverage of the fibre area would be achieved and a more representative and accurate study of the soiling process could be obtained.

The experiments with clay particle suspensions showed that the light transmission method can be applied to realistic systems, but the results from this system were not easily described by the theory developed in Chapter 3. This was due to the many unknowns of the clay system, such as the orientation of the deposited particles on the fibre surface. Further studies of the orientation of the clay particles and their shape would help in characterising the light transmission signal. Further, the experiments of the deposition of clay particles onto polyester fibre from an aqueous phase showed that the attenuation in light signal is quite small compared to the emulsions. Reasons may include the stability of the clay suspension, the small particle size, and the surface charge of the fibre. A more hydrophilic fibre surface, which can be achieved by plasma treatment, would benefit the deposition process of clay particles, and should result in a higher light attenuation. It is likely that such a system would give significantly higher effects of the clay deposition on the light transmission.

Finally, after looking at the soiling process one could also look directly at the removal of deposited soil from the fibre surface. A soiled fibre, for instance one such as obtained from the emulsion experiment, could be used in this study. The removal of soil according to detergency involves the addition of surfactant material into the emulsion system to investigate whether the deposited oil drops on the fibre surface will be removed. Having a record of the soiling process would help in characterising the removal efficiency of the surfactants studied. Knowing the values for light transmission for clean and soiled fibre, one could work out the removal efficiency of the surfactants.

The light transmission method possesses promising properties as a tool to

investigate interfacial interactions. Here, it has been shown that the method can be used to study the kinetics of the soiling process of single fibres. Further investigation has to be carried out to reduce the size of the fibre to make it more relevant for the detergency industry.
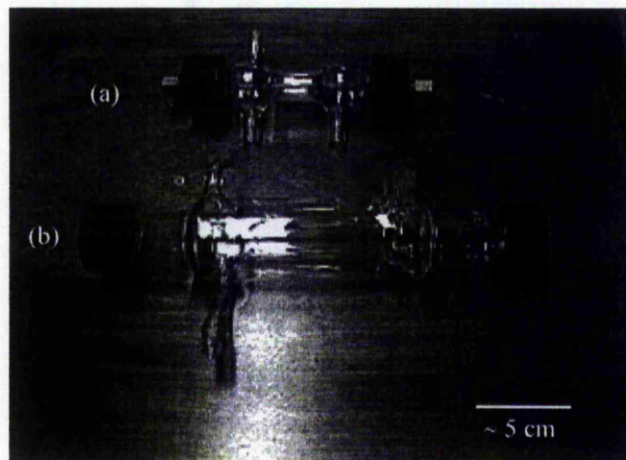
# Appendices

## Appendix 1: Glass flow cells used in the investigation.



Figure A1. Flow cells used in immersion and emulsion experiments. (a) short flow cell with inlet and outlet ports; used in clay deposition experiments. (b) long flow cell with inlet and outlet ports and thermostatic jacket; used in immersion experiments.

## <u>Appendix 2</u>: C-program to determine the wetted and the covered area of fibre.

```c
// Calculation from plan image of fibre area wet by a clam droplet
// Output is in the form of planar pixel areas
//
#include "pr_mem.h"

// Type definitions for main functions

float WetArea(BYTE **InIm, int r, int c,float radius,float *MaxWA,float *MinWA);
long PlanArea(BYTE **InIm, int r, int c,long *MaxPA,long *MinPA);
void DisplayResults(long PlanArea,long MaxPA,long MinPA,
                                          float area,float MaxWA,float
MinWA,float rad);

int main(int argc,char *argv[])
{
BYTE **InIm;

int Rows, Cols;
char fi[50];
float Radius,Area,MaxWA,MinWA;
long PlanarArea,MaxPA,MinPA;

if (argc<3)
  {
  printf("\nsyntax is\t%s infile.bin rows cols\n\n",argv[0]);
  printf("Assumptions:\\n");
  printf("\t\tfibre axis is along horizontal in the image\n");
  printf("\t\tfibre image has top and bottom equating to fibre edges\n");
  printf("\t\tdroplet outline is highlighted in white (255)\n");
  printf("\t\tCo-ords have top left as row 0\n");
  return 1;
  }
else
  {
  Rows=atoi(argv[2]);
  Cols=atoi(argv[3]);
  strcpy(fi,argv[1]);

  InIm=ImByteAlloc(Rows,Cols);          // These allocate memory space

// using routines in pr_mem.c
  GetByteImage(InIm,Rows,Cols,fi);       // Read in byte image

  Radius=(float)Rows/2.0;
  Area=WetArea(InIm,Rows,Cols,Radius,&MaxWA,&MinWA);
  PlanarArea=PlanArea(InIm,Rows,Cols,&MaxPA,&MinPA);
  DisplayResults(PlanarArea,MaxPA,MinPA,Area,MaxWA,MinWA,Radius);
  ImByteFree(InIm,Rows);                // Free up memor
  return 0;
  }
}
//
float WetArea(BYTE **InIm, int Rows, int Cols,float Rad,float *Max,float *Min)
{
float WA,geodesic,Rel_Pos,Sum_Col,Sum_Max,Sum_Min;
int bounds[1000],nb;
int i,j,k;
```

```
*Max=0.0,*Min=0.0;
for (j=0;j<Cols;j++)
  {
  nb=0;
  for (i=0;i<Rows;i++)
    if (InIm[i][j]==WHITE) {bounds[nb]=i;nb++;}

                                                // complex outline
  if (nb>2)
    {
    printf("\nWetted area calculation - POSSIBLE ERROR in outline\n");
    printf("\t\t\trow %d, col %d with number of whites=%d\n",i,j,nb);
    }

  if (nb>=2)
    {
    Sum_Max=0.0;
    Sum_Min=0.0;
    for (k=bounds[0];k<=bounds[nb-1];k++)
      {
      Rel_Pos=((float)k-Rad)/Rad;
      geodesic=1.0/pow(1.0-Rel_Pos*Rel_Pos,0.5);
      Sum_Max=Sum_Max+geodesic;
      if ((k!=bounds[0])&&(k!=bounds[nb-1]))
          Sum_Min=Sum_Min+geodesic;
      }
    *Max=*Max+Sum_Max;
    *Min=*Min+Sum_Min;
    }
  }
WA=0.5*(*Max+*Min);
return WA;
}
long PlanArea(BYTE **InIm, int Rows, int Cols,long *MaxPA,long *MinPA)
{
long PA=0;
int bounds[5000],nb;
int i,j;

*MaxPA=0,*MinPA=0;
for (j=0;j<Cols;j++)
  {
  nb=0;
  for (i=0;i<Rows;i++)
    if (InIm[i][j]==WHITE) {bounds[nb]=i;nb++;}

                                                // complex outline
  if (nb>2)
    {
    printf("\nPlanar area calculation - POSSIBLE ERROR in outline\n");
    printf("\t\t\trow %d, col %d with number of whites=%d\n",i,j,nb);
    }
  if (nb>=2)
    {
    PA=PA+abs(bounds[nb-1]-bounds[0]);            // length of line
    *MaxPA=*MaxPA+abs(1+bounds[nb-1]-bounds[0]);
    *MinPA=*MinPA+abs(bounds[nb-1]-bounds[0]-1);
    }
  }
return PA;
}
```

```
void DisplayResults(long PlanarArea,long MaxPA,long MinPA,
                                        float Area,float MaxWA,float MinWA,float
Rad)
{
printf("\n\n===================================================");
printf("\n\nFibre pixel radius \t= %.2f\n",Rad);
printf("Planar pixel area \t= %ld \t%ld\t%ld\n",PlanarArea,MinPA,MaxPA);
printf("Wetted pixel area \t= %.0f \t%.0f\t%.0f\n",Area,MinWA,MaxWA);
printf("\nConvert areas by multiplying by calibrations\n");
printf("\n===================================================\n");
}
```

## <u>Appendix 3</u>: Immersion of coiled PMMA optical fibre in a series of alkanes
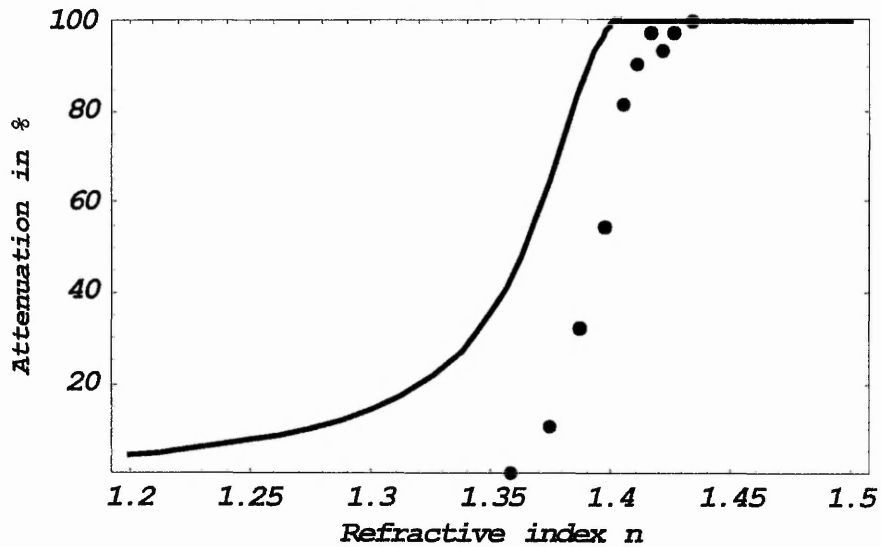


Figure A3. Plot of experimental data (dots) and theoretical predictions (solid line) obtained from the light guiding model for the immersion of coiled PMMA optical fibre in alkanes.

Coiling of a PMMA optical fibre gives rise to skew rays, which are not considered in the light guiding model. Figure A3 above shows that whilst an exact numerical match is not possible qualitatively experimental data can be approximated by the theory.

## Appendix 4: Determination of contact area of latex particles on glass



(a)



(b)

(c)
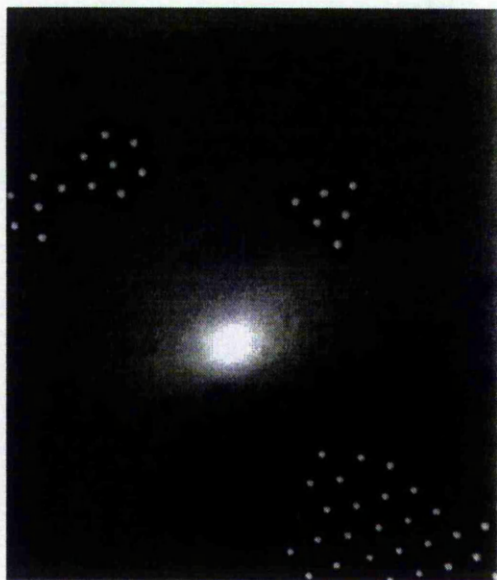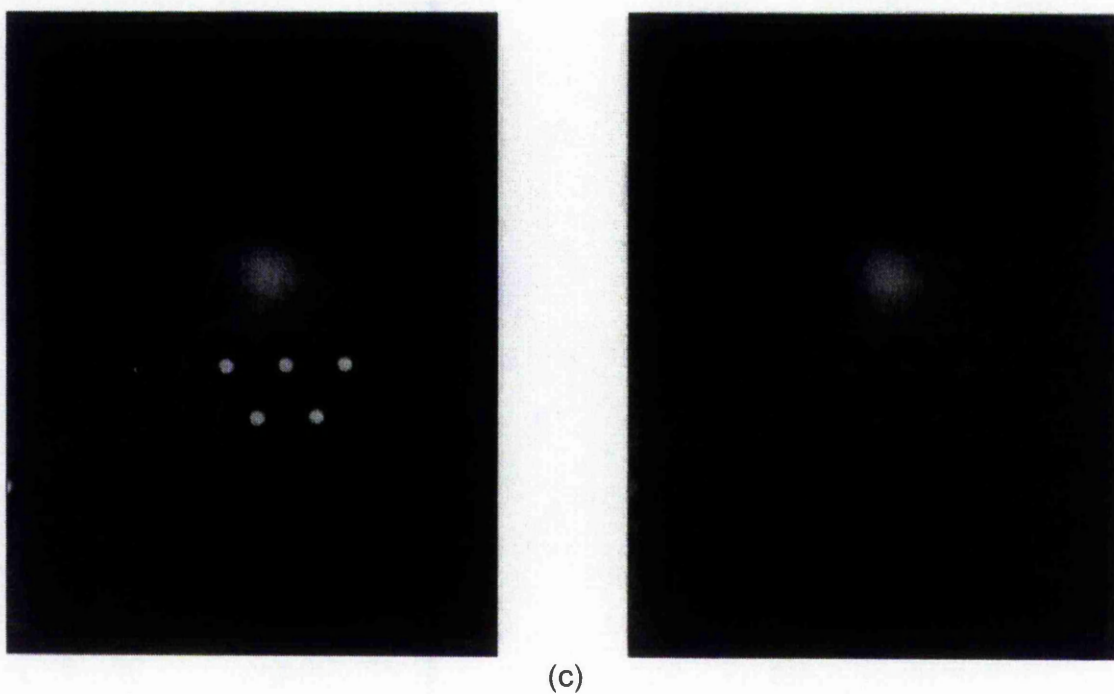
Figure A4. Transmission microscope pictures of particles (right pictures) and their contact areas (light spot in left pictures) with glass. (a) 3.15, (b) 5, and (c) 10 μm latex particles.

## Appendix 5: Evaporation of a drop of 3.15 μm latex particle suspension on polyester fibre.
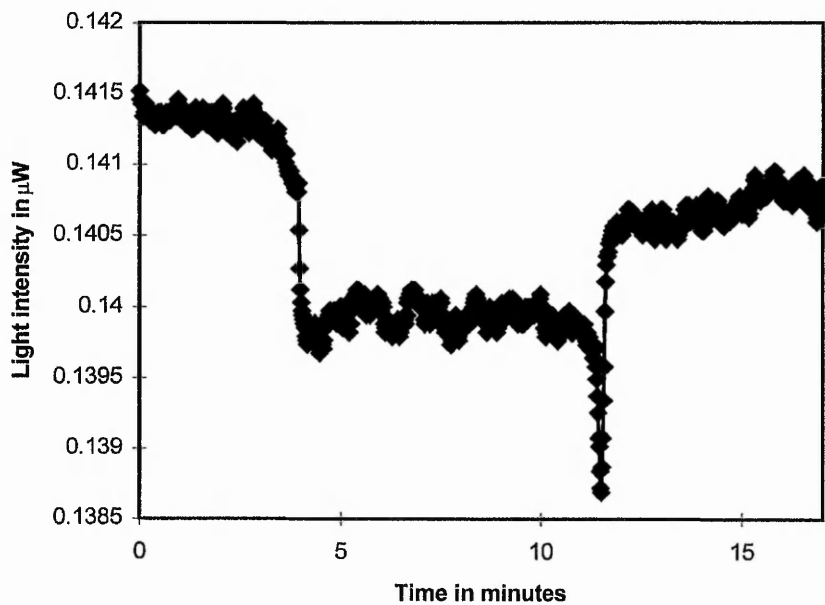


Figure A5. The effect of the deposition of 3.15 μm latex particles on light transmission in 800 μm polyester fibre via evaporation of suspension droplet. Suspension drop volume is 0.5 μl and the solid content is 1%.

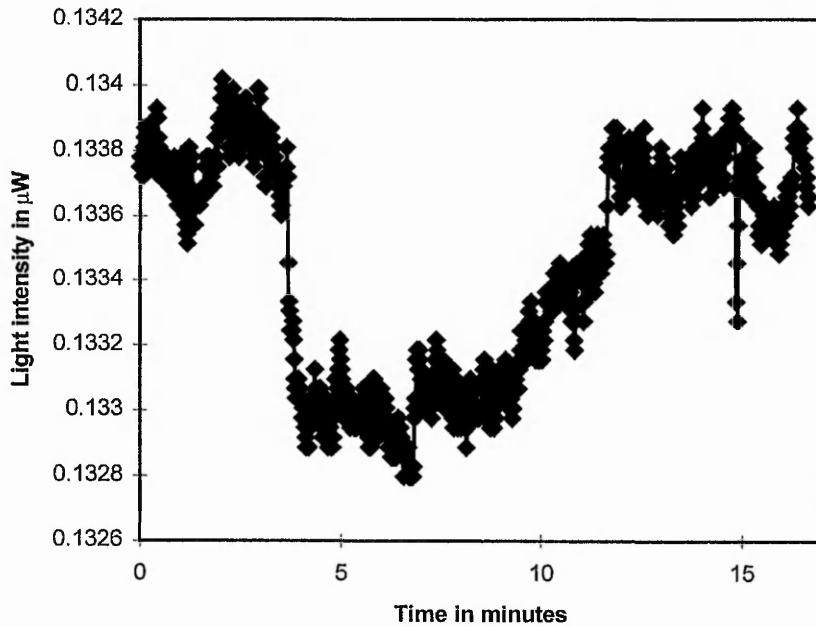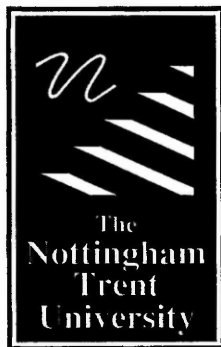## Appendix 6: Evaporation of a drop of 10 μm latex particle suspension on polyester fibre.



Figure A6. The effect of the deposition of 10 μm latex particles on light transmission in 800 μm polyester fibre via evaporation of suspension droplet. Suspension drop volume is 0.5 μl and the solid content is 1%. It is notable that the signal above looks quite similar to that of evaporation of pure water on polyester fibre, suggesting that the fibre does not optically see the particles.

# Libraries & Learning Resources